

©2016

Xiao Qian

ALL RIGHTS RESERVED

FROM LIGHT TO DARK: MAPPING FLUXES OF MODEL
CYANOBACTERIA FOR BIOFUEL APPLICATIONS

by

XIAO QIAN

A dissertation submitted to the

Graduate School-New Brunswick

Rutgers, The State University of New Jersey

In partial fulfillment of the requirements

For the degree of

Doctor of Philosophy

Graduate Program in MICROBIAL BIOLOGY

Written under the direction of

G. Charles Dismukes

And approved by

New Brunswick, New Jersey

May 2016

ABSTRACT OF THE DISSERTATION

From light to dark: Mapping fluxes of model cyanobacteria for biofuel applications

By XIAO QIAN

Dissertation Director:

Dr. G. Charles Dismukes

Cyanobacteria are a diverse class of prokaryotes that are the simplest oxygenic photoautotrophs. They harvest light energy during the daytime to assimilate inorganic carbon (predominately CO_2 and HCO_3^-) from the environment. Photosynthetically fixed carbons are used to synthesize the majority of cellular components, including proteins, lipids, carbohydrates, nucleic acids, pigments, etc. that are used for diverse functions. Among these, proteins are the major carbon products formed during growth in excess nutrients and light, when cell division is fastest. By contrast, carbohydrates, typically glycogen, accumulate during periods of nutrient limitation in sufficient light and CO_2 .

They serve as carbon and energy storage components for dark periods when light energy is low (no photophosphorylation) or carbon is scarce. These two biomass components together may account for up to 85% of the cellular dry weight. Now, scientists are using technologies to try to make cyanobacterial “cell factories” that produce valuable chemicals and biofuel. Accomplishing such ambitious redesign requires a comprehensive understanding of cyanobacterial metabolism at a system level picture under various conditions.

The objective of the first part of this thesis was to quantitatively measure and predict the carbon flux distributions in a model cyanobacterium *Synechococcus* sp. PCC 7002 under various light and nutrient conditions. For this, I employed two different approaches, flux balance analysis (FBA) and metabolic flux analysis (MFA), to map carbon flux distributions under different growth conditions. The FBA approach is simplest to apply but more primitive. It relies upon a steady-state (non-kinetic) representation of enzymatic fluxes between metabolites inferred to exist based on the presence in the genome of encoded enzymes and from comparison to classical pathways. FBA was able to simulate one important metabolic transition: from active carbon allocation (growth) to carbon and energy storage mode that occurs as light intensity increases. Integration of transcriptomic information with the FBA modeling further enabled the prediction of steady-state carbon flux distribution under nitrogen deprivation. The relative flux of fixed carbon into storage carbohydrates under nitrogen deprivation was predicted to increase by 200%, compared to a predicted 30% decrease of carbon flux through the lower glycolytic pathway and into the TCA cycle. This prediction was

validated by the experimental-based MFA approach that measures metabolic flux directly using ^{13}C -labelled precursors.

In addition to quantifying the carbon fluxes into different terminal products, the FBA and MFA approaches together illustrated several important metabolic routes that were overlooked by scientists in the past. The FBA approach predicted a hybrid gluconeogenesis-pentose phosphate (hGPP) pathway was equally possible to convert fixed CO_2 intermediates into glycogen, rather than the conventional gluconeogenesis-only pathway. Using the MFA approach, I provided quantitative experimental proof showing the alternative hGPP pathway to be the major pathway under nitrogen deprivation, 4.4-fold more active than conventional gluconeogenesis. Again using ^{13}C -labelling and the MFA approach, I generated quantitative results proving that the newly discovered pair of enzymes of the succinic semialdehyde (SSA) shunt, previously postulated to complete the TCA cycle of cyanobacteria ($\text{AKG} \rightarrow \text{SSA} \rightarrow \text{SUCC}$), actually operate to catalyze these reactions during photosynthesis. Furthermore, deletion of one or both of these enzymes led to a 10~15% reduction of the photosynthetic growth rate, and 50~80% reduction of the pool size of the downstream product, succinate. The MFA results showed the flux through the SSA shunt accounts for $> 6.4\%$ of the corresponding RuBisCO carboxylation flux under photoautotrophic conditions. Lastly using the MFA approach, I showed: 1) the dominant role of a cyclic route ($\text{PEP} \rightarrow \text{OXA} \rightarrow \text{MAL} \rightarrow \text{PYR} \rightarrow \text{PEP}$) via the malic enzyme for generating PYR and OXA needed for photoautotrophic biosynthesis; and 2) the increased synthesis of glycogen that occurs under nitrogen deprivation results from the combination of two pathways at the 3PG and G6P branching points that contribute precursors.

The goal of the second part of the thesis was to construct a *Synechococcus* 7002 mutant capable of producing H₂ in the dark at high rates by anaerobic fermentation in the presence of nitrate. Cyanobacteria catabolize the storage carbohydrates (glycogen) synthesized during photosynthesis under dark anaerobic conditions (denoted auto-fermentation). *Synechococcus* 7002 bears a H₂-producing enzyme, Hox hydrogenase, which produces H₂ during auto-fermentation by consuming reductant generated through glycogen catabolism. A knockout mutant of the reductant consuming nitrate reductase, *AnarB*, showed a 6-fold higher dark fermentative H₂ evolution rate than the WT when fermenting on nitrate. Combining the mutation with a “milking” strategy, which continuously removes H₂ from the fermentation medium, resulted in a 49-fold combined increase in the net H₂ evolution rate during 2 days of fermentation compared to the WT.

In summary, my dissertation quantitatively maps the carbon flux distribution, using a combination of computational and experimental approaches, under both photoautotrophic growth at different light intensities and nutrient conditions and under dark autofermentation in the model cyanobacterium *Synechococcus* 7002. These studies reveal the capacity for using cyanobacteria as cell factories for carbon and solar energy storage and H₂ production, respectively.

Acknowledgements

There is a Chinese old saying: *One day as a teacher, one life as a father*. This is the spirit of how we Chinese people respect our mentors. I am deeply grateful to my Ph.D. advisor, Professor G. Charles Dismukes. The moment I received his invitation to join the lab as a doctoral trainee was one best moment in my life at Rutgers University. The way Professor Dismukes mentored me allowed me to not only master my experimentation and independent critical thinking skills, but also explore the potential of myself, the potential to make impossible possible again. I would also like to thank my Ph.D. co-advisor, Professor Desmond S. Lun for his professionalism in work and patience in me, and guiding me through the path to a new world of biology – computational biology. In addition, I would like to thank the other two members of my dissertation committee, Professor Jeff Boyd and Professor Debashish Bhattacharya for their encouragement and assistance in completing this dissertation work.

I want to specially acknowledge my undergraduate advisor, Dr. Barbara Zilinskas. If she did not make the phone call to help me get my General Biology credits transferred from Canada to Rutgers, I would have remained undergraduate for one additional year, my life path would be completely altered, and I would have missed all these important people I met later in my life.

When friendship is blended with collaboration, the outcome is magnificent. I would like to acknowledge all my lab mates and friends, Dr. Gennady Ananyev, Dr. Kumaraswamy G. Kenchappa, Dr. Anagha Krishnan, Dr. Tiago Guerra, Dr. David Vinyard, Dr. Elizabeth Burrows, Yuan Zhang, Colin Gates and Shannon Chang. Collaborations with these great scientists accelerated my progress to become a real

philosophical scientist. They created a joyful laboratory experience for me at Rutgers. Outside of Rutgers, I should thank Dr. Donald A. Bryant and his student Dr. Shuyi Zhang from Penn State University for their great contributions to my thesis work.

Also, I would like to acknowledge all other members of the Dismukes' chemistry subgroup, Dr. David Robinson, Dr. Clyde Cady, Dr. Paul Smith, Graeme Gardner, and Dr. Anders Laursen for being great companions from another discipline.

I would always like to thank my lovely parents, Guoqing Qian and Suqin Fei, who are the best parents in this world. They offered me love since I was carried, offered me patience since I started to behave, and offered me support since I decided to move forward in my life. For the past ten years, they have suffered the “emptiness” at my home in China due to my absence. Yet, they never complained, because all they want is to see me realize my dreams and be happy. The next person I would like to acknowledge is my girlfriend and hopefully wife in the future, Qi Zhang. She spent her golden years with me throughout my doctoral training life at Rutgers, and provided me love, courage and confidence.

Friendship is essential, and I am so grateful that I am always supported by so many true friends. I would like to thank my former roommates and still life buddies, Suowei Wu and Hao Tong. These two gentlemen shared my happiness and sorrowness for years since we met in the Macro Economics class. I would also like to acknowledge another life buddy, Amy Fan, who has been a good listener of my “weird” and “naïve” thoughts, and backs me up when I need help.

Here, I would like to acknowledge several other friends who open my eyes to another path of being a scientist. Dr. Wei Li was my special mentor and like my brother,

who enlightened me with the great idea of forming a new collaborative relationship between scientists and business men, so that more scientists hopefully can do their research of own interest. Great ideas shall always accompany with loyal encouragers and criticizers. Therefore, I shall thank one best encourager friend, Dr. Ying Zhang, and one best criticizer friend, Ke Sun.

Lastly, my doctoral work was supported by Department of Energy (DOE-EERE, grant DE-EE0003373), Air Force Office of Scientific Research (MURI grant FA9550-05-1-0365), and National Science Foundation (NSF-MCB, grant 1515511).

Table of contents

ABSTRACT OF THE DISSERTATION	ii
Acknowledgements.....	v
Chapter 1: Introduction	1
1. <i>Cyanobacteria for biofuel</i>	2
1.1) Liquid hydrocarbon fuel	2
1.2) Carbohydrate feedstocks.....	2
1.3) Hydrogen	5
2. <i>Photoautotrophic growth of cyanobacteria</i>	9
3. <i>Dark autofermentative H₂ production</i>	18
3.1) Increasing total reductant equivalent pool size.....	21
3.2) Increasing the fraction of reductant equivalents directed H ₂ production.....	21
3.3) Increasing Hox Hydrogenase concentrations and/or activities.....	22
4. <i>Scope of the thesis</i>	24
Chapter 2: Beyond conventional flux balance analysis of photoautotrophic metabolism: Light intensity dependent partitioning of carbon into different cellular products	27
<i>Summary</i>	28
1. <i>Introduction</i>	30
2. Experimental Procedures	33
2.1) Metabolic Network Reconstruction.....	33
2.2) Biomass composition and vBOF	38
2.3) Linear programming problem formulation.....	41
2.4) Optimization strategy	42
2.5) Flux boundaries	42
2.6) Bacterial cultivation and model validation.....	42
2.7) Transcriptomic data constrained carbon metabolic fluxes under nitrogen deprivation	43
2.8) ¹³ C isotope kinetics measurements under photoautotrophic condition	45
3. <i>Results and Discussion</i>	47
3.1) Model validations	47
3.2) Photoautotrophic metabolic fluxes under low light and high light conditions.....	55

3.3) Transcriptomic-constrained analysis of metabolism under nitrogen deprived condition in <i>Synechococcus</i> 7002	67
4. <i>Conclusion</i>	72
5. <i>List of abbreviations</i>	73
6. <i>Supplemental Information</i>	74
Chapter 3: Closing the truncated tricarboxylic acid cycle in the cyanobacterium <i>Synechococcus</i> sp. PCC 7002	78
<i>Summary</i>	79
1. <i>Introduction</i>	80
2. <i>Experimental Procedures</i>	84
2.1) Cloning, protein purification and identification	84
2.2) Enzyme assays.....	85
2.3) Mutant construction and segregation.....	87
2.4) Strains, growth conditions and culture preparation	92
2.5) Intracellular metabolites analysis	94
2.6) Determination of intracellular SSA	95
2.7) O ₂ evolution rate, dark respiration rate, and Chlorophyll-a concentration	96
3. <i>Results</i>	97
3.1) Determination of SSA-DNPH derivates.....	97
3.2) ¹³ C labeling of SSA under light and dark conditions	99
3.3) Intracellular metabolite analysis of TCA cycle mutants	101
3.4) Growth phenotypes and succinate levels in mutant strains	104
3.5) GABA shunt enzymatic assays.....	106
3.6) Construction of glutamate decarboxylase expression strains	109
3.7) Metabolic profiling of glutamate decarboxylase expression strains	111
4. <i>Discussion</i>	115
Chapter 4: Quantitative fluxomics analysis of the carbon partitioning into cellular products in the cyanobacterium <i>Synechococcus</i> sp. PCC 7002.....	120
<i>Summary</i>	121
1. <i>Introduction</i>	122
2. <i>Experimental Procedures</i>	127

2.1) Culture growth and experimental conditions.....	127
2.2) Intracellular metabolite extraction and analysis	127
2.3) Intracellular steady state validation	128
2.4) Carbon labeling experiment.....	128
2.5) Semi-quantitative analysis.....	129
2.6) Isotopically nonstationary metabolic flux analysis (INST-MFA).....	129
3. <i>Results</i>	131
3.1) Requirement for stable cultures for INST-MFA analysis	131
3.2) How do carbon metabolite pool sizes change with growth conditions	133
3.3) Semi-quantitative determination of carbon flux distributions.....	135
3.4) Quantitative analysis of carbon flux distribution	140
4. <i>Discussion</i>	146
4.1) Changes of carbon flux distributions at metabolic branches under -N.....	146
4.2) The OPP pathway	147
4.3) Metabolic channeling	148
4.4) The hGPP pathway	148
4.5) The malic cyclic route	149
4.6) The SSA route	151
5. <i>Conclusion</i>	152
6. <i>Supplemental Information</i>	153
Chapter 5: Inactivation of nitrate reductase alters metabolic branching of carbohydrate fermentation in the cyanobacterium <i>Synechococcus</i> sp. strain PCC 7002	161
<i>Summery</i>	162
1. <i>Introduction</i>	163
2. <i>Experimental Procedures</i>	167
2.1) Mutant construction and segregation.....	167
2.2) Strains, growth conditions and culture preparation	170
2.3) Fermentative conditions	171
2.4) Analytical assays	171
2.5) Measurements of instantaneous H ₂ production rate and pyridine nucleotide concentrations	172

3. <i>Results</i>	174
4. <i>Discussion</i>	192
5. <i>Conclusion</i>	202
Chapter 6: Conclusions	203
References	208

Table of Figures

Figure 1-1 Scheme of photosynthesis of <i>Synechococcus 7002</i>	11
Figure 1-2 Autofermentative metabolism of cyanobacteria	19
Figure 1-3 Overall scheme of subjects studied in the thesis	26
Figure 2-1 Pipelines to construct and optimize <i>iSyp821</i>	35
Figure 2-2 PSII ETR and weight fraction of protein and carbohydrates at different light intensities	40
Figure 2-3 Prediction of growth rates and C_i uptake rates at different PSII ETRs	50
Figure 2-4 Prediction and validation of PSI/PSII ETR ratio by <i>iSyp821</i>	53
Figure 2-5 A relative flux map for photoautotrophic growth under low and high light conditions	58
Figure 2-6 ^{13}C -labeling kinetics of F6P, FBP and S7P monitored under low and high light conditions	63
Figure 2-7 Carbon flux redistribution under nitrogen deprivation photoautotrophic conditions as predicted by transcriptomic modified FBA	69
Figure S2-1 Dry weights of <i>Synechococcus 7002</i> culture at different optical densities....	74
Figure S2-2 Dry weight densities of <i>Synechococcus 7002</i> cultures grown under different light conditions.....	75
Figure S2-3. Oxygen evolution of <i>Synechococcus 7002</i> cultures supplemented with different concentrations of $NaHCO_3$	76
Figure 3-1 Scheme showing the TCA cycle, glyoxylate cycle and GABA shunt	82
Figure 3-2 Scheme for mutant construction and verification of the TCA cycle mutants ..	88
Figure 3-3 LC-MS method to determine intracellular SSA contents	98
Figure 3-4 Quantification of intracellular SSA.....	100
Figure 3-5 Metabolites profiling of TCA cycle metabolites in mutant strains	103
Figure 3-6 Characterizations of purified recombinant proteins	107
Figure 3-7 Verification of the constructed GABA shunt mutant strains	110
Figure 3-8 Metabolites profiling of GABA shunt mutant strains	113
Figure 4-1 Pool size stability tests of indicator metabolites in bioreactor culture.....	132
Figure 4-2 A comparison of metabolite pool sizes +N vs. -N	134

Figure 4-3 ¹³ C-labeling parameters of carbon metabolites +N vs. -N	137
Figure 4-4 Carbon flux distribution maps +N vs. -N	143
Figure S4-1 Pool size stability tests of 12 indicator metabolites in batch culture	153
Figure 5-1 <i>narB</i> deletion mutant construction and confirmation	168
Figure 5-2 Growth curves of WT and the $\Delta narB$ strain.....	175
Figure 5-3 Nitrite excretion and nitrate uptake.....	178
Figure 5-4 Excretion of fermentative end products	183
Figure 5-5 The ratio of intracellular metabolite concentrations +N vs. -N.....	185
Figure 5-6 Autofermentative H ₂ evolution rates measured via H ₂ rate electrode and NAD(P)H concentrations measured by fluorescence +N vs. -N.....	189
Figure 5-7 Plot of autofermentative H ₂ evolution rate against intracellular NAD(P)H concentration.....	190
Figure 5-8 Autofermentative reductant balances	197
Figure 5-9 A quantitative schematic representation of overall effects of deleting the <i>narB</i> gene in <i>Synechococcus</i> 7002.....	198

Table of Tables

Table 1-1 Energetic requirements for the synthesis of biomass components.....	14
Table 2-1 Comparison of the <i>iSyp821</i> FBA model to the two existing <i>Synechococcus</i> 7002 models, <i>iSyp611</i> and <i>iSyp708</i>	49
Table 2-2. Summary of fluxes into metabolite precursor for making carbohydrate, protein and lipids under both high light and low light conditions	59
Table 2-3 Parameters determined by ¹³ C labeling of target metabolites	64
Table S2-1. Total carbohydrate and total protein contents of photoautotrophic cultures of wildtype <i>Synechococcus</i> 7002 before and after 1 hour of nitrogen deprivation.....	77
Table 3-1 Primers used in this study.....	91
Table 3-2 Growth rates, Chlorophyll <i>a</i> contents, oxygen evolution and respiration rates of mutant strains	105
Table 4-1 Carbon flux distribution patterns at branching points	139
Table 4-2. Photoautotrophic carbon flux distributions at different branching points.....	145
Table S4-1. Pool sizes of metabolites in cultures +N vs. -N	154
Table S4-2 Absolute metabolic flux rates of all metabolic reactions	160
Table 5-1 Primers used to generate <i>narB</i> deletion mutant.....	169
Table 5-2 Chlorophyll-a, total reduced sugar content and total protein content	176
Table 5-3 Reduced sugar catabolism and metabolite excretion.....	180
Table 5-4 Reductant balance calculations.....	182
Table 5-5 Intracellular concentrations of adenosine phosphates and pyridine nucleotides +N vs. -N.....	186
Table 5-6 Comparison of H ₂ evolution rates in the vial experiments and “milking” experiments	191
Table 5-7 ATP yield per glucose equivalent catabolized through the glycolytic pathway during autofermentation.....	195

Chapter 1. Introduction

Recent economic and political impacts have driven the world price of crude oil from \$140 / barrel in 2008 to less than \$40 / barrel in 2016 (Bloomberg). However, oil market price fluctuation does not resolve the energy crisis we may have to face in the near future. BP estimates that the total proven reserves of oil, natural gas and coal can only meet 52.5 years, 54.1 years and 110 years of global productions, respectively (BPstats, 2015). Renewable sources of energy such as hydroelectricity, nuclear, solar, wind, and biofuel, are considered potential alternatives to fossil fuels. In 2014, renewable energy accounted for ~15% of world energy consumption. Biofuel is a promising alternative energy option, though its current contribution to total world energy consumption is still small (0.55% of by 2014) (BPstats, 2015).

Owing to the advantages of lower carbon footprint and not competing with crops for arable land (Liu et al., 2013; Dismukes et al., 2008), algal-based biofuel has the potential to become a major renewable energy resource in the future. Algal-based biofuel can be derived from three ecologically diverse classes of aquatic microbial oxygenic photoautotrophs (AMOPs): cyanobacteria, green algae and diatoms. Compared to terrestrial plants, AMOPs benefit from their higher photosynthetic efficiency in light to biomass conversion, and account for more annual global biomass production (Ducat & Silver, 2012; Dismukes et al., 2008). Algal biomass accumulated during photoautotrophic growth can be converted into different forms of biofuel either directly or indirectly by biological or chemical strategies.

1. Cyanobacteria for biofuel

Due to their fast growth, ability to fix CO₂, ease of cultivation, modifiable genomes, and ability to produce metabolites of interest without external reduced carbon sources, cyanobacteria are an ideal platform for biofuel production. On March 2013, a US based company, *Algenol*, announced production of 9,000 gallons per acre per year of ethanol from their ethanol-tolerant strains of photosynthetic cyanobacteria. This yield is larger than corn ethanol, which at the time yielded only 400 gallons per acre per year. As a biotechnological platform, cyanobacteria can be used to synthesize many other energy-rich products, which can be categorized into the following three product groups: 1) liquid hydrocarbon fuel, 2) carbohydrate feedstocks, and 3) H₂ gas (Nozzi et al., 2013; Hays & Ducat, 2015; Machado & Atsumi, 2012).

1.1) Liquid hydrocarbon fuel

The main algal liquid fuels include alcohols (ethanol, isopropanol and butanol), isoprenoids (-C₅H₉- oligomers), and fatty acids (Quintana et al., 2011). Many cyanobacteria naturally produce ethanol at a basal rate under fermentative conditions (Heyer & Krumbein, 1991; Ananyev et al., 2012). Several studies have genetically wired ethanol production to photosynthetic carbon influx by introducing or manipulating pyruvate decarboxylase and alcohol dehydrogenase in cells (Deng & Coleman, 1999; Gao et al., 2012). Such a strategy successfully increased the ethanol yield in cyanobacteria up to 5.5 g L⁻¹. Moreover, cyanobacteria can synthesize longer-chain alcohols that possess a higher energy density than that of ethanol. Introduction of a heterologous isobutanol biosynthetic pathway and overexpression of native RuBiSCO led to the production of isobutyraldehyde and isobutanol (1.1 g L⁻¹ and 0.45 g L⁻¹,

respectively) in *Synechococcus elongates* PCC 7942 (Atsumi et al., 2009). Other chemicals that have been synthesized in cyanobacteria include 2,3-butanediol (2.4 g L⁻¹), 1-butanol (29.9 mg L⁻¹), 2-methyl-1-butanol (0.2 g L⁻¹), acetone (36 mg L⁻¹), ethylene (0.171 g L⁻¹ day⁻¹), isoprene (0.05 mg g⁻¹ DW day⁻¹), and isopropanol (146 mg L⁻¹) (Nozzi et al., 2013; Gao et al., 2016).

1.2) Carbohydrate feedstocks

Cyanobacteria are promising candidates for generating carbohydrate feedstocks (-CH₂O-), which can be fermented by secondary microorganisms to produce value-added metabolites (Hays & Ducats, 2015). Cyanobacteria naturally store carbons in the form of glycogen and exopolysaccharide layers, in contrast to algae and plants which use starch and a cellulosic cell wall as intracellular glucose sinks. Under ideal growth conditions, cyanobacteria have a general biomass composition of low carbohydrate and lipid levels (10-30% and 5-10%, respectively), and high protein levels (40-79%). However, several nutrient limited and stress conditions stimulate cyanobacteria to accumulate a lot more carbohydrates, although cultures under these conditions are usually coupled with compromised growth. Nitrogen starvation has been widely used to stimulate storage carbohydrates (mainly glycogen) synthesis in cyanobacteria (up to 60%) (Taikhao et al., 2014; Hasunuma et al., 2013; Miller et al., 2002; Vu et al., 2013; Yoo et al., 2007). During nitrogen starvation, glycogen serves as a primary carbon and reductant sink (Luque & Forchhammer, 2008). Osmotic stress induction can significantly increase soluble sugar content in cyanobacteria (up to 50%) (Carrieri et al., 2010; Guerra et al., 2013a). Such stress-induced soluble sugars are used to correct the osmotic imbalance and prevent cellular dehydration. Additionally, by expressing specific efflux transporters

exporting carbohydrates in several cyanobacterial species, scientists successfully used these strains to excrete large quantities of glucose, fructose, lactose or sucrose in the presence of osmotic stress induction (Ducat et al., 2012; Du et al., 2013; Niederhltmeyer et al., 2010; Xuan et al., 2013). Alternatively, when the glycogen synthesis pathway knockout mutant of *Synechococcus* 7002 ($\Delta glgA-I glgA-II$) was cultivated in hypersaline environment, soluble carbohydrates were spontaneously excreted into the media without need for changing transporters (Xu et al., 2013). In this particular mutant strain, total intracellular soluble carbohydrate content increased by 70%, while growth rate decreased by 15%.

To avoid slower growth caused by manipulation of environmental conditions, scientists have used several bioengineering approaches to improve cyanobacterial biomass and compositions. The first approach is increasing the light utilization efficiency of liquid cultures in cultivation chambers or ponds. In cultivation chambers or ponds, light is largely absorbed by surface layer cells, causing cells further from the surface to receive reduced light, reducing overall biomass productivity and cell density (Melis 2009). Deletion of the *apcE* gene encoding a protein product involved in the interaction between the thylakoids and phycobilisome caused antenna truncation in *Synechocystis* 6803, and led to increased yields of photosynthetic biomass (60%) and glycogen productivity (255%) at atmospheric CO₂ levels with light intensity at 50 $\mu\text{mol m}^{-2} \text{s}^{-2}$. in 15 days (Joseph et al., 2014). The $\Delta apcE$ mutant strain showed a slower initial photoautotrophic doubling time (21.25 h) as compared to the wildtype (WT) strain (24.88 h), and the increased biomass yield in 15 days is actually due to the higher final cell density of the $\Delta apcE$ culture. In the $\Delta apcE$ culture, absorption of light by cells at the

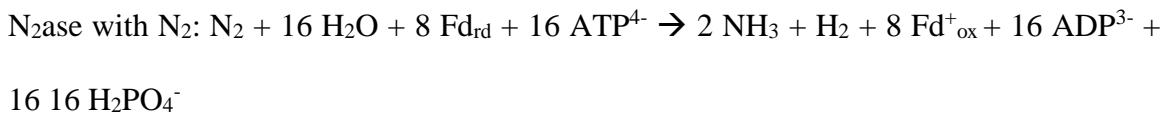
surface layer was decreased, and therefore cells below the surface layer received more light and grew better. The authors suggested that the increased glycogen productivity of the *ΔapcE* mutant was caused by the redirection of carbons from phycobilisome to glycogen in the mutant.

The second approach is to increase the intracellular inorganic carbon (*C_i*) availability. Overexpressing genes encoding a *C_i* transporter (*ictB*) and a carbonic anhydrase (*ecaA*) led to elevated photosynthetic activity and biomass productivity of 49% and 36%, respectively, in *Synechococcus* 7942 (Chow et al., 2014). By addition of a second photosynthetic carbon sink (cellulose), by co-expressing heterologous cellulose synthase gene (*acsAB*) together with *ictB* and *ecaA*, the co-expression strain produced a 2.9-fold more total carbohydrate in 3 days.

The third approach is to overexpress the flux-limiting gluconeogenic enzyme, glyceraldehyde-3-phosphate dehydrogenase 1 (GAP1), to funnel more carbons into glycogen. This mutant strain in *Synechococcus* 7002 increased the glycogen content by 20%, while the mutant had a same photoautotrophic growth rate as WT. This observation was interpreted as evidence that GAP1, which converts 3PG to GAP, is the kinetic bottleneck in gluconeogenesis activity (Kumaraswamy et al., 2013).

1.3) Hydrogen

Many cyanobacterial species are capable of synthesizing H₂ through nitrogenase or [NiFe]-hydrogenase activities, represented by the following equations (Brentner et al., 2010; Carrieri et al., 2011):



Nitrogenases from N_2 -fixing cyanobacteria produce H_2 as a required byproduct. However, this process is very energy consuming, requiring a minimum of 4 ATP molecules to form each molecule of H_2 in the absence of N_2 gas. As a result, nitrogenase activity is preferred under light conditions in phototrophs that supply cells with enough ATP. However, this introduces inhibition of nitrogenase which is oxygen-sensitive in most cases (Bothe et al., 2010). In filamentous heterocystous cyanobacteria, such as *Anabaena*, this problem is reduced by the lack of photosynthetic machinery in their nitrogenase-bearing heterocyst cells. In most nonheterocystous cyanobacteria that fix N_2 gas, nitrogenase activity occurs at night, when intracellular O_2 is respired to create an anaerobic environment for nitrogenase. Yet, there are exceptions in nonheterocystous *Gleothoece* and *Cyanothece* species that exhibit nitrogenase activity under aerobic conditions by unknown mechanisms. Several nitrogenase-bearing cyanobacterial strains have been employed to produce photo- H_2 in the presence or absence of O_2 (Dutta et al., 2005). Anaerobic conditions for some of the strains under light was achieved by sulfur deprivation which impairs Photosystem II activity, or by purging with argon gas to continuously flush O_2 out of the system. The highest reported photo- H_2 evolution rate is $530 \mu\text{mol mg}^{-1} \text{chl}a \text{ h}^{-1}$ by a mutant strain of heterocystous *Nostoc* PCC 7120 that lacks functional uptake hydrogenase (Nyberg et al., 2015). The highest reported photo- H_2

evolution rate by nonheterocystous nitrogenase-bearing cyanobacteria is $373 \mu\text{mol mg}^{-1} \text{chla h}^{-1}$ by *Cyanothece* sp. ATCC 51142 under an argon atmosphere that is in the absence of N_2 and O_2 (Bandyopadhyay et al., 2010). This study also demonstrated the superior O_2 tolerance of the nitrogenase carried by this strain, whose aerobic Photo- H_2 rate is $> 150 \mu\text{mol mg}^{-1} \text{chla h}^{-1}$ (or $2.34 \mu\text{mol mg}^{-1} \text{DW h}^{-1}$).

Many cyanobacteria harbor a bidirectional [NiFe]-hydrogenase belonging to the pentameric Hox class, which catalyzes reversible hydrogen (H_2) production/uptake using NAD(P)H/NAD(P)^+ , while some strains use flavodoxin or ferredoxin as the electron carriers (Aubert-Jousset et al., 2011; Cournac et al., 2004; Carrieri et al., 2011; Ghirardi et al., 2007; Gutekunst et al., 2014). Although Hox hydrogenases in cyanobacteria are immediately inactivated by atmospheric levels of O_2 , the anaerobic reactivation process is fully reversible and can take only a few minutes to complete (Cournac et al., 2004). Moreover, a protein film electrochemistry (PFE) study of the Hox hydrogenase from the cyanobacterium *Synechocystis* 6803 indicated that this enzyme is more biased toward proton reduction, and is able to retain 25-50% activity under microaerobic conditions (1% O_2) (McIntosh et al., 2011). These two advantages make Hox hydrogenase a more suitable starting point than FeFe-hydrogenase for commercial applications. Dark fermentative hydrogen production rates of different cyanobacteria have been reviewed by Taikhao et al. (2015) and Carrieri et al. (2011). The two highest Hox-driven dark fermentative H_2 evolution rates reported so far are $0.094 \mu\text{mol mg}^{-1} \text{DW h}^{-1}$ ($13.8 \mu\text{mol mg}^{-1} \text{chla h}^{-1}$) in *Aphanothece halophytica* (Taikhao et al., 2015), and $0.074 \mu\text{mol mg}^{-1} \text{DW h}^{-1}$ (or $4.5 \mu\text{mol mg}^{-1} \text{chla h}^{-1}$) in *Arthrospira maxima* (Ananyev et al., 2012). Nonetheless, the highest transient initial fermentative hydrogen evolution rate is reported

to be $44.2 \mu\text{mol mg}^{-1} \text{chl}a \text{ h}^{-1}$ in the cyanobacterium *Lyngbya aestuarii* BL J (Kothari et al., 2014). Strategies to increase Hox-driven dark fermentative H_2 productions is further discussed in the “*Dark Autofermentative H_2 production*” section (Section 3). In addition, the introduction of a high turnover rate *Clostridium acetobutylicum* [FeFe]-hydrogenase into a cyanobacterium has also been shown to further increase the H_2 evolution rate by 500-fold for *Synechococcus elongates* sp. 7942, but only in the presence of light and a PSII inhibitor to avoid O_2 evolution (Ducat et al., 2011). The H_2 production rate was $2.8 \mu\text{mol mg}^{-1} \text{chl}a \text{ h}^{-1}$ and lasted for 96 h.

2. Photoautotrophic growth of cyanobacteria

A scheme of cyanobacterial primary energy conversion and CO₂ fixation is shown in Figure 1-1. Light-driven linear electron flow (LEF) in cyanobacteria occurs through two photosystems that are functionally analogous to those in plants. Each oxygen molecule formed by LEF (via Photosystem II-cytb₆f-PSIFerredoxin-FNR) results in the equivalent of 12 protons being pumped across the thylakoid membrane. Upon the formation of one oxygen molecule, 4 electrons are transferred through the entire LEF to FNR and reduce 2 NADP⁺ to NADPH. If 4.67H⁺/ATP are used for ATP synthesis (Vollmar, et al., 2009), LEF will hypothetically produce a fixed ratio of ATP/NADPH of ~1.3. However, this ATP/NADPH ratio is not sufficient to fully support cellular activity during photosynthesis, such as nitrogen assimilation and protein and lipid biosynthesis. In C₃ plants, the combined energy requirements for CO₂ fixation under photorespiring conditions and nitrate assimilation to glutamate are ~1.43 ATP/NADPH, which leads to a deficit of ~0.13 ATP molecules per NADPH molecule (Kramer et al., 2004). Marine cyanobacteria strains, such as *Synechococcus* 7002, have many other ATP-requiring cellular activities compared to C₃ plants, such as salt pumping (Elanskaya et al., 2002) and osmolyte synthesis (Guerra et al., 2013a). Therefore, LEF alone is not sufficient to provide the energy needed by marine or halophilic cyanobacteria. Cyclic electron flow (CEF) provides ion gradients and ATP production mechanisms for cells in addition to LEF. In CEF, electrons can be forced back to the plastoquinone (PQ) pool from various electron carriers, including ferredoxin, NADPH and NADH, through specific PQ oxidoreductases for each of these cofactors (Vermaas, 2001). There are three types of CEF pathways found in cyanobacteria: 1) type 1 NADPH dehydrogenase (NDH-1)

complex; 2) Fd-PQ oxidoreductase (FQR); and 3) type 2 NDH (NDH-2) (Kramer & Evans, 2011; Howitt et al., 1999; Ooyabu, et al., 2008). NDH-1 is suggested to pump protons across the thylakoid membrane during NADPH oxidation. Upon oxidation of each NADPH, 2 protons are directly pumped by NDH-1 and 2 protons are removed from cytoplasmic side by quinone per electron transferred. FQR is suggested to facilitate electron exchange between Fd and PQ, and removes 2 protons from cytoplasmic side by quinone per pair of Fd_{rd} oxidized. In addition to these two pathways, cyanobacteria possess a NDH-2 which oxidizes NADH and NADPH without pumping protons across the thylakoid membrane.

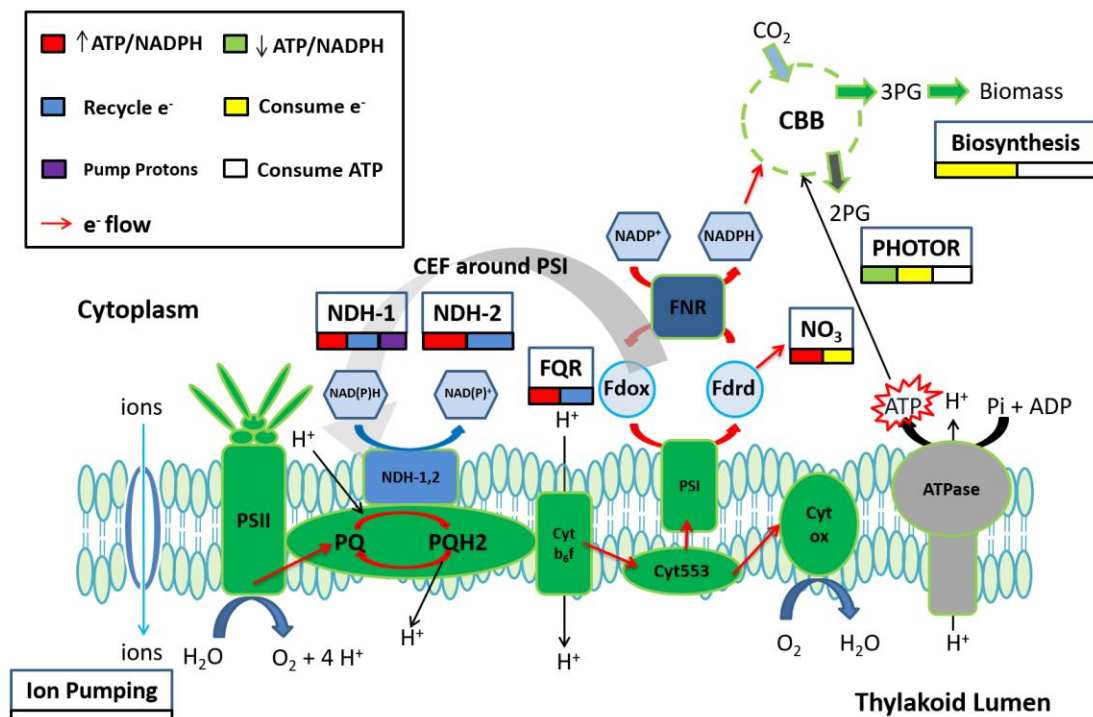


Figure 1-1 Scheme of photosynthesis in a model cyanobacterium *Synechococcus* 7002. Energetic outcomes of different reactions involved in photosynthesis were labeled in colored bar(s) underneath the reaction names. PQ: Plastoquinone; Cyt ox: Cytochrome Oxidase c; ATPase: ATP synthase; Fd_{ox} (or Fd_{rd}): oxidized (or reduced) ferredoxin; NDH-1: type 1 NADPH dehydrogenase; NDH-2: type 1 NAD(P)H dehydrogenase; FQR: ferredoxin:plastoquinone oxidoreductase; FNR: ferredoxin:NADP⁺ oxidoreductase; NO₃: nitrate reduction; PHOTOR: photorespiration; CBB: Calvin-Benson-Basham cycle.

Once ATP and NADPH are produced from photosynthetic electron transport activity, they can be used to fix CO₂, maintain other biosynthesis reactions and cellular homeostasis, get dissipated through photorespiration, or spontaneously revert back to ADP and NADP⁺, respectively (Figure 1-1). CO₂ molecules are assimilated into the system primarily through the Calvin-Benson-Basham cycle (CBB), which uses 2 NADPH and 3 ATP molecules to fix each CO₂ molecule into 3-phosphoglycerate (3PG). Alternatively, phosphoenol pyruvate carboxylase (*PPC*), which incorporates one CO₂ molecule by converting one phosphoenol pyruvate (PEP) molecule into one oxaloacetate (OXA) molecule has been reported to be active in cyanobacterial species during photosynthesis (Shylajanaciyar et al., 2015; Young et al., 2011; Jia et al., 2014). The major function of *PPC* in cyanobacteria is suggested to be replenishing carbon intermediates in the TCA cycle that are consumed in biosynthesis reactions (Shylajanaciyar et al., 2015). *PPC* activity is reported to be ~10% of the RuBisCO activity during the photosynthesis of *Synechocystis* 6803 (Young et al., 2011). *PPC* activity is also quantified in *Synechococcus* 7002 in this thesis (Chapter 4), and the *PPC* reaction rate is found to be substantially higher, ~70% of the RuBisCO activity during photosynthesis. In another study, overexpression of *PPC* in *Anabaena* sp. PCC 7120 was reported to increase the net photosynthetic efficiency of the mutant by 23% (Jia et al., 2014). After being synthesized, 3PG is then directed to three major terminal carbon sinks: protein, carbohydrates and lipids. Precursors of these terminal carbon sinks are synthesized in the pentose phosphate pathway (PP), the glycolysis/gluconeogenesis pathway and the tricarboxylic acid pathway (TCA). Lipid content is generally low in cyanobacteria, with few exceptions (Quintana et al., 2011). Protein is the major terminal

carbon sink during photoautotrophic growth, while environmental stresses (nutrient deprivation, high salinity, light exposure, etc.) can stimulate the redirection of the carbon flux into storage carbohydrates with compromised cell growth (Hays & Ducats, 2015; Carrieri et al., 2010; Konopka & Schnur, 1980). The tradeoff between synthesis of storage carbon products and growth can be controlled by thermodynamic requirements. Biosynthesis of the three major biomass components (carbohydrates, lipids, protein) costs both ATP and reductant equivalents yet at different quantities. Such energetic requirements were calculated in Subramanian et al. (2013) and Raven (1982), and are summarized in Table 1-1.

Biomass Component	ATP requirement (per C)	NADPH requirement (per C)
Carbohydrates	4.2	2
Lipids (TAG)	5.84	2.84
Protein	4.98	2.77

Table 1-1 Energetic requirements for the synthesis of carbohydrates, lipids and protein in algae summarized from Subramanian et al. (2013) and Raven (1982).

In addition to the thermodynamic requirements, there are other kinetic factors that can affect the choice and rate of carbon product formation: photon energy utilization efficiency, kinetic rate constants of electron transfer reactions, availability of substrate metabolites, metabolic compartmentalization, feedback control, respiration rates, and cell division (Cardol et al., 2011; Radakovits et al., 2010). Therefore, understanding how metabolism works in a cyanobacterium at a system level is complicated but essential to know to determine the maximum theoretical yields of carbon products and biomass (Woolston et al., 2013).

Measurements of the rate of consumption of initial substrates (e.g. glucose, CO₂, etc.) and yields of terminal products cannot provide information on the instantaneous fluxes of the intermediate reactions, which is required to systematically understand cyanobacterial cellular metabolism. Herein we use two powerful approaches to obtain fluxomic information: 1) the modeling approach called flux balance analysis (FBA) (Steuer et al., 2012) and, 2) the experimental approach called metabolic flux analysis (MFA) (Adebisi et al., 2015).

FBA is a mathematical constraint-based method that simulates cellular metabolism under different growth conditions in genome-scale metabolic reconstructions. FBA can rapidly (within several seconds) predict outcomes of the metabolic network as a single complete entity, with the tradeoff of lacking detailed metabolic kinetic constraints, such as enzymatic regulations and metabolic pool sizes. One major application of FBA is predicting fluxomic outcomes of genetic and environmental perturbations, which potentially speeds up our experimental progress to understand whole cell metabolism and to optimize the production of desired metabolites. FBA has been extensively used to

study metabolism of several cyanobacteria at different growth modes (photoautotrophic, photo-mixotrophic, heterotrophic, fermentative) (Shastri & Morgan, 2005; Nogales et al., 2012; Knoop et al., 2010; Hamilton & Reed, 2012). Recently, the predictive power of FBA has been further expanded to simulate the kinetic diurnal growth of cyanobacteria (Knoop et al., 2013; Knies et al., 2015; Rügen et al., 2015). Additionally, FBA is used to help determine genetic modification targets that optimize production of metabolites of interest from cyanobacterial cell factories (Fu, 2009; Vu et al., 2013; Anfelt et al., 2015; Knoop Steuer, 2015). Nonetheless, the major drawback of FBA, lack of enzymatic regulation and pool size information as input constraint, sometimes leads to fluxomic predictions that are biologically unacceptable (Steuer et al., 2012). The experiment-based MFA approach quantifies the steady state carbon fluxes at the whole cell level, which illustrates a traffic diagram of *in vivo* activity of metabolic enzymes, and therefore can overcome the mentioned shortcomings of FBA approach. MFA uses ^{13}C labeling patterns generated from organisms fed with ^{13}C -labeled substrates, metabolite pool sizes and excretion rates, nutrients uptake rates, cellular growth rates, and cellular biomass compositions as constraint input (Adebiyi et al., 2015). Applications of MFA include 1) to identify major intracellular pathways and branch points in the metabolic network, 2) to understand flux control at metabolic branch points, 3) to calculate rates of unmeasurable pathways, 4) to identify kinetic bottlenecks and 5) modification targets for redirecting flux to desirable products (Woolston et al., 2013; Vallino & Stephanopoulos, 1994; Antoniewicz et al., 2007). In cyanobacteria, MFA has been applied to study heterotrophic, photoheterotrophic, and photomixotrophic metabolism, which uncovered valuable fluxomic information of the OPP pathway, the malic enzyme pathway, and the TCA

cycle during these various growth conditions (Yang et al., 2002; You et al., 2014; Nakajima et al., 2014; Feng et al., 2010; Alagesan et al., 2013). Interestingly, MFA has only been applied in one cyanobacterial photoautotrophic growth study of *Synechocystis* 6803 (Young et al., 2011), although photoautotrophic growth is one major phase to produce desired metabolites.

In this thesis, the whole cell carbon fluxomic information of a model cyanobacterium *Synechococcus* 7002 during photosynthesis under different light and nitrogen conditions are obtained through both FBA and MFA approaches in Chapter 2 and 4, with some FBA predicted pathways being further experimentally validated in Chapter 3.

3. Dark autofermentative H₂ production

Under dark anaerobic conditions, cyanobacteria can catabolize their own carbohydrate storage (glycogen) synthesized during photosynthesis to produce ATP and keep cells alive (Stal & Moezelaar, 1997). This process is called autofermentation. During autofermentation, glycogen is oxidized through the EMP (glycolysis) and OPP pathways, and reduces NAD(P)⁺ molecules with different stoichiometries (2 and 7, respectively, see Figure 1-2). These reductant equivalents are consumed through the excretion of fermentative products, including lactate, alanine, succinate, alcohol, formate, H₂ gas and others (Carrieri et al., 2011; Stal & Moezelaar, 1997). When nitrate is in the growth media, reductant equivalents are largely consumed to produce nitrite and ammonia, catalyzed by nitrate reductase and nitrite reductase respectively (McNeely et al., 2014). Increasing the production of Hox-driven autofermentative H₂ production can be achieved by three major strategies: 1) increasing the total reductant equivalent pool size, 2) increasing the fraction of reductant equivalent directed to H₂ production, and 3) increasing Hox Hydrogenase concentrations and/or activities.

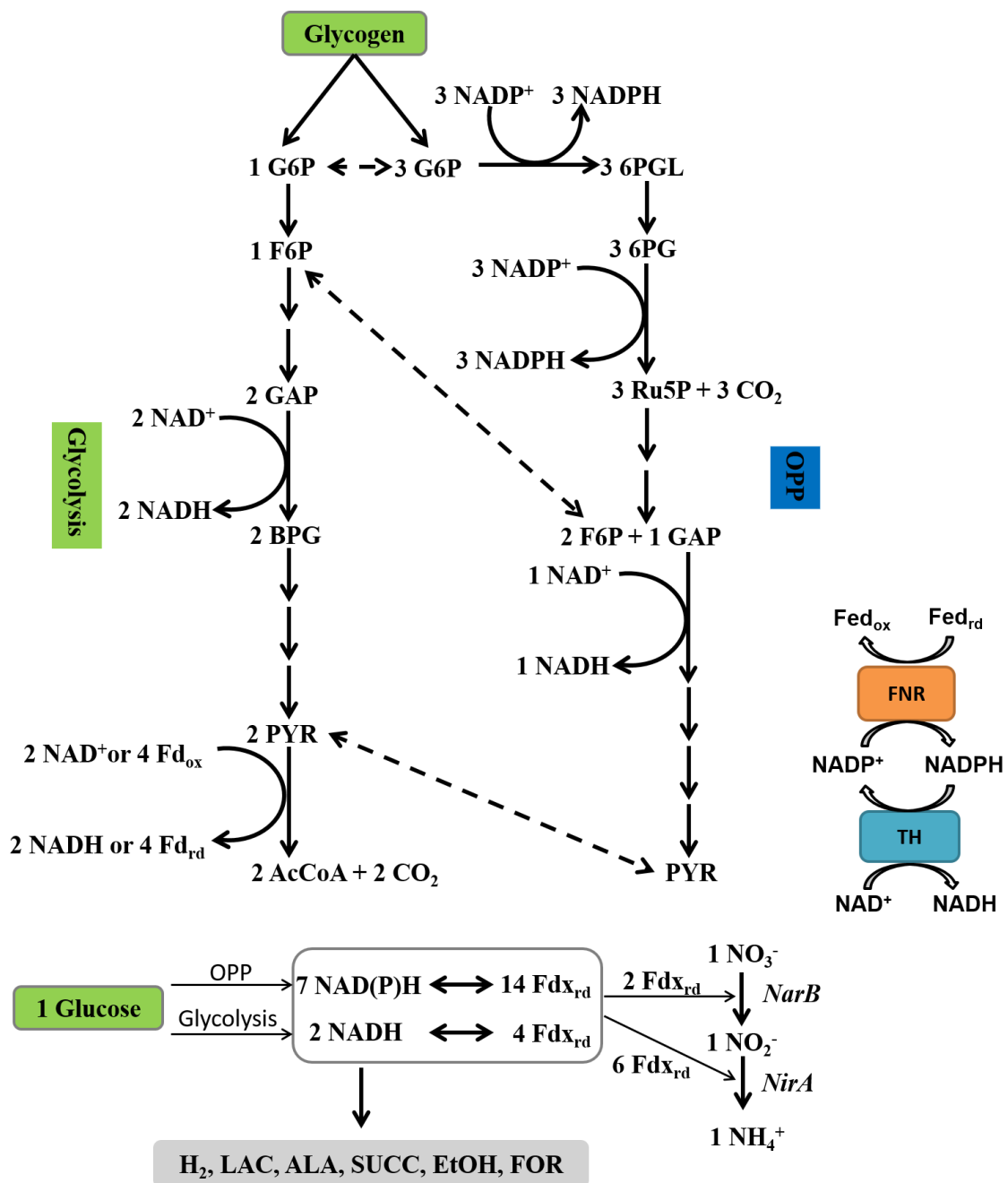


Figure 1-2 Autofermentative metabolism of cyanobacteria under dark anaerobic conditions. Glycogen is catabolized through the glycolysis pathway and the OPP pathway, which will generate different numbers of reductant equivalent. Electrons can be passed from reduced ferredoxin (Fed_{rd}) to NAD(P)⁺ through ferredoxin-NADP⁺ reductase (FNR)

and transhydrogenase (TH) activities. Reductant equivalent can be consumed to produce fermentative products including H₂, lactate (LAC), alanine (ALA), succinate (SUCC), ethanol (EtOH) and formate (FOR), or to reduce nitrate (NO₃⁻) to nitrite (NO₂⁻) or ammonia (NH₄⁺).

3.1) Increasing total reductant equivalent pool size

Both physiological stresses and genetic modifications can improve autofermentative H₂ production by increasing the total pool size of reductant equivalent. Firstly, increased glycogen content can significantly increase reductant availability through a faster catabolism of glycogen during autofermentation, and sometimes increase autofermentative hydrogen evolution rates by folds in cyanobacteria (Antal & Lindblad, 2005; Carrieri et al., 2010; Troshina et al., 2002; Taikhao et al., 2013). Strategies to increase glycogen contents have been described in section “*Cyanobacteria for biofuel*” (Section 1). Genetic modification of bottleneck enzymes in the glycogen catabolism pathway is another strategy to increase the intracellular reductant equivalent pool. Over-expression of the NAD⁺-dependent glyceraldehyde-3-phosphate dehydrogenase (GAPDH-1) in *Synechococcus* 7002 elevated the autofermentative glycogen catabolic rate by 58% in the mutant, which resulted in an increase in the NADH pool size, the NADPH pool size and H₂ yields by 4.0-fold, 2.9-fold and 3.0-fold, respectively (Kumaraswamy et al., 2013). Interestingly, while the knockout mutant of GAPDH-1 maintained a similar glycogen catabolic rate compared to WT, the mutant forced more glycogen to be catabolized through the OPP pathway. Consequently, the reductant equivalent pool size and the H₂ yield during autofermentation of the knockout mutant increased by 5.7-fold and 2.3-fold, respectively.

3.2) Increasing the fraction of reductant equivalents directed to H₂ production

Knocking out reductant competing pathways by genetic modifications is a common strategy to improve autofermentative H₂ production in cyanobacteria. Knockout

mutants of enzymes catalyzing the production of other fermentative metabolites can significantly increase the autofermentative H₂ yield by folds (McNeely et al., 2010; Krishnan et al., 2015). In the case of the D-lactate dehydrogenase knockout of *Synechococcus* 7002, H₂ yield was increased by 5-fold of the mutant. Alternatively, increasing H₂ yield can be achieved by a “milking” strategy that continuously removes H₂ by an electrochemical cell, which in one case resulted in an 11-fold increment (Ananyev et al., 2012). Removing nitrate from fermentative media has been a common strategy to increase fermentative H₂ productions, and inhibition or elimination of the nitrate reduction pathway through either molybdate substitution by tungstate or genetic modifications significantly increases H₂ production rates (Gutthann et al., 2007; Baebrasert et al., 2011). When both nitrate reductase and nitrite reductase were knocked out in *Synechocystis* 6803, the double mutant produced H₂ at a rate 140-fold faster than WT in the presence of nitrate (Baebrasert et al., 2011). In Chapter 5 of the thesis, a nitrate reductase knockout mutant of *Synechococcus* 7002 that eliminates reductant consumption by nitrate reduction is described to illustrate how to redirect reductant equivalents to increase autofermentative H₂ yield.

3.3) Increasing Hox Hydrogenase concentrations and/or activities

Increasing the concentration of matured Hox hydrogenase could potentially elevate H₂ productivities. Simultaneous overexpression of the endogenous proteins HoxEFUYH and maturation enzymes HypABCDEF in *Synechocystis* 6803 increased H₂ productivity by 3-fold without supplementing Ni²⁺ in the growth media. Supplementation of Ni²⁺ to the overexpression mutant further increased H₂ productivity by 14-fold (Ortega-Ramos et al., 2014). Supplementation of Ni²⁺ or Fe³⁺ was well known to increase

Hox hydrogenase activity in cyanobacteria (Taikhao et al., 2013). In addition, nitrogen deprivation during the photosynthetic growth phase can also enhance hydrogenase activity (Troshina et al., 2002). Nitrogen-deprived incubation leads to a ~4-fold increment of *in vitro* hydrogenase activity in the cyanobacterium *Gloeocapsa alpicola*.

4. Scope of the thesis

The scope of this thesis is two-fold (see Figure 1-3): Chapter 2, 3 and 4 focus on understanding fluxes from primary carbon and energy metabolism during the growth phase under light, so that we can answer the question, “How do cyanobacterial cells determine the production of different biomass components during photosynthesis?”. Predictions of carbon fluxes and utilized biochemical pathways described in Chapter 2 are experimentally validated in Chapter 3 and 4. Chapter 5 focuses on understanding the NAD(P)H flux during dark autofermentation. In Chapter 5, I present the results of an engineered cyanobacterial strain lacking nitrate reductase, which is capable of high autofermentative hydrogen yield in the presence of nitrate. The rationale of this mutant strain is based on our prior knowledge of cyanobacterial fermentation. As a result, the findings in Chapter 5 help answer the question, “How to optimize H₂ production during autofermentation?”. In summary, the overall goal of my research is generating quantitative predictions and interpretations of cyanobacterial metabolism for harnessing the potential of cyanobacteria as biofuel production platforms.

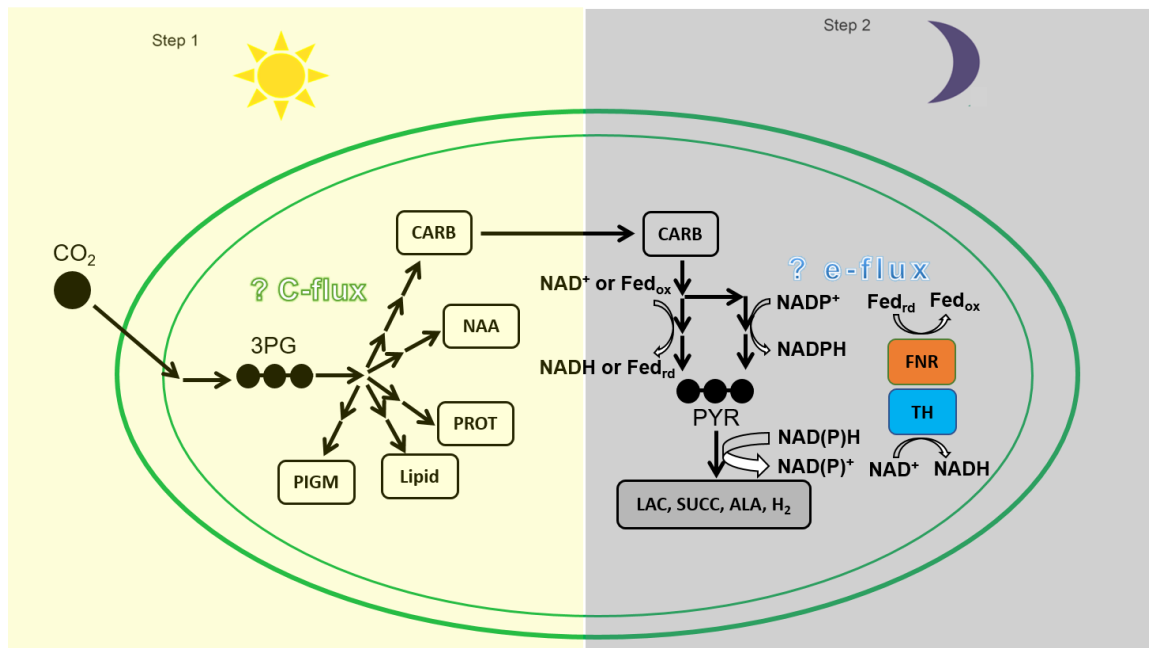


Figure 1-3 Overall scheme of subjects studied in the thesis. In the model cyanobacterium *Synechococcus* 7002, external CO₂ is assimilated during photosynthesis to produce biomass components including carbohydrates (CARB), nucleic acids (NAA), protein (PROT), lipids and pigments (PIGM) (left half). When cyanobacteria are transferred to dark anaerobic conditions, carbohydrates are catabolized to generate ATP and NAD(P)H reductant equivalent (right half). Reductant equivalents are consumed to produce fermentative products. The overall goal of the thesis is to understand carbon flux (C-flux) distributions under light, and understand reductant equivalent flux (e-flux) distributions under dark, which together will enhance our knowledge of using cyanobacteria for biofuel applications.

The following four manuscripts presented as four separate chapters in the dissertation are:

- 1) Xiao Qian, Min Kyung Kim, G. Kenchappa Kumaraswamy, Ananya Agarwal, Desmond S. Lun*, & G. Charles Dismukes*. Beyond conventional flux balance analysis of photoautotrophic metabolism: Light intensity dependent partitioning of carbon into different cellular products. Submitted to *The Plant Journal*.
- 2) Shuyi Zhang^a, Xiao Qian^a, Shannon Chang, G. Charles Dismukes, and Donald A. Bryant. Revisit the tricarboxylic acid cycle in cyanobacteria. *In prep*
- 3) Xiao Qian, Yuan Zhang, Desmond S. Lun, & G. Charles Dismukes. Quantitative fluxomics analysis of the carbon flux distributions under different nitrogen conditions in the cyanobacterium *Synechococcus* sp. PCC 7002. *In prep*
- 4) Xiao Qian, G. Kenchappa Kumaraswamy, Shuyi Zhang, Colin Gates, Gennady Ananyev, Donald A. Bryant & G. Charles Dismukes. (2015) In activation of nitrate reductase alters metabolic branching of carbohydrate fermentation in the cyanobacterium *Synechococcus* sp. Strain PCC 7002. *Biotechnology and Bioengineering*, epub DOI: 10.1002/bit.25862.

An overall summary in Chapter 6 highlights the main conclusions of the work.

Chapter 2: Beyond conventional flux balance analysis of
photoautotrophic metabolism: Light intensity dependent
partitioning of carbon into different cellular products

Coauthors: Min Kyung Kim, G. Kenchappa Kumaraswamy, Ananya Agarwal,

Desmond S. Lun and G. Charles Dismukes

Summary

Computational models of genome-scale metabolism predicted for cyanobacteria during steady-state photoautotrophic growth have been previously developed. However, these lack flexibility in accounting for light-dependent carbon partitioning among the major biomass components. We have constructed and experimentally tested a comprehensive genome-scale model of photoautotrophic growth, denoted *iSyp821*, for the cyanobacterium *Synechococcus* sp. PCC 7002. In contrast to previous genome-scale models, *iSyp821* incorporates a variable biomass objective function (ν BOF), in which stoichiometries of the major biomass components vary according to light intensity. ν BOF was constrained to fit the measured cellular carbohydrate/protein content under different light intensities. *iSyp821* provides rigorous agreement with experimentally measured cell growth rates and inorganic carbon uptake rates as a function of light intensity. In addition, *iSyp821* simulates two observed metabolic transitions that occur as light intensity increases: 1) from cyclic to linear electron flow through PSI, and 2) from active carbon allocation (growth) to carbon and energy storage mode. *iSyp821* predicts significant flux through a hybrid gluconeogenesis-pentose phosphate (PP) pathway that partitions fixed CO₂ intermediates into glycogen by an alternative pathway than conventional gluconeogenesis. Dominant flux through this pathway was verified experimentally by following the kinetics of formation of ¹³C metabolites from ¹³CO₂ fixation. *iSyp821* can also utilize experimentally measured transcriptomic data to estimate changes in concentrations of gene products (enzymes) under nutrient stress. We found that using this strategy, *iSyp821* correctly predicts the observed redistribution pattern of carbon products under nitrogen depletion, including decreased rates of CO₂ uptake, amino acid synthesis,

and increased rates of glycogen and lipid synthesis. Genetic engineering of photosynthetic organisms is typically phenomenological with many attempts failing and others producing unanticipated changes in metabolic functions, while advances in mathematical modeling of whole cell metabolism has emerged as a powerful diagnostic tool for prediction of the outcome of metabolic engineering. Herein, we demonstrate the application of an advanced modeling tool to a new discovery in cyanobacterial metabolism. We predict, and subsequently experimentally validate, flux through a previously disregarded metabolic pathway.

1. Introduction

Cyanobacteria and microalgae are examples of unicellular aquatic microbial oxygenic photoautotrophs (AMOPs), whose members include organisms that are recognized as the most efficient photosynthetic organisms at converting carbon dioxide, water and nutrients into complex molecules and biomass using solar energy (Quintana et al., 2011; Parmar et al., 2011). For this reason, they are being pursued as leading candidates for producing chemical and biofuel precursors. Key attributes of these organisms that are important for these applications include biomass composition (lipids, carbohydrates, pigments, and proteins), nutrient and solar input requirements for growth, tolerance to environmental stress, and ease of genetic transformation. As these attributes differ greatly among species, there is considerable interest in understanding species variations in metabolism and its regulation under environmental stimuli.

Genetic modification is a successful strategy for redirecting metabolic intermediates into biotechnological interesting chemicals. Removing competing pathways, overexpression of native pathways or addition of new pathways have each been applied to elevate the yield of desired biochemicals (Qian et al., 2015; Qi et al., 2013; Kumaraswamy et al., 2013; Varman et al., 2013; Radakovits et al., 2010). However, simple transgenic mutants often exhibit undesired attributes such as slower growth rate, susceptibility to environmental stresses or unanticipated products, because of modified regulation of metabolic pathways and misbalance of energy resources (Zhang & Bryant, 2011; Suzuki et al., 2010; McNeely et al., 2010). Researchers have explored more complex genetic changes involving replacement of whole metabolic pathways and transcriptional regulation of multiple gene targets (Wang et al., 2013; Liu et al., 2011).

These complex strategies are time consuming and costly, and are best implemented together with a computational model of metabolism capable of simulating genetic modifications.

So far, genome-scale models have been constructed for more than 100 organisms (Feist et al., 2009). Among these organisms, *Synechocystis* sp. PCC 6803, a fresh water strain, is the most well modeled and extensively studied cyanobacterium (Shastri & Morgan, 2005; Fu, 2009; Nogales et al., 2012; Knoop et al., 2013; Knoop et al., 2010). In addition, genome-scale models have also been constructed for a marine cyanobacterial strain, *Synechococcus* sp. PCC 7002 (Hamilton & Reed, 2012; Vu et al., 2013). This strain has a fast growth rate (0.20 h^{-1}), well studied genomic database and mature transformation protocol (Frigaard et al., 2004; Xu et al., 2011).

There are currently two published genome-scale models of *Synechococcus* 7002: *iSyp611* (Hamilton & Reed, 2012) and *iSyp708* (Vu et al., 2013). In *iSyp611*, the authors used fixed weight fractions of macromolecules measured from *Synechocystis* 6803 to formulate the biomass objective function (BOF). In a later version, *iSyp708*, the BOF was improved and all major biomass components in the BOF were experimentally measured (Vu et al., 2013). Moreover, the model was assigned with content of biomass components measured at three suboptimal growth conditions to account for the biomass composition at various growth conditions. This formulation however, is still not sufficiently flexible to capture changes in biomass composition with light intensity, which is a fundamental property of all photoautotrophically growing microorganisms (Cornet et al., 1998; Konopka & Schnur, 1980; Olguín et al., 2001).

In the present study we constructed a metabolic model, *iSyp821*, incorporating a variable biomass objective function (v BOF) to simulate this fundamental attribute of light intensity dependent biomass composition. This is represented as a transition between linear and cyclic electron flow through the two photosystems. This transition rebalances the yields of products of linear flux through the two photosystems (O_2 , NADPH and ΔpH) with those from cyclic flux around PSI only (ΔpH). This strategy is used by cells to adjust the amounts of NADPH to ATP available to match the different cellular processes such as CO_2 , and production of glycogen, amino acids and lipids. Experimentally, we identified unequal linear correlations (different slopes) between photosystem II (PSII) electron transfer rate (ETR) and the amount of the two major carbon products made: proteins and total carbohydrates (Figure 2B). These linear correlations were used as constraints for the v BOF computational model. v BOF allows flux through pathways that satisfy the final carbon product distribution under different light intensities. To achieve this agreement, the model predicted flux through an unconventional gluconeogenesis-pentose phosphate (PP) pathway that partitions fixed CO_2 intermediates into glycogen. Use of this novel hybrid pathway was experimentally validated by detection of ^{13}C -fluxes. Additionally, we used transcriptomic data as constraints to *iSyp821* to simulate the change of carbon flux distribution under nitrogen deprivation, a photoautotrophic growth condition important for biotechnological applications.

2. Experimental Procedures

2.1) Metabolic Network Reconstruction.

A web-based tool denoted Model SEED (available at <http://www.theseed.org/models/>) was used to input the map of metabolic reactions based on available curated genomic data. The model was constructed according to the step-wise guidance introduced by Henry et al. (Henry et al., 2010). In addition, the biocuration process of the model was further enhanced by following the most recently published genome-scale network reconstruction rules (Heavner & Price, 2015; Monk et al., 2014; Ravikrishnan & Raman, 2015). An xml format of the reconstruction iSyp821 with references of some biochemical reactions were deposited in RUCore. iSyp821 included all the reactions and genes in the two previously published *Synechococcus* 7002 models. A comprehensive literature review was carefully done to assign accurate confidence scores and proper references to all the reactions in the network. MOST (<http://most.ccib.rutgers.edu/>) (Kelly et al., 2015) was used to correct errors in the draft model, arriving at our final reaction network. Specific details of model construction, biocuration, and database usage are provided in Figure 2-1. A confidence interval of 1~4 was assigned to each reaction in the model to indicate whether the reaction 1) has no gene annotated but is required in the model to produce biomass; 2) gene annotated; 3) gene-protein association is verified in vivo; and 4) protein is characterized in vitro. Lists of new genes and reactions along with their descriptions and references were deposited in RUCore. Photosynthetic electron transfer chain was manually added into the metabolic network after the automated procedures were finished. Both linear electron transfer route and several alternative electron transfer routes were included. In total five alternative

electron pathways are included in *iSyp821*. They are: 1) the type-1 NADH dehydrogenase pathway (proton pumping, both NADH and NADPH are substrates); 2) the type-2 NADH dehydrogenase pathway (non-proton pumping, NADH is the only substrate); 3) the ferredoxin quinone reductase (FQR) pathway; 4) the Mehler reaction; and 5) the cytochrome-c oxidase (COX) pathway.

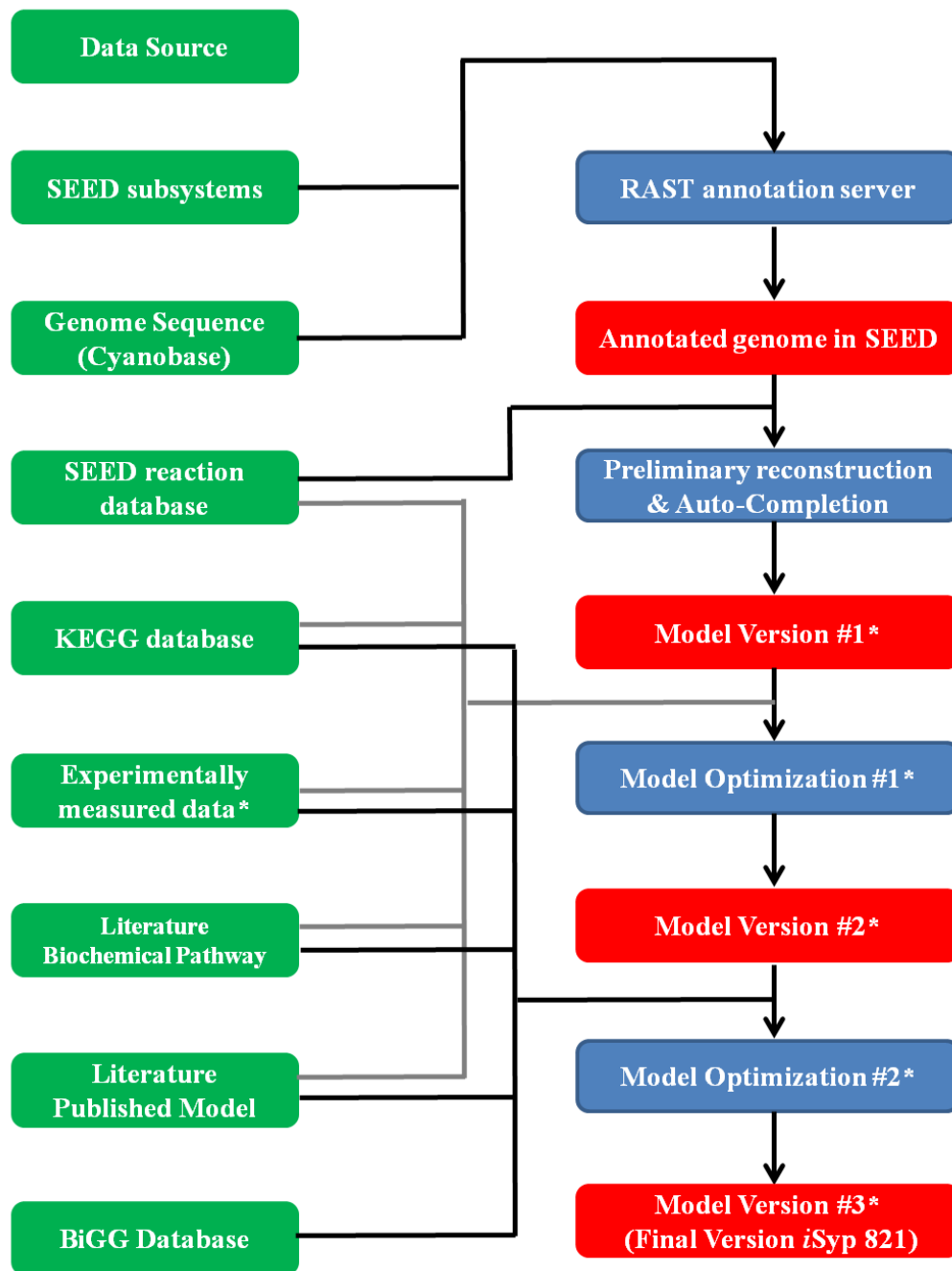


Figure 2-1 Pipelines to construct and optimize *iSyp821*. Database and experimental data are colored in green, major construction steps are colored in blue, and versions of model are colored in red.

- **Version #1*** draft contains 848 metabolic reactions, and a biomass objective function (BOF) from an *E. coli* model. All metabolic reactions are bidirectional. Reaction, metabolite and gene were in SEED-style nomenclature. No Reaction Confidence Level. There were 2 Compartments: cytoplasm and extracellular. No photosynthetic system;
- **Model Optimization #1*** includes: 1) Biolog consistency analysis to find out missing/redundant reactions; 2) Gene essentiality consistency analysis to add or correct GPRs; 3) GapFill & GapGen to correct reversibility constraints of biochemical reactions, add missing metabolic reactions and remove redundant metabolic reactions; 4) Determination of species-specific BOF;
- **Experimental measured data*** includes cell dry weight, CO₂ uptake rates, O₂ evolution rates, growth rates, and protein/sugar/chlorophyll-a/DNA/RNA/Lipid contents under different light intensities;
- **Version #2*** draft contains 724 metabolic reactions, a *Synechococcus* 7002 specific biomass objective function (BOF), a completed photosynthetic system including both LEF and AEFs, GPR, Confidence level of reactions, literature references supporting metabolic reactions, and one additional cellular compartment: periplasm;
- **Model Optimization #2*** includes: 1) Manually conversion of KEGG nomenclature to BiGG nomenclature for reaction names, metabolite names and gene names; 2) Consolidation: aimed to including all the reactions and genes missed in our model draft but covered in the two published metabolic models: *iSyp611* and *iSyp708*; 3) inclusion of a light-dependent variable biomass

objective function (vBOF);

- **Version #3*** (Final Version) *iSyp821* contains 794 metabolic reactions and a vBOF.

2.2) Biomass composition and ν BOF.

Biomass components (carbohydrates, proteins, nucleic acids, lipids, pigments) were experimentally measured as described in Guerra et al. (2013a and 2013b) using at least 3 biological replicates. Dry weights at different optical densities under different light conditions were estimated based on a standard curve (Figure S2-1) measured under the reported optimal growth condition (Zhang & Bryant, 2011) of *Synechococcus* 7002. Mass densities at different light conditions (Figure S2-2) were measured and compared to validate the usage of this standard curve. The intracellular concentrations of inorganic ions in the objective function were taken from a *Synechocystis* sp. PCC 6803 model (Nogales et al., 2012). The ATP requirement for basic cellular maintenance (2.3 mmol/gDW/h) was calculated based on the experimentally measured dark respiration rate (0.35 mmol O₂ /gDW/h) of wild type *Synechococcus* 7002 assuming that all ATP produced during dark respiration was used to keep cells alive and not for cell division. Measurements of protein and carbohydrate contents under different light conditions (Figure 2-2 B) were used to construct the ν BOF. Protein and carbohydrate contents both have good linear correlations against PSII electron transfer rates calculated based on total O₂ evolution rate (Figure 2-2 A). We did not consider any circadian effects on biomass component changes, since our experiments were conducted under 24-h continuous light. The content of lipids, nucleic acids and pigments at each light intensity were assumed to be proportional to the protein content, as these three biomass components together accounted for less than 10% of our measured dry weight. Thus, we only measured the content of lipids, nucleic acids and pigments under optimal growth conditions in the bioreactor (400 μ E/m²/s, red light, 25 mM bicarbonate, 38 °C), and calculated the content

under other light intensities based on the change of protein content. In the ν BOF, the stoichiometries of the biomass components were as follows:

$$(0.0484 * V_{O_2} + 1.155) \text{ Carbohydrate} + (-10^{-5} * V_{O_2} + 0.0007) \text{ Protein} + (-10^{-5} * V_{O_2} + 0.0006) \text{ Lipid} + (-2 * 10^{-5} * V_{O_2} + 0.0009) \text{ DNA} + (-2 * 10^{-6} * V_{O_2} + 0.0001) \text{ RNA} + (-0.0004 * V_{O_2} + 0.0199) \text{ chlorophyll-a} + (-0.0002 * V_{O_2} + 0.0097) \beta\text{-carotene} + \alpha \text{ intracellular cofactors} + \beta \text{ inorganic ions} \rightarrow 1 \text{ Biomass}$$

V_{O_2} is the total oxygen evolution rate of cells under a given light intensity, and α and β are fixed coefficients. BOFs yielded from this ν BOF stoichiometries calculation rule and used for different FBA simulations described in this manuscript were deposited in RUCore.

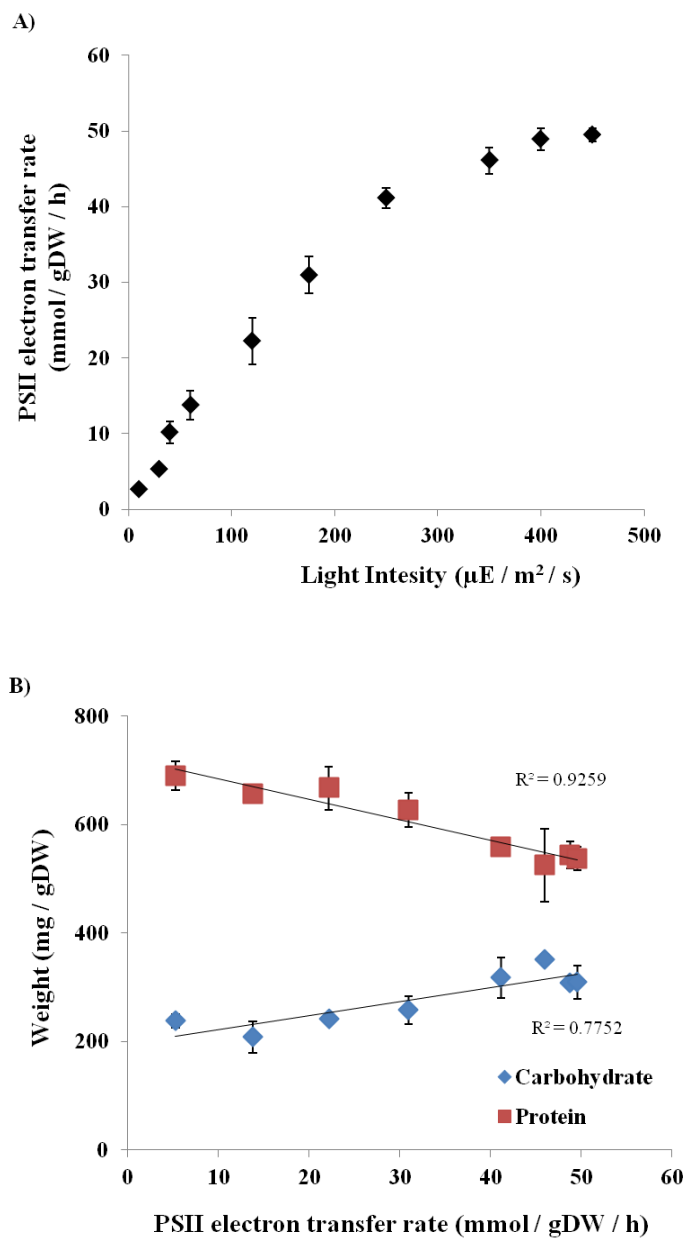


Figure 2-2 A) PSII electron transfer rate (estimated based on the total O_2 evolution rate) measured at different light intensities; B) Experimentally measured weight fraction of two major biomass components in *Synechococcus* 7002, proteins and carbohydrates, as a function of the PSII ETR (light intensity dependent). R^2 values are 0.9259 and 0.7752 for protein and carbohydrate, respectively. The error bars represent standard errors from 3 biological replicates.

2.3) Linear programming problem formulation.

Flux-balance analysis (FBA) was performed as previously described (Lun et al., 2009). Briefly, from the metabolic reconstruction, we obtain a stoichiometric matrix S , a reaction flux vector v with lower bound a , and upper bound b , and an objective vector f . For FBA (Orth et al., 2010; Raman & Chandra, 2009), a biologically optimal flux distribution is obtained by solving

$$\begin{aligned} & \max && f v \\ \text{subject to} && S v = 0, && (1) \\ && a \leq v \leq b, \end{aligned}$$

where v contains flux predictions for all reactions in the model, and \leq indicates component-wise inequality.

In our simulations, we used a second objective vector g to further constrain the space of solutions for v . Let z be the optimal value of equation (1). We implement the second objective vector by calculating

$$\begin{aligned} & \max && g v \\ \text{subject to} && S v = 0, && (2) \\ && a \leq v \leq b, \\ && f v = z. \end{aligned}$$

Solutions to optimization problems (1) and (2) were calculated using Gurobi Optimizer (Gurobi Optimization, Inc., Houston, Texas) and Matlab (The Mathworks, Inc., Natick, Mass.). We used flux variability analysis (FVA) (Mahadevan & Schilling, 2003) to find the range possible for each individual reaction flux in the optimal space defined by equation (2).

2.4) Optimization strategy.

We used a dual-optimization strategy to perform simulations of photoautotrophic growth. We set our first objective to maximize the biomass production rate with a net CO₂ input of 8.37 mmol/gDW/h (experimentally measured in our lab). Then we set our second objective to minimize the total photon utilization.

2.5) Flux boundaries.

It is necessary to put constraints on several reactions to perform accurate simulations of photoautotrophic growth. The maximum net CO₂ consumption rate was set to be 8.37 mmol/gDW/h, which was observed at the maximum photoautotrophic growth rate (Figure 3). There was initially no constraint on total photon input rate (or photosystem I (PSI) or PSII electron transfer rate). Our simulations of growth under photoautotrophic conditions determined that the total photon input rate required to reach maximum growth in the *Synechococcus* 7002 wild type strain was 99.6 mmol/gDW/h. Thus, 99.6 mmol/gDW/h was set as the maximum photon input rate for all photoautotrophic growth simulations described in this paper.

2.6) Bacterial cultivation and model validation.

Wild type *Synechococcus* 7002 culture was grown in a photobioreactor (Photon System Instruments, Model FMT 150/400). There were no additional barriers other than a glass vessel wall between the light source and the cells. A⁺ medium (Stevens & Porter, 1980) supplemented with 1 mg/mL NaNO₃ and 25mM of NaHCO₃ (saturating bicarbonate concentration, see Figure S2-3) was used as the cultivation medium. The pH was controlled at 8.0 ± 0.1 and temperature at 38°C. Growth was monitored

spectrophotometrically by measuring the optical transmission of cultures at 730 nm. Red LED lights (wavelength = 680 nm) were used as the sole light source for growth and for oxygen evolution measurements. Depending on the requirement for each experiment, the light intensity varied. Growth rate was determined by the flow rate, according to the following equation:

$$\text{Growth Rate (h}^{-1}\text{)} = \text{flow rate (mL/h)} / \text{total bioreactor volume (mL)}$$

The bioreactor volume was 410 mL. PSII electron transport rate (ETR) was determined electrochemically by measuring oxygen evolution rates using both oxygen rate and concentration type electrodes. The O₂ evolution rate transferred through PSII was converted to electrons by multiplication by 4. Net carbon consumption rates (photosynthesis minus respiration) were determined by gas chromatography. The goodness of fit of was calculated using the chi-squared test. The reduced chi-squared was achieved by the following equation:

$$\chi_{\text{red}}^2 = \frac{\chi^2}{\nu} = \frac{1}{\nu} \sum \frac{(O - E)^2}{\sigma^2}$$

where σ^2 is the known variance of the observation, O is the observed data, and E is the theoretical data, ν is the number of degrees of freedom, given by $N - n - 1$, where N is the number of observations, and n is the number of fitted parameters.

2.7) Transcriptomic data constrained carbon metabolic fluxes under nitrogen deprivation.

Two growth conditions were used with this method: nitrate-replete and nitrate-starved. Nitrate was the sole external nitrogen source in all experiments. The nitrate-

starved culture was incubated in nitrate-free media for hours allowing at least one doubling to occur, and therefore we can assume the culture is under the metabolic steady-state. The mathematical constraints and strategy for integration of transcriptomic data in genome-scale metabolic model were carried out as described by Kim et al. (*submitted*). Experimentally measured transcriptomic data from *Synechococcus* 7002 under the conditions of interest (Ludwig & Bryant, 2012) were integrated into the genome-scale metabolic model using the gene-protein-reaction (GPR) association relationships. Briefly, we modified the standard FBA problem (1) by setting the objective function to maximize correlation between the flux vector and the gene expression data. To calculate the correlation, we used the uncentered Pearson product-moment correlation, which is a popular measure of the linear correlation between two variables:

$$\max \frac{v_{\text{irr}} \cdot g_{\text{irr}}}{\|v_{\text{irr}}\| \|g_{\text{irr}}\|}$$

$$\text{subject to } \begin{cases} Sv = 0 \\ a_j \leq v_j \leq b_j \end{cases}$$

where v_{irr} is a flux vector representing the reaction rates of the irreversible reactions in the network, and g_{irr} is a vector indicating corresponding gene expression data. We used the set of irreversible reactions when maximizing the correlation, since the directions of reversible reactions are unknown a priori, whereas gene expression data values are always positive. The predicted flux was normalized by growth rates experimentally measured under different nitrogen conditions (0.19 h⁻¹ with nitrate, 0.08 h⁻¹ without nitrate). The rationale behind this method is that, given a limited translational efficiency and a limited accumulation of enzyme over the time, the level of mRNA can be related to

metabolic reaction rates. We have observed good correlations with this method for ^{13}C -determined *in vitro* fluxes for both *Escherichia coli* and *Saccharomyces cerevisiae* (Kim et al., *submitted*).

2.8) ^{13}C isotope kinetics measurements under photoautotrophic condition.

Synechococcus 7002 cultures were grown under constant light ($250 \mu\text{E}/\text{m}^2/\text{s}$ and $30 \mu\text{E}/\text{m}^2/\text{s}$ for high light and low light, respectively) and CO_2 level (2% v/v with air) to reach exponential phase ($\text{OD}_{730\text{nm}}$ at ~ 0.5). Then, a $\text{NaH}^{13}\text{CO}_3$ stock solution was injected into the culture with rapid mixing to a final concentration of 25 mM. Extraction followed a method modified from Bennette et al. (Bennette et al., 2011). Subsequently, 2 mL samples were withdrawn and rapidly quenched by mixing with 4 mL of quenching solution (60% methanol in water, $-20 \text{ }^\circ\text{C}$) at time points of 0, 10, 30, 60, 120, 240, 480 and 720 seconds. Quenched samples were then centrifuged for 15 min at 6000g and $-20 \text{ }^\circ\text{C}$. The supernatant was discarded and the cell pellet was then extracted with 300 μL 80:20 methanol-water solution at $-20 \text{ }^\circ\text{C}$. Extracts were then analyzed by the LC-MS/MS method described in Bennette et al. (Bennette et al., 2011) to measure the total enrichment of ^{13}C in the three target metabolites, FBP, F6P and S7P. After $^{13}\text{CO}_2$ is fixed by Rubisco to make 3PG, 3PG is used to synthesize either GAP/DHAP or PEP. Therefore, GAP/DHAP is the only ^{13}C -labeled precursor to synthesize ^{13}C -labeled FBP and S7P, which are located at two different downstream pathways. Thus, under the assumed steady state conditions, the ^{13}C enrichment kinetics and pool sizes of FBP and S7P can be used to quantitatively compare the fluxes of the two metabolites. If the pool size of S7P is larger than or the same as FBP, while the ^{13}C labeling rate constant (k-value) of S7P is larger than FBP, then the carbon flux of $\text{GAP/DHAP} \rightarrow \text{S7P}$ is larger than the carbon

flux of GAP/DHAP \rightarrow FBP. The k-value was calculated by fitting the total ^{13}C enrichment curve of the metabolite to the exponential equation $y = A_0 (1 - e^{-kt})$ (Huege et al., 2011), where A_0 is the maximum ^{13}C -enrichment level, and t is the time.

3. Results & Discussion

3.1) Model validations.

In *iSyp821* we use a semi-automated web-based resource, Model SEED, and newly published biochemical data to construct the most comprehensive stoichiometric biochemical network of the central metabolism of *Synechococcus* 7002 to date. Compared to the two existing *Synechococcus* 7002 models, *iSyp821* includes more genes, metabolites and reactions (Table 2-1), and the first light intensity dependent carbon partitioning function, ν BOF. The photoautotrophic growth rates and inorganic carbon C_i uptake rates were determined experimentally over a range of intensities from 10~450 $\mu\text{E}/\text{m}^2/\text{s}$, the latter representing the upper limit of intensities achievable in our bioreactor. Both data sets exhibit a linear correlation (R^2 equals to 0.9259 for protein and 0.7752 for carbohydrate) when plotted as a function of the electron flux through PSII measured at each intensity, as determined by oximetry (Figure 2-2). PSII flux is a measure of the photochemical redox energy production rate and a major portion of the proton ion gradient energy (excludes contributions from PSI cyclic electron flow) (Allen, 2003). The PSII flux increases with light intensity until reaching a saturated rate at 400~450 $\mu\text{E}/\text{m}^2/\text{s}$. The experimental photoautotrophic growth rate at this maximum PSII flux is 0.19 ± 0.02 (h^{-1}). This growth rate is consistent with earlier growth rate measurements for *Synechococcus* 7002 (Nomura et al., 2006). Figure 2-3 A&B shows that the growth rate and inorganic carbon uptake rate can be fit simultaneously over the full range of light intensities by *iSyp821* using a single set of model parameters that yield excellent quantitative representations ($\text{Chi}_{\text{red}}^2$ equal to 1.37 and 1.11, respectively). *iSyp821*

predicts that the fall off in rates at light intensities less than $400 \mu\text{E}/\text{m}^2/\text{s}$ is due to insufficient photon energy for supporting maximum growth.

		<i>iSyp611</i> (Hamilton et al, 2012)	<i>iSyp708</i> (Vu et al, 2013)	<i>iSyp821</i> (This paper)
Genes		611	708	821
Reactions (Metabolic and Transport)	GPR	517	568	723
	NGPR	35	34	21
Exchange Reactions		37	44	48
Metabolites		554	581	777
Experimentally measured BOF		NO	YES	YES

Table 2-1 Comparison of the *iSyp821* FBA model to the two existing *Synechococcus* 7002 models, *iSyp611* and *iSyp708*.

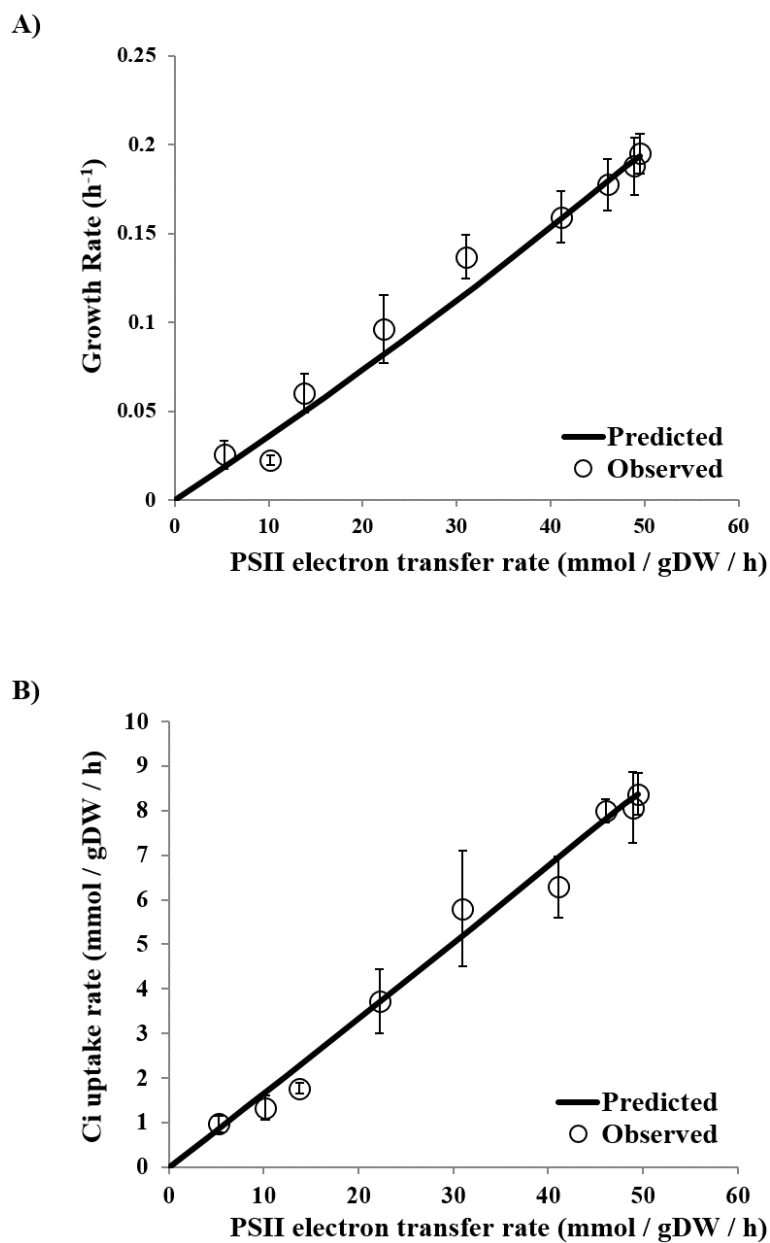


Figure 2-3 Prediction of growth rates (GR) and C_i uptake rates at different PSII electron transfer rates. The experimental (circles) and predicted (lines) growth rates (A) and C_i uptake rates (B) of *Synechococcus* 7002 plotted as a function of the PSII electron transfer

rate measured at different incident light intensities. The error bars represent standard errors from 3 biological replicates. Culturing was done on A⁺ medium.

Next, we used *iSyp821* to predict the PSI/PSII ETR ratios at different light intensities below the optimal light intensity (450 $\mu\text{E}/\text{m}^2/\text{s}$) (Figure 2-4 A). This prediction results from the changing biomass composition, which comes from the vBOF, and the ATP maintenance requirement of the cell interacting with our assumption of minimum total photon utilization. The ratio of PSI/PSII ETR fluxes is used by photosynthetic cells to control the balance between proton ion gradient generation (precursor to downstream ATP photophosphorylation) and redox energy generation. Cells control this flux ratio by at least three mechanisms: 1) adjusting the number of functional PSI/PSII reaction centers, 2) adjusting their optical cross sections (functional antenna size), and 3) adjusting the ratio of linear to cyclic electron flow around PSI (Allen, 2003). So far, there is no published data on PSI/PSII ETR ratios of cyanobacteria or algae at different low light intensities, but there is for a higher plant, rice, to help validate our predictions for cyanobacteria (Yamori et al., 2015). *iSyp821* predicts a smooth nearly hyperbolic dependence of PSI/PSII ETR ratio on light intensity (Figure 2-4 A): starting from a high value of 2.7 at lowest light intensity (10 $\mu\text{E}/\text{m}^2/\text{s}$), decreasing rapidly in the range 10 to 30 $\mu\text{E}/\text{m}^2/\text{s}$, and finally decreasing much more slowly until the optimal growth light intensity is reached (denoted by arrow). For comparison we plot the experimental PSI/PSII ETR ratio for rice reported by Yamori et al. (2015) in the light range of 40~500 $\mu\text{E}/\text{m}^2/\text{s}$ in Figure 2-4 B. These data provide good support for the validity of our predicted PSI/PSII ETR ratio for *Synechococcus* 7002 in this light intensity range. In this same study of rice, a mutant strain lacking cyclic electron flow was reported that has

lower plant dry biomass and grain production at low light ($200 \mu\text{E}/\text{m}^2/\text{s}$) of 11% and 28%, respectively. Such deficiencies of biomass accumulation and grain yield disappeared once the light intensity was increased to $800 \mu\text{E}/\text{m}^2/\text{s}$. These findings and the model predictions together suggest that in photosynthetic organisms, the PSI/PSII ETR ratio needs to be higher at low light intensities than at the optimal growth light intensity to maintain a homeostatic ATP/NADPH flux ratio, which is predicted to be ~ 1.7 (Figure 2-4 C). The exceptionally high PSI/PSII ETR ratio predicted at the low light intensity range of $10\sim 30 \mu\text{E}/\text{m}^2/\text{s}$ represents the requirement of hyper-active cyclic electron flow to support cellular survival and growth. Experimental data for PSI/PSII ETR ratio in photosynthetic organisms at such extreme low light conditions are not yet available.

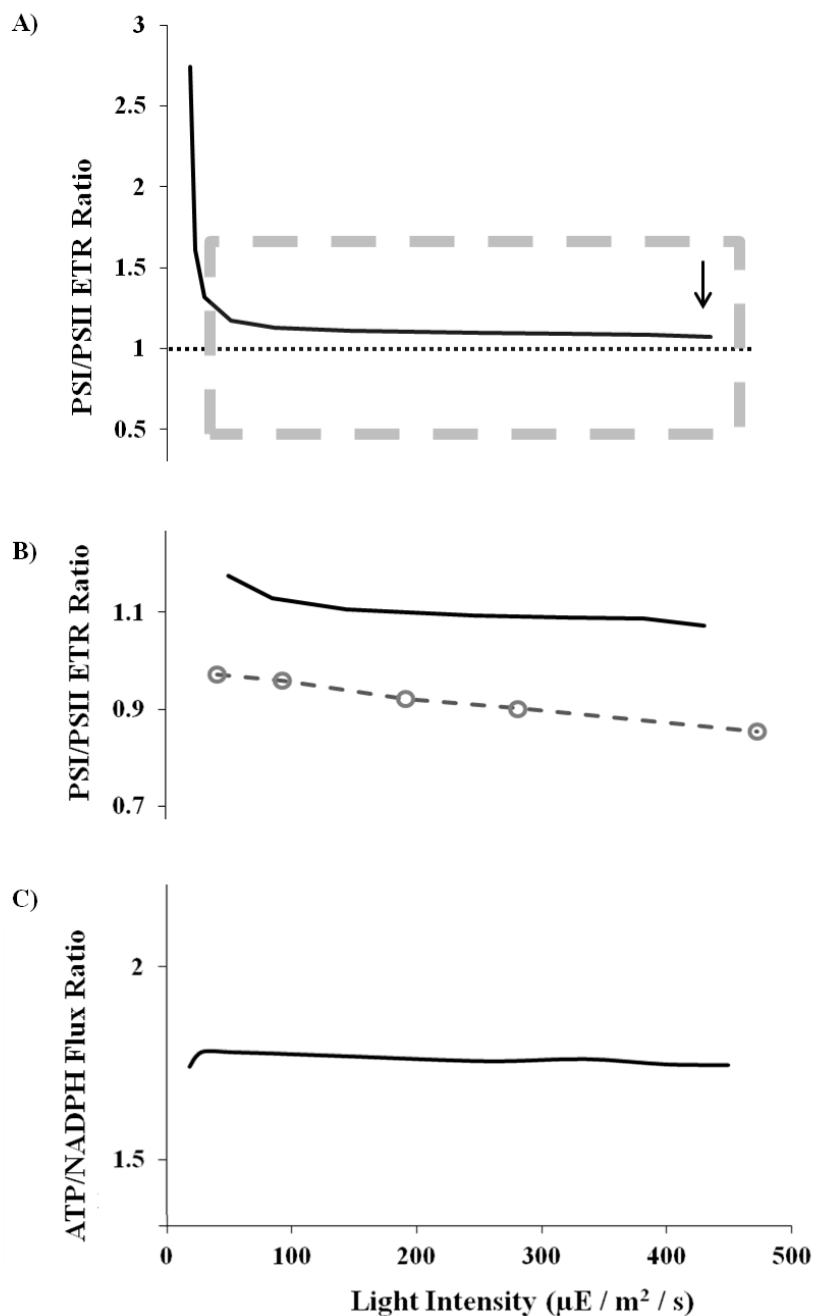


Figure 2-4 A) Predicted PSI/PSII ETR ratio by *iSyp821*; B) a comparison of PSI/PSII ETR ratio predicted by *iSyp821* (black line) vs. experimentally measured PSI/PSII ETR ratio of WT rice (grey circle) from Yamori et al. (2015); C) predicted ATP/NADPH flux ratio by *iSyp821*. The part in the grey box in (A) was used to compare with the PSI/PSII

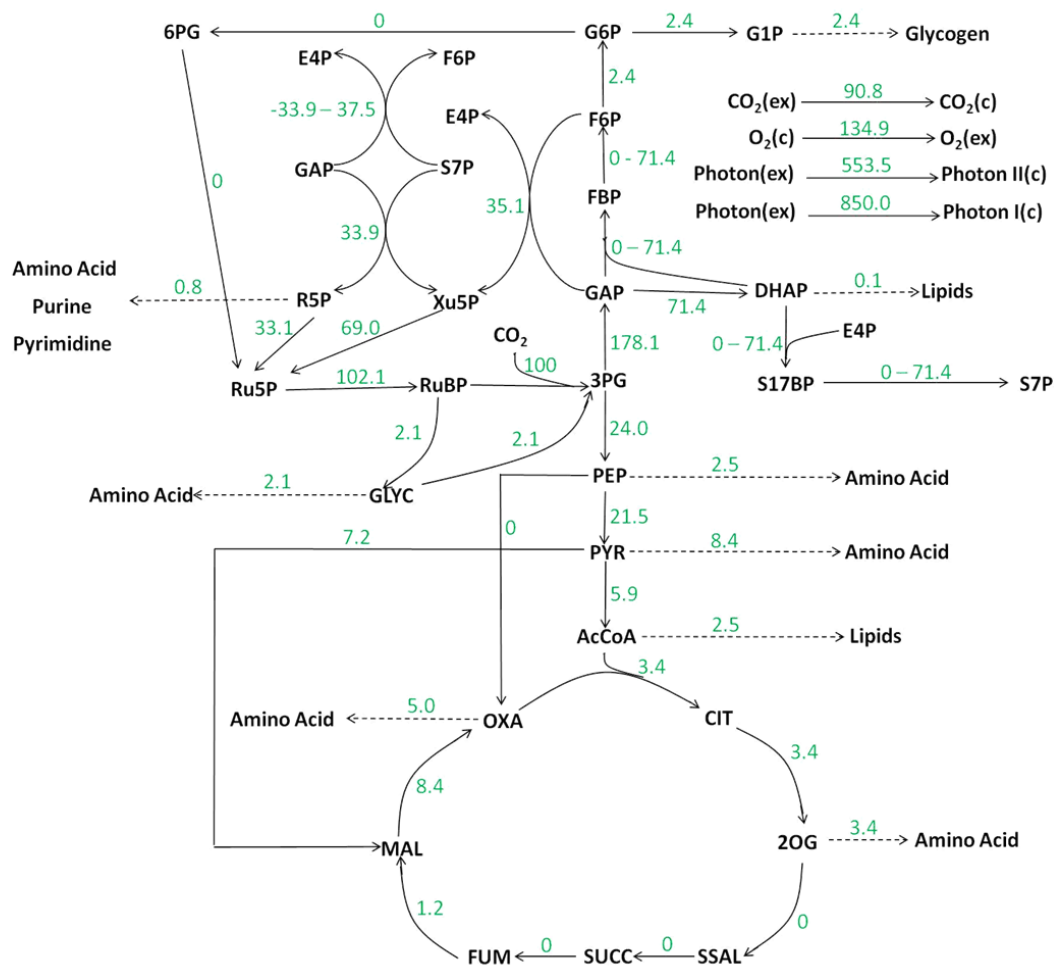
ETR ratio of rice measured at a similar light intensity range. The PSI/PSII ETR ratio data of WT rice (grey open circles) was normalized to the PSI/PSII ETR ratio of the NDH deficient mutant *crr6* before plotting. The arrow in (A) indicates the optimal growth light intensity (the minimal light intensity needed to support the optimal growth rate of 0.19 h^{-1}).

3.2) Photoautotrophic metabolic fluxes under low light and high light conditions.

Next we investigated the individual fluxes through central carbon metabolic pathways at high ($400\mu\text{E}/\text{m}^2/\text{s}$) and low ($12.5\mu\text{E}/\text{m}^2/\text{s}$) light intensities to learn how the dark reactions respond to the change in PSI/PSII ETRs. The high light intensity corresponds to that for optimal growth rate (0.19 h^{-1}), maximum C_i uptake rate ($8.37\text{ mmol}/\text{gDW}/\text{h}$) and PSII ETR ($49.6\text{ mmol}/\text{gDW}/\text{h}$) (Figure 2-3), while the low light intensity was selected as it exhibits a higher PSI/PSII flux ratio (predicted to be 1.53 at PSII ETR = $4\text{ mmol}/\text{gDW}/\text{h}$, Figure 2-5 A). All other fluxes were free to vary. Graphic overview of the predicted flux maps at two different light intensities are shown in Figure 2-5. All the fluxes were normalized to Rubisco carboxylase activity (100%), and units are $\text{mmol}/\text{gDW}/\text{h}$. FBA does not necessarily produce a unique solution. Thus, flux variability analysis was performed, and some flux solutions indicate a range of values rather than a single value to reflect the range of values that can be achieved in the optimal FBA solution. The difference in flux values for a single pathway under the two light conditions can be very small, but it is their cumulative effect into terminal sinks that count. Hence, we compared their carbon fluxes in terms of three categories “making amino acids”, “making carbohydrates (glycogen)”, and “making lipid precursors” (Table 2-2). The term “cumulative” refers to “the sum of carbon flux into the same category”. The cumulative difference is significant, with 80.0 units and 14.4 units of carbon equivalent flux predicted to produce amino acids and glycogen, respectively, under low light condition. This contrasts with 72.4 units and 22.2 units of carbon equivalent flux, respectively, under the high light condition. This High light vs. Low light flux comparison represents an improvement in predictive power of our model *iSyp821* compared to the previously

published versions (*iSyp708* and *iSyp611*). Relative flux maps under different light conditions predicted by these two earlier model versions are not significantly different, as the proportions of carbohydrate and protein are fixed in their BOFs.

A)



Precursor Catagory	Precursor Reaction	High Light Flux	Low Light Flux
Carbohydrate	G1P → Glycogen	3.7	2.4
Protein	R5P → Amino Acid	0.7	0.8
Protein	GLYC → Amino Acid	1.9	2.1
Protein	PEP → Amino Acid.	2.3	2.5
Protein	PYR → Amino Acid	7.6	8.4
Protein	2OG → Amino Acid	3.1	3.4
Protein	OXA → Amino Acid	4.5	5.0
Lipid	AcCoA → Lipid	2.2	2.5
Lipid	DHAP → Lipid	0.1	0.1
Cumulative Carbohydrate	Metabolite → Glycogen	22.2*	14.4*
Cumulative Protein	Metabolite → Protein	72.4*	80*
Cumulative Lipid	Metabolite → Lipid	4.7*	5.3*

Table 2-2. Summary of fluxes into metabolite precursor for making carbohydrate, protein and lipids under both high light and low light conditions, as shown in Figure 5. Units are mmol/gDW/h.

* Unit in “carbon equivalent”, calculated as: G1P = 6 units; R5P = 5 units; GLYC, PEP, PYR, DHAP = 3 units; 2OG = 5 units; OXA = 4 units; AcCoA = 2 units

Rubisco combines RuBP and CO₂ to synthesize 3PG, which can be recycled either back to regenerate RuBP to sustain the Calvin-Benson-Bassham (CBB) cycle, or used to synthesize biomass components. Modeling results suggest the possibility that synthesized GAP/DHAP can be converted into G6P through either the conventional gluconeogenesis pathway: GAP/DHAP → FBP → F6P → G6P, or a hybrid gluconeogenesis-PP pathway: GAP/DHAP → S17BP → S7P → F6P → G6P (shown in Figure 2-5 A). This hybrid pathway involves a reaction sequence previously postulated in multiple FBA papers (Knoop et al., 2013; Vu et al., 2013; Knoop et al., 2010), but its role in synthesizing storage carbohydrate was never emphasized nor experimentally tested. In this hybrid pathway, a part of the non-oxidative phase of the PP pathway is utilized, and no extra reducing power is introduced into the system. Three major functions have so far been assigned to the PP pathway in photoautotrophic bacteria: 1) to regenerate RuBP for light-driven CO₂ fixation, 2) to generate precursors of nucleotides and aromatic amino acids, and 3) to produce reducing power (NAD(P)H) for ATP generation through oxidative respiration in the dark (Herrmann & Weaver, 1999). To our knowledge, the importance of this hybrid pathway in converting fixed CO₂ into storage carbohydrates in any autotrophic bacteria has not been pointed out in the literature. Interestingly, fructose-bisphosphate aldolase class I and II (encoded by genes *A0010* and *A1352* in *Synechococcus* 7002), are likely to be bifunctional and capable of converting GAP/DHAP into FBP as well as S17BP, which is the precursor of S7P (White, 1995). The existence of these two bi-functional enzymes further increases the likelihood that this hybrid pathway is a major route for converting fixed CO₂ into storage carbohydrates in *Synechococcus* 7002.

To test the model's prediction of the function of this hybrid pathway, we conducted ^{13}C kinetic labeling experiments using LC-MS to determine the pool sizes and the first-order rate constants of three target metabolites (FBP, F6P and S7P) under photoautotrophic conditions for *Synechococcus* 7002. The results show that the GAP/DHAP \rightarrow S7P route is favored over the GAP/DHAP \rightarrow FBP route (Figure 2-6 and Table 2-3). The ^{13}C labeling rate constant of S7P was significantly larger than that of FBP under two different light conditions, while the pool size of S7P was significantly larger than that of FBP at 250 $\mu\text{E}/\text{m}^2/\text{s}$ light and similar at 30 $\mu\text{E}/\text{m}^2/\text{s}$ light. These results indicate a faster carbon influx into S7P than FBP starting from ^{13}C labeled CO_2 . If F6P were completely synthesized from FBP through the gluconeogenesis pathway, then F6P should be labeled slower than FBP. In our experiments, however, we observed that the labeling of F6P was significantly faster than that of FBP at 250 $\mu\text{E}/\text{m}^2/\text{s}$ light, while they are similar at 30 $\mu\text{E}/\text{m}^2/\text{s}$ light (Figure 2-6). Thus, we hypothesize that at least a significant part of the F6P pool was synthesized through the hybrid pathway we mentioned earlier. Interestingly, slower labeling of FBP than S7P in Arabidopsis Rosette under photoautotrophic growth condition was previously reported (Szecowka et al., 2013). The authors explained this observation as the compartmentalization effect of FBP pool, which causes a portion of the FBP pool to never be labeled and the overall percentage of labeling to be lower than its downstream metabolites. An alternative explanation is "metabolic channeling", which has been discussed by Huege et al. (2011) and Young et al. (2011). In these two publications, slower labeling of upstream metabolites than downstream metabolites was explained by the existence of multi-enzyme complexes, which transfer intermediates directly between catalytic sites without

diffusion into the bulk phase of the cell. In future work, we plan to conduct a more comprehensive metabolic flux analysis by adapting the methodology described in (Young et al., 2011) to further investigate this hypothesis.

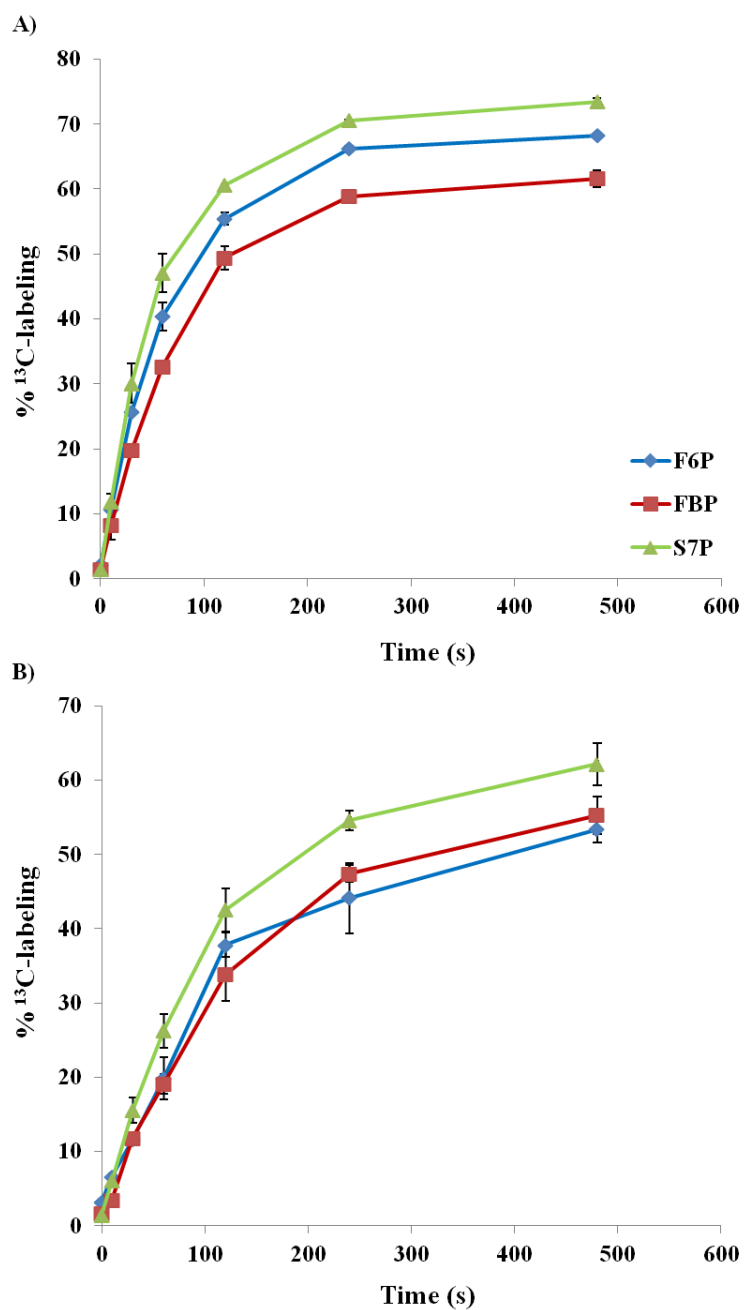


Figure 2-6 ¹³C-labeling kinetics of three carbon metabolites F6P (blue diamond), FBP (red square) and S7P (green triangle) monitored under A) 250 $\mu\text{E}/\text{m}^2/\text{s}$ and B) 30 $\mu\text{E}/\text{m}^2/\text{s}$ actinic light. Labeling rate constants and pool sizes of corresponding metabolites are summarized in Table 2. The error bars represent standard errors from 3 biological replicates.

Light Condition	Metabolite	Pool Size (10^{-3} mmol/gDW)	k-value (s^{-1})
250 μE/m²/s	FBP	0.19 ± 0.01	0.0129 ± 0.0004
	S7P	1.11 ± 0.23	0.0172 ± 0.0008
	F6P	0.10 ± 0.01	0.0148 ± 0.0006
30 μE/m²/s	FBP	0.27 ± 0.07	0.0072 ± 0.0004
	S7P	0.35 ± 0.02	0.0093 ± 0.0004
	F6P	0.04 ± 0.01	0.0075 ± 0.0007

Table 2-3 Experimental pool sizes and first-order rate constants (k-value) determined by ¹³C labeling of three target metabolites under photoautotrophic conditions for *Synechococcus* 7002. Pool size values are the average values of 3 biological replicates under the two corresponding light conditions.

Although the oxygenase reaction of Rubisco leads to a loss of fixed carbon, a small portion of RuBP went through this reaction to synthesize several essential amino acids such as glycine in our simulation. The reaction KEGG EC# order to synthesize glycine from RuBP is [3.1.3.18] + [1.1.3.15] + [2.6.1.45]. Glycine can be synthesized through a less energetically wasteful alternative pathway, and therefore the validity of this prediction needs to be further tested by addition ^{13}C labeling experiments. The zero flux prediction of the PEPC reaction in Figure 5A is unexpected. This prediction is caused by the photon utilization minimization assumption we used for modeling (see Methods). Pyruvate kinase, which catalyzes $\text{PEP} \rightarrow \text{PYR}$, yields one ATP per PYR molecule, while the PEPC reaction does not. This one molecule of ATP will reduce the over photon requirement, and therefore it is favored during the simulation. Although utilization of the bidirectional malic enzyme that catalyzes $\text{PYR} \rightarrow \text{MAL}$ reaction consumes one NADH, this consumed NADH is compensated by the subsequent $\text{MAL} \rightarrow \text{OXA}$ reaction that produces one molecule of NADH. The discovery of genes encoding 2-oxoglutarate decarboxylase (2-OGDC) (A2770) and succinic semialdehyde dehydrogenase (SSADH) (A2821) in *Synechococcus* 7002 completed the modified TCA cycle in this cyanobacterial strain (Zhang & Bryant, 2011). However, our model predicted an insignificant flux going through this 2-OGDC-SSADH pathway under the two illumination conditions examined. 2OG was exclusively used for synthesis of amino acids and pyrimidine, and fumarate was generated as a result of aspartate metabolism ([6.3.4.5] + [4.3.2.1]). Computational knockout analysis of these two genes did not cause any reduction in the predicted growth rate, unlike an observed 30% reduction in growth rate for the experimentally tested knockout mutant (Zhang & Bryant, 2011). This

disagreement might be caused by the lack of flux constraints on the alternative pathway that bypasses this $2OG \rightarrow SSAL \rightarrow SUCC$ process in our model. *In vitro* activities of enzymes involved in the alternative pathways need to be determined in order to place such flux constraints.

Because of the ν BOF, less carbon flux went into precursor metabolites for protein synthesis (and more into carbohydrate synthesis) under high light than low light (Figure 2-5). Konopka & Schnur (1980) used $NaH^{14}CO_3$ to study carbon partitioning under different light conditions in two cyanobacterial strains, *Merismopedia tenuissima* and *Oscillatoria rubescens*. In both strains, an inverse relationship was observed between incorporation of radioisotope into polysaccharides versus into proteins with increasing light intensities. Under high light, more polysaccharides and fewer proteins were ^{14}C labeled. A similar effect on chemical composition has also been observed in *Arthrospira* sp. (Olguín et al. 2001). A 5% reduction in relative protein content and a 25% increase in relative polysaccharide content were observed when *Arthrospira* sp. was cultivated in 144 μE light intensity as opposed to 66 μE light intensity. The inverse relationship between carbohydrates and proteins can be explained by the different availabilities of NADPH and ATP when light increases. When light intensity is low, cells need to invest photon energy to keep cells alive and try to grow, and therefore NADPH and ATP are invested towards protein synthesis. As light intensity increases, NADPH and ATP become more abundant, and therefore can be stored in the form of glycogen, which could be catalyzed in the dark to satisfy the cellular maintenance requirement.

3.3) Transcriptomic-constrained analysis of metabolism under nitrogen deprived condition in *Synechococcus* 7002.

Nitrogen removal from growth media is widely used to stimulate redistribution of stored carbon from proteins into carbohydrates in cyanobacteria and into lipids in microalgae (Taikhao et al., 2014; Hasunuma et al., 2013; Nigam et al., 2011). We adapted *iSyp821* to model these changes by including transcriptomic data collected from Ludwig & Bryant (2012) into the model to account for changes in mRNA levels. The carbon flux distribution of photoautotrophic cultures grown under nitrogen-deprived condition was then simulated and compared to nitrate-replete growth condition (Figure 2-7). We observed that, under simulated nitrogen deprived conditions, 1) the absolute fluxes of most of the pathways in the map, except fluxes into glycogen and Malonyl-CoA (lipid precursor) (Figure 2-7 A), and 2) the relative fluxes going into the lower glycolytic pathway (3PG → AcCoA) into the TCA cycle (Figure 2-7 B) were predicted to decrease more than 30%, while 3) the relative fluxes going into glycogen synthesis and lipid synthesis were predicted to increase more than 2-fold (Figure 2-7 B). All of these observations were validated by existing literature or experimental data, as described next.

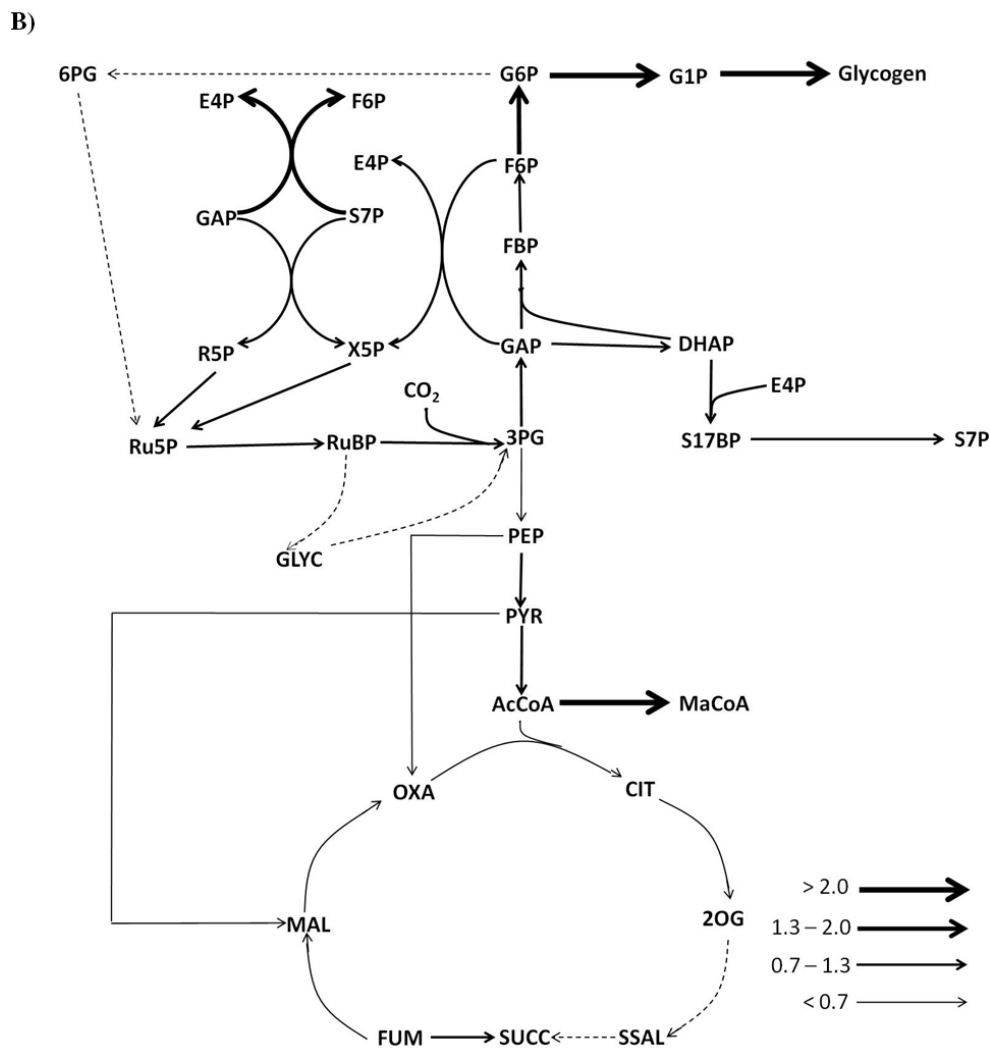


Figure 2-7 Carbon flux redistribution under nitrogen deprivation photoautotrophic conditions as predicted by transcriptomic modified FBA. A) Absolute carbon flux distributions (without normalization to CO_2 uptake and B) normalized carbon flux distribution (with normalization to CO_2) are shown here. The increasing thickness of the arrows represents the fold-increase of the reaction fluxes under nitrogen deprivation versus nitrate repleted condition. Dashed arrows indicate insignificant carbon fluxes going through these pathways under nitrogen deprivation.

It is well known that during nitrogen deprivation, pigment catabolism (chlorosis) and protein catabolism occur in cyanobacteria as a means to recycle nitrogen for survival (Stevens et al., 1981; Sauer et al., 2001). Our prediction of greater than 30% reduction in relative carbon flux going into both lower glycolysis pathway and TCA cycle agrees well with a lowered protein synthesis rate under nitrogen deprivation. These two pathways are the major sources of carbon precursors for protein synthesis (Figure 2-5). Associated with the loss of photosynthetic pigments and phycobilisomes, the photosynthetic apparatus activities drastically reduced. In the cyanobacterium *Synechococcus* sp. PCC 7942, the PSII and PSI activities of nitrogen-deprived cells retained only 0.1% of the activities of active growing cells (Sauer et al., 2001). Additionally, it has been shown that Rubisco is depleted during nitrogen-deprived photoautotrophic conditions in *Synechocystis* 6803 (Duke & Allen, 1990). Reduced PSII and PSI activities along with reduced Rubisco abundance under nitrogen deprivation will lower the CO₂ fixation rate, in accord with our flux prediction of reduced absolute CO₂ fixation rate.

Triacylglycerides (neutral lipids) are not typically stored in most cyanobacteria, while polar lipids comprise the main components of membranes. Although minor components of total biomass, lipid content has been shown to increase in several cyanobacterial species under nitrogen deprivation and photoautotrophic growth (Griffiths & Harrison, 2009; Tedesco & Duerr, 1989). Using *iSyp821* the transcriptomic modified FBA model predicted that relative flux into malonyl-CoA, the precursor of lipid synthesis, increased by 2-fold under nitrogen deprivation (Figure 2-7 B). In most cyanobacteria, glycogen rather than protein becomes the major carbon sink under nitrogen deprived photoautotrophic conditions (Taikhao et al., 2014). Nitrogen starvation during 24 hour of

photoautotrophic growth with continuous light increased the total carbohydrate content by 5-fold (mainly glycogen) in *Synechococcus* 7002 (Guerra et al., 2013a). Consistent with this observation and our model predictions, we observe a 27% increase in the total carbohydrate content in the first hour of nitrogen deprivation, as determined experimentally (Table S2-1). Using *iSyp821* the transcriptomic modified FBA model predicted that the flux into glycogen synthesis increased by more than 2-fold under nitrogen deprived growth (Figure 2-7).

4. Conclusion

The most comprehensive metabolic FBA model to date, *iSyp821*, was constructed for photoautotrophic growth and tested against experimental data for cyanobacterium *Synechococcus* 7002. Incorporation of a light-dependent PSI/PSII ETR algorithm into *iSyp821* allows reliable simulations of photoautotrophic growth at different light intensities. Application of this variable Biomass Objective Function (ν BOF) within the metabolic FBA model was validated experimentally with data from biomass growth rate, C_i uptake rate and the carbohydrate/protein content as a function of light intensity. The model's prediction reveals the important transition with changing light intensity from photon distribution between PSI and PSII, and carbon distribution favoring growth or carbon storage. Additionally, the model predicted an unconventional gluconeogenesis-PP pathway that converts fixed CO_2 into carbohydrates and carries the major flux under some conditions. This hybrid pathway was experimentally verified by kinetic ^{13}C metabolite labeling experiments. By incorporation of transcriptomic data to approximate enzyme concentration changes, we extended *iSyp821* to simulate photoautotrophic carbon flux redistribution under nitrogen stress conditions. We obtained quantitative agreement with the experimental trends in accumulation of carbohydrates and lipids, and loss of CO_2 uptake, amino acid synthesis.

5. List of abbreviations

GAP: glyceraldehyde-3-phosphate; S17BP: Sedoheptulose 1, 7-bisphosphate; S7P:

Sedoheptulose-7-phosphate; FBP: Fructose 1, 6-bisphosphate; F6P: Fructose-6-phosphate;

DHAP: Dihydroxyacetone phosphate; PEP: Phosphoenolpyruvate; 2OG: Alpha-

ketoglutarate; SSAL: Succinyl-semialdehyde; SUCC: Succinate.

6. Supplemental files

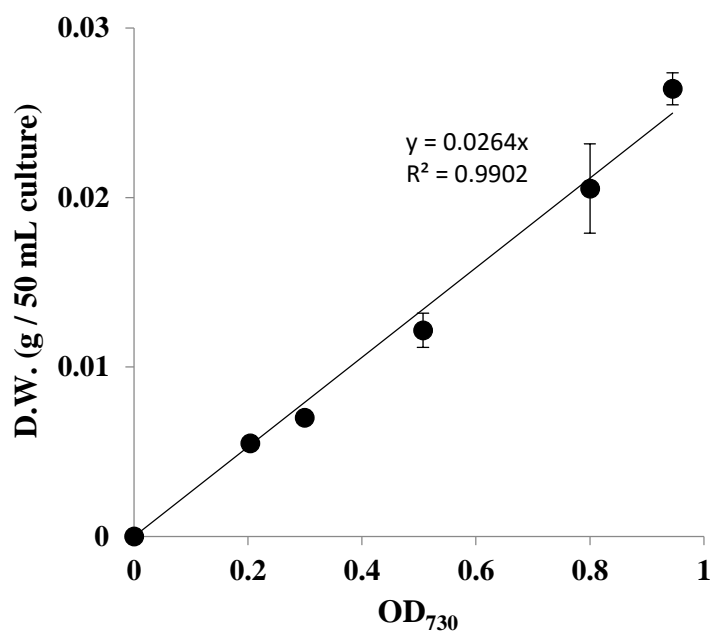


Figure S2-1 Dry weights of *Synechococcus* 7002 culture at different optical densities illuminated with $250 \mu\text{E} / \text{m}^2 / \text{s}$ actinic light condition. The results are the mean values of three biological replicates.

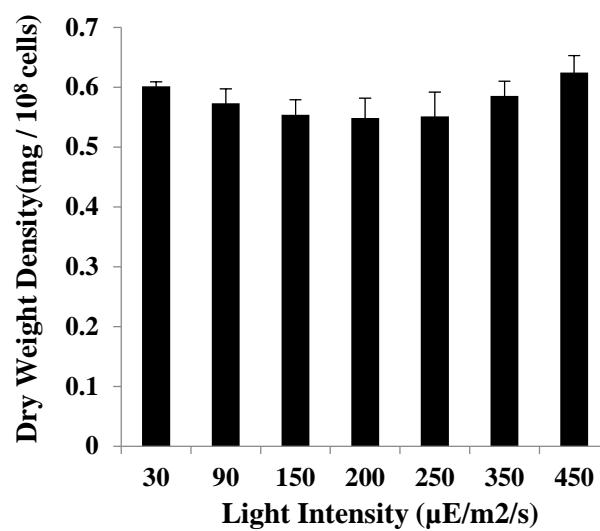


Figure S2-2 Dry weight densities of *Synechococcus* 7002 culture grown under different light conditions. The results are the mean values of three biological replicates. By performing one way ANOVA test at 1% significance level of the test, we showed that dry weight densities at different light intensities are same.

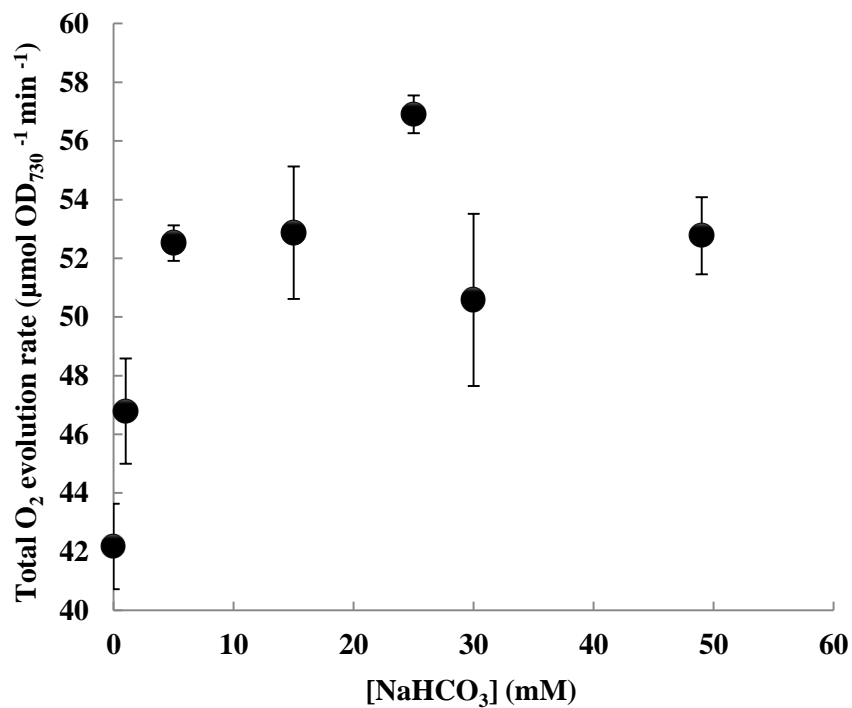


Figure S2-3. Total oxygen evolution rates of *Synechococcus* 7002 cultures supplemented with different concentrations of NaHCO₃ under the saturating red light (700 μE m⁻² s⁻¹). The results are the mean values of three biological replicates.

Condition	Total carbohydrate content (mol / 10¹⁷ cells)	Total protein content (mol / 10¹⁷ cells)
Before N-deprivation	486 ± 2	7.8 ± 0.1
After N-deprivation	618 ± 4	6.9 ± 0.2

Table S2-1. Total carbohydrate and total protein contents of photoautotrophic cultures of wildtype *Synechococcus* 7002 before and after 1 hour of nitrogen deprivation. The results are the mean values of three biological replicates.

Chapter 3: Revisit the tricarboxylic acid cycle in cyanobacteria

Coauthors: Shuyi Zhang, Shannon Chang, G. Charles Dismukes and Donald A. Bryant

Summary

For nearly half century, it was believed that cyanobacteria had an incomplete tricarboxylic acid (TCA) cycle, as the 2-oxoglutarate dehydrogenase (2-OGDH) was missing. In addition, the existence of gamma-Aminobutyric acid (GABA) shunt, a variant of the TCA cycle, is also ambiguous and poorly understood because the GABA aminotransferase is missing in many cyanobacteria. Recently, a succinic semialdehyde (SSA) route, which utilizes 2-oxoglutarate decarboxylase (2-OGDC) and succinic semialdehyde dehydrogenase (SSADH) to convert 2-OG into succinate, was identified and thus completed the TCA cycle in cyanobacteria. In this study, the glutamate decarboxylase and N-acetylornithine aminotransferase were biochemically characterized and our results demonstrated that N-acetylornithine aminotransferase could also function as GABA aminotransferase. Furthermore, the glutamate decarboxylase from *Synechocystis* sp. PCC 6803 was expressed in *Synechococcus* sp. PCC 7002, which originally lacks the enzyme, to study the metabolic correlations between the SSA route and the GABA shunt. *in vivo* metabolite profiling studies of 7 *Synechococcus* sp. PCC 7002 mutant strains related to these two routes were also conducted to further examine their physiological importance and connections. Our results showed that all SSA route mutants suffered reduced rates of photoautotrophic growth and oxygen evolution, and had lower chlorophyll *a* contents. Metabolites profiling also indicated that, compared to 2-oxoglutarate decarboxylase, the GABA shunt is less efficient in converting 2-oxoglutarate to succinic semialdehyde in *Synechococcus* sp. PCC 7002. The metabolic profiling study of these two TCA variants will provide new insights to carbon and nitrogen metabolism as well as pathway evolution of the TCA cycle in cyanobacteria.

1. Introduction

Global CO₂ annual emission rate has been rapidly rising for the past two decades, and, unfortunately, this increasing trend of annual CO₂ emission appears to continue. While major countries around the world are trying to cut down their CO₂ emission, scientists and engineers are seeking ways to effectively remove CO₂ from the atmosphere. Cyanobacteria are one group of essential oxygenic photosynthetic organisms and are projected to play a pivotal role in supplying future renewable energy needs as well as CO₂ sequestration. Owing to the straightforward genetic modification methodologies, many cyanobacteria species have been metabolically engineered into cell factories using CO₂ and light as “free” carbon and energy sources (Lan et al., 2012; Yu et al., 2013; Ducat et al., 2011a). Thus, our abilities to understand and utilize these organisms efficiently are extremely important. This capability is directly dependent on fundamental studies to understand key metabolic pathway interactions and regulatory processes in these organisms (Zhang et al., 2015; Krishnan et al., 2015; Qian et al., 2015).

The tricarboxylic acid (TCA) cycle is a central metabolic pathway that generates energy to support cellular survival and growth, as well as precursors for cellular components biosynthesis (Tang et al., 2011; Zhang & Bryant, 2014). As such, the identification of a complete, non-canonical, TCA cycle (via the 2-OGDC/SSADH bypass) in most cyanobacteria not only corrects a long-held misconception that these organisms have an incomplete TCA cycle due to the absence of 2-OGDH, but also provides much useful knowledge illustrating the occurrence and physiological functions of the TCA variants in these bacteria (Zhang & Bryant, 2014; Zhang & Bryant, 2011). Nonetheless, this route has not been supported by any *in vivo* metabolic evidences under any of the

growth conditions (e.g. photoautotrophic, photoheterotrophic and dark aerobic). Particularly, the involvement of this SSA route under photoautotrophic and photoheterotrophic growth conditions in *Synechococcus* sp. PCC 7002 (*Synechococcus* 7002) are so far unclear.

In addition, the existence of GABA shunt, another TCA cycle variant, in cyanobacteria is still mystery and poorly understood. The GABA shunt pathway is composed of glutamate decarboxylase, GABA aminotransferase and succinic semialdehyde dehydrogenase, and the shunt results in the conversion of glutamate to succinate with GABA and succinic semialdehyde as intermediates (Figure 3-1). However, the glutamate decarboxylase, which catalyzes the first step in the GABA shunt, presents in some cyanobacteria species but is apparently lacking in other cyanobacteria strains. In addition, another key enzyme in the GABA shunt, the GABA aminotransferase, is also missing in many cyanobacteria. Considering the intrinsic links between the GABA shunt and the TCA cycle, both of which can convert 2-oxoglutarate to succinate, it is likely that these two cycles are also functionally connected. Indeed, it was reported in *Bradyrhizobium japonicum* that the GABA shunt was used in a mutant lacking the 2-oxoglutarate dehydrogenase (Green et al., 2000). A recent study has reported that N-acetylornithine aminotransferase from *Synechocystis* sp. PCC 6803 (*Synechocystis* 6803) could also function as GABA aminotransferase, which together with glutamate decarboxylase forms the GABA shunt in cyanobacteria (Xiong et al., 2014). However, the biochemical validation of the putative bi-functional N-acetylornithine aminotransferase was not performed yet.

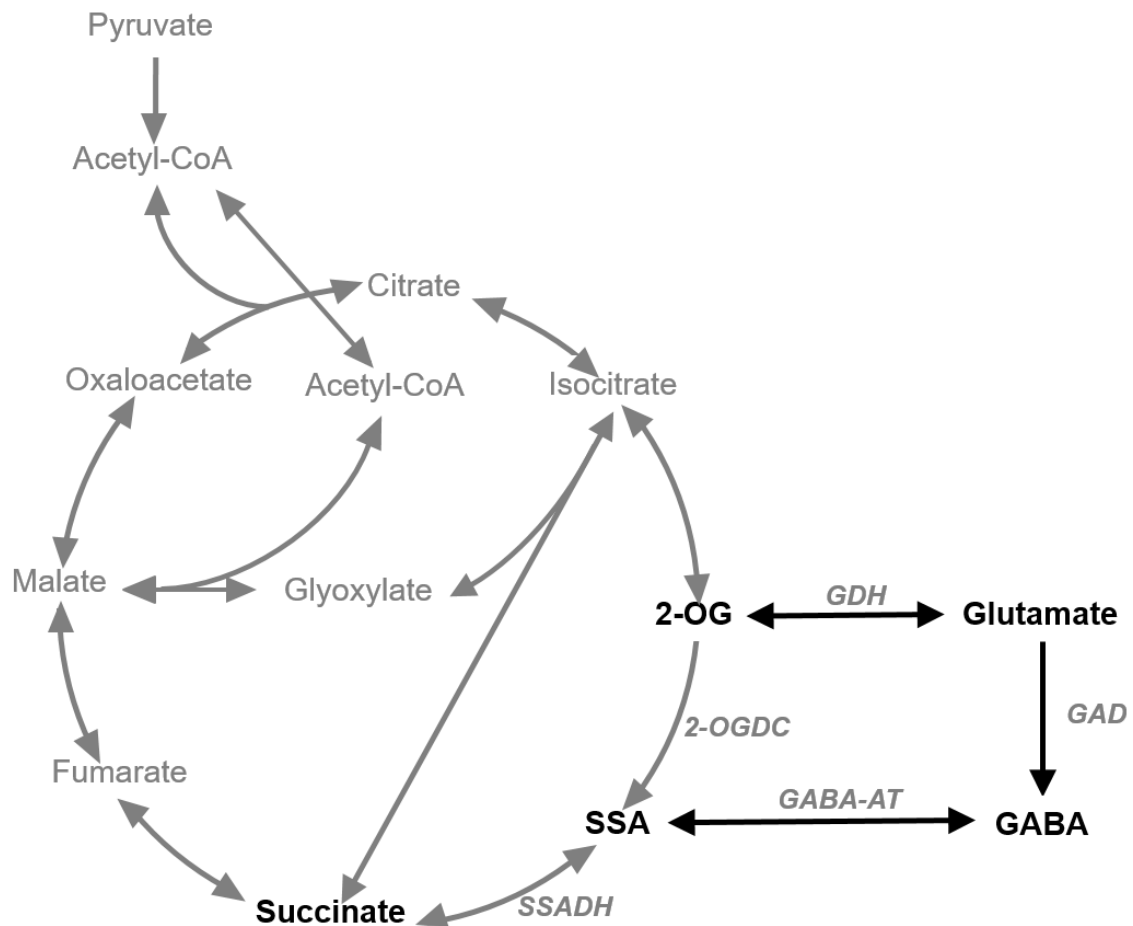


Figure 3-1 Scheme showing the TCA cycle, glyoxylate cycle and GABA shunt. Abbreviations: 2-OG, 2-oxoglutarate; SSA, succinic semialdehyde; GABA, gamma-Aminobutyric acid; GABA-AT, GABA aminotransferase; GAD, glutamate decarboxylase; GDH, glutamate dehydrogenase; 2-OGDC, 2-oxoglutarate decarboxylase; SSADH, succinic semialdehyde dehydronease.

In this study, a cyanobacteria-specific protocol was successfully developed to extract and analyze intracellular SSA from *Synechococcus* 7002. Our findings demonstrate the significant involvement of the SSA route under photoautotrophic, photoheterotrophic and dark aerobic growth conditions in *Synechococcus* 7002. Additionally, we biochemically validated that N-acetylornithine aminotransferase could also function as GABA aminotransferase. Furthermore, the glutamate decarboxylase from *Synechocystis* 6803 was also transformed and expressed in *Synechococcus* sp. PCC 7002 which normally lacks this enzyme. Intracellular metabolite concentrations were measured in this overexpression strain and potential interactions between the GABA shunt and the TCA cycle was investigated. The biochemical and metabolic characterizations in this work validates the occurrence of these pathways in cyanobacteria and provides possible insights into pathway evolution as well as future metabolic engineering.

2. Experimental Procedures

2.1) Cloning, protein purification and identification

Open reading frames *sll1641*, encoding the glutamate decarboxylase and *slr1022*, encoding the N-acetylornithine aminotransferase of *Synechocystis* sp. PCC 6803; open reading frames SYNPC7002_A0326, encoding the N-acetylornithine aminotransferase of *Synechococcus* sp. PCC 7002 were amplified by polymerase chain reaction (PCR) with Phusion DNA polymerase (New England Biolabs, Ipswich, MA) and cloned into plasmid pAQ1Ex-*P_{cpcBA}* (Xu et al., 2011). Primer set GADF-GADR was used to amplify *sll1641*; primer set 6803ArgDF-6803ArgDR was used to amplify *slr1022*; and primer set 7002ArgDF-7002ArgDR was used to amplify SYNPC7002_A0326 (Table 1). An N-terminal [His]₁₀-tag was introduced into all the enzymes to facilitate subsequent protein purification.

The resulting plasmids pAQ1Ex-*P_{cpcBA}:: sll1641*, pAQ1Ex-*P_{cpcBA}:: slr1022*, and pAQ1Ex-*P_{cpcBA}:: A0326* were verified by DNA sequencing and were transformed into *E. coli* strain DH5-alpha. Cells were grown overnight in 1 liter Luria-Bertani (LB) medium containing 50 µg ml⁻¹ gentamycin, harvested by centrifugation at 4°C at 5,000 × *g*, and washed once with 50 mM Tris-HCl buffer, pH = 8.0. Cells were disrupted by three passages through a chilled French pressure cell operated at 138 MPa. Soluble lysates were obtained by centrifugation at 20,000 × *g* for 30 min and were loaded onto a Ni²⁺-NTA affinity resin (Goldbio, St. Louis, MO), which was pre-equilibrated with 10 mM imidazole in 50 mM Tris-HCl, pH 8.0, and washed with 30 mM imidazole in 50 mM Tris-HCl, pH 8.0, 300 mM NaCl. Proteins were eluted stepwise with 50, 100, 150, 200,

and 250 mM imidazole in 50 mM Tris-HCl, pH 8.0, 300 mM NaCl. Fractions containing the recombinant proteins were monitored by polyacrylamide gel electrophoresis in the presence of sodium dodecylsulfate (SDS-PAGE) and were concentrated by ultrafiltration using Centriprep columns (Millipore, Billerica, MA). Purified proteins were further analyzed by SDS-PAGE and immunoblotting with commercial antibodies (Rockland, Limerick, PA) to the poly-[His] tags. Proteins were also positively identified by tryptic peptide mass fingerprinting as previously described (Zhang & Bryant, 2011).

2.2) Enzymatic assays

For enzyme assays with glutamate decarboxylase, the reaction mixture (0.2 ml) contained 1 mM glutamate, 50 mM K-phosphate, pH 4.5 and 50 μ g purified sll1641, and control experiments were performed similarly but without the addition of the purified enzyme. The mixture was incubated at RT for 1 h, and the produced GABA was detected by using Edman's reagent as previously described with modifications (Tank & Bryant, 2015). In details, an aliquot (30 μ l) of the reaction mixture was transferred to a glass test tube and dried by flushing with nitrogen. The dried sample was then dissolved in 100 μ L coupling solution (mixture containing 50% acetonitrile, 25% pyridine, 10% triethylamine and 15% water) and the resulting solution was dried again. Then the dried sample was dissolved in 100 μ L coupling solution, after which 5 μ L of PITC was added to the solution and reaction was allowed to proceed for 5 minutes at RT. After reaction, the liquid sample was dried and the resulting pellet was dissolved in 250 μ L analysis solvent. An aliquot (20 μ L) of the solution was injected on Shimadzu LC-20AB HPLC system equipped with 254-nm UV detector SPD-20A. Different components in the solution were separated on a Kinetex 5- μ m C18 100Å column (15 cm \times 4.6 174 mm ID) protected by a

SecurityGuard ULTRA cartridge UHPLC C18 for 4.6-mm ID columns 175 (Phenomenex, Torrance, CA, USA). The HPLC analysis method consisted of a 2-solvent gradient (solvent A and B) developed over a 20-min period with a flow rate of 0.5 ml/min at 30 °C. The initial condition was 100% solvent A (0.14 M sodium acetate, pH 6.2 containing 0.5 mM triethanolamine), which decreased over 10 min to 82.5% and from 10-15 min to 0%. Solvent B was a 40:60 (v/v) mixture of HPLC-grade water and acetonitrile. The elution times and concentrations of substrates and products were determined by comparison of results obtained from analyses of individual standard compounds with the same procedure.

For enzyme assays with N-acetylornithine aminotransferase, the reaction mixture (0.2 ml) contained 1 mM L-ornithine, 1 mM 2-oxoglutarate, 50 mM K-phosphate, pH 9 and 50 µg purified slr1022 or SYNPPCC7002_A0326. The mixture was incubated at RT for 1 h, and an aliquot (30 µl) of the reaction mixture was further analyzed using the same procedure as described in the enzyme characterization of glutamate decarboxylase to detect product formation. Control experiments were performed similarly but without the addition of the purified enzyme. The elution times and concentrations of substrates and products were determined by comparison of results obtained from analyses of individual compounds.

For enzyme assays with GABA aminotransferase, the reaction mixture (0.2 ml) contained 1 mM GABA, 1 mM 2-oxoglutarate, 50 mM K-phosphate, pH 9 and 50 µg purified slr1022 or SYNPPCC7002_A0326. The mixture was incubated at RT for 1 h, and an aliquot (30 µl) of the reaction mixture was further analyzed using the same procedure as described in the enzyme characterization of glutamate decarboxylase to detect product

formation. Control experiments were performed similarly but without the addition of the purified enzyme. The elution times and concentrations of substrates and products were determined by comparison of results obtained from analyses of individual compounds.

2.3) Mutant construction and segregation

The coding sequences of SynPCC7002_A2770, SynPCC7002_A2771, *sdhA* (SynPCC7002_A2569), *sdhB* (SynPCC7002_A1094), or the operon of *sucCD* (SynPCC7002_A0890 and SynPCC7002_A0891) were deleted and replaced by a DNA cassette that confers certain antibiotic resistance to produce the corresponding mutant strains of *Synechococcus* 7002 using homologous recombination method (Figure 3-2 A). The generated mutant strains are named as $\Delta A2770$, $\Delta A2771$, $\Delta A2569$, $\Delta A1094$, and $\Delta A9091$, respectively. In addition, the operon encoding SynPCC7002_A2770 and SynPCC7002_A2771 was further deleted in strain $\Delta A2569$ to generate the double mutant $\Delta A2569A7071$; and SynPCC7002_A1094 as well as the operon of SynPCC7002_A2770 and SynPCC7002_A2771 were deleted in strain $\Delta A9091$ to generate the triple mutant $\Delta A1094A7071A9091$. Transformation and selection were performed as previously described (Frigaard et al., 2004). Complete segregation was verified by PCR with template DNAs derived from the wild type and mutant strains (Figure 3-2 B, C&D). The primers used are listed in Table 3-1.

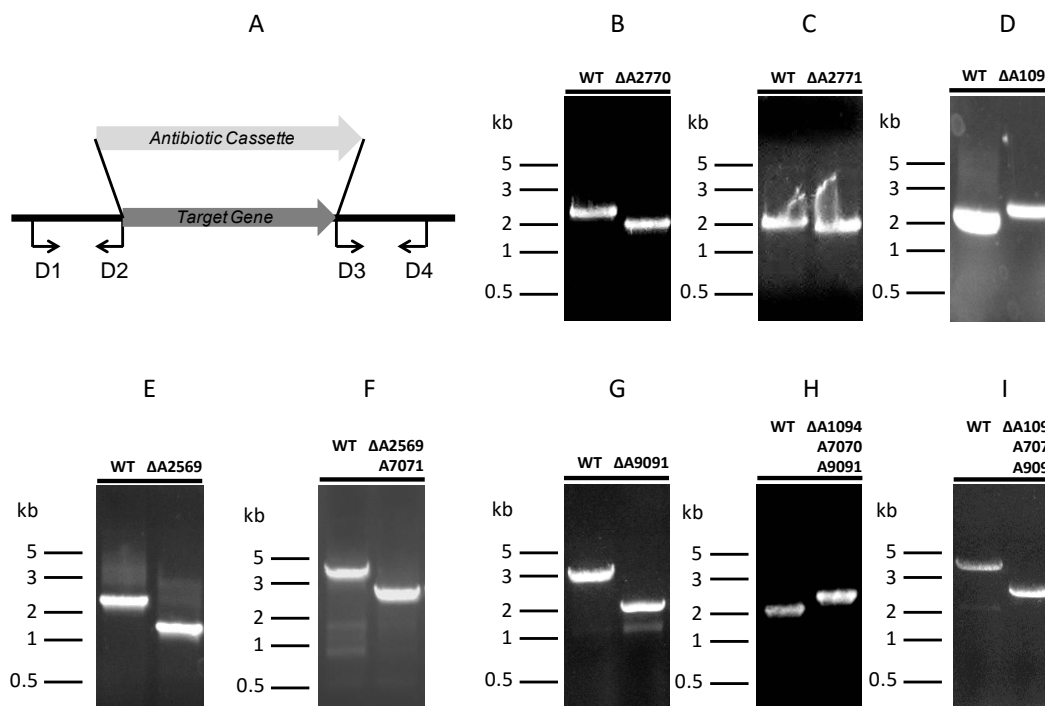


Figure 3-2 Scheme for mutant construction and verification of the TCA cycle mutants. A. Upstream and downstream flanking regions for a gene of interest were amplified using primer pairs D1-D2 and D3-D4, and these fragments were ligated to the antibiotic cassette. The resulting construction was transformed into *Synechococcus* sp. PCC 7002 to generate fully segregated mutants based on homologous recombination. B~I. Agarose gel electrophoretic analysis of amplicons from PCR reactions using primer set D1-D4 and template DNA derived from wild type (WT) or mutant strains $\Delta A2770$ (B), $\Delta A2771$ (C), $\Delta A1094$ (D), $\Delta A2569$ (E) and $\Delta A9091$ (G), verifying the complete segregation of alleles of corresponding genes. Additionally, deletion of the operon of SynPCC7002_A2770 and SynPCC7002_A2771 in the $\Delta A2569$ A7071 strain (F), and deletions of SynPCC7002_A1094 (H) as well as the operon of SynPCC7002_A0890 and

SynPCC7002_A0891 (I) in the Δ A1094A7071A9091 strain were also verified using the same method.

Name	Sequence (5' to 3')
A2770D1	TGCAGTGGATCCGGACGATCGCCT
A2770D2	ATGTAAAAGCTTGTCGTA CTGGGG
A2770D3	GCCTTGGTCAGTGAGCCAATTTG
A2770D4	AATGGTCAATCTTGTATTGCGGCG
A2771D1	AATCGAAGTCGTCTTTTTACCCGCCGAGCA
A2771D2	AATGATGGATCCA ACTCTCTCCTTTGCCGC
A2771D3	TGAATGAAGCTTCCCCCGACTTTATCCA
A2771D4	TAGATTTTTTTCACGACCATCCCGCTGGAGG
A2569D1	ATAACAGCGATCGCCAATTACGCCCGTGT
A2569D2	CGGCGCTCTAGAAAACTCAGGGGT TATTC
A2569D3	GCTTAAGCATGCCAGCCCTTCTCAAAGATG
A2569D4	GTCGATTTTATCGCTACCGAAAACCCCGAC
A1094D1	TTGTGAACACTCACCCGATAGGTCGGCTCT
A1094D2	GTCCGTGGATCCCCTCTTTTTGCCACAAAT
A1094D3	GCGCGCAAGCTTAAATGAGGGGGCTTAAAT

A1094D4	CGAAGGCGATCGCCCACTGTCTTTTTTTC
A9091D1	ACCCAAATCTGTTTGAAGCTCAAATCCGCC
A9091D2	GAGCAAAAGCTTTAGCGCAGAGGCAACCTC
A9091D3	ACGACCGGATCCATTTGCACCGCTTAGATC
A9091D4	CTTCGAGGGGGATGTGATATTCCTTGAGCA
GADF	GGCCGGCATATGGTGCATAAAAAAATTGAC
GADR	AATACTGGATCCCTAATGGCTAAAGTGGGA
6803ArgDF	GGTGATCATATGACCTATTCCCCTGTTGTT
6803ArgDR	TTAGATGGATCCTCAAACCAAAGTGGCGAT
7002ArgDF	AGTATTCATATGAGTCCCCAAACGCTACTG
7002ArgDR	AATGGTCAATCTTGTATTGCGGCG

Table 3-1 Primers used in this study.

In order to construct a *Synechococcus* 7002 strain expressing the glutamate decarboxylase, the pAQ1Ex-*P_{cpcBA}::sll1641* plasmid was transformed into wild-type *Synechococcus* 7002 as previously described (Frigaard et al., 2004). The presence of the desired glutamate decarboxylase gene in 7002-GAD was confirmed by PCR using primer set GADF-GADR. Immunoblotting was also performed with commercial antibodies (Rockland) to the His₁₀-tag as previously described (Shen et al., 2002), to validate expression of the recombinant glutamate decarboxylase. The resulting strain was named GAD-Ex.

To further investigate metabolic correlations between the GABA shunt and the TCA cycle in cyanobacteria, the gene encoding 2-oxoglutarate decarboxylase (SYNPCC7002_A2770) was deleted and replaced by a DNA fragment encoding an antibiotic resistance gene (*aphAII*, kanamycin resistance), the generated strain was denoted as Δ 2770-GAD-Ex. Primer sets A2770D1-A2770D2 and A2770D3-A2770D4 (Table 3-1) were used to amplify the upstream and downstream regions of SynPCC7002_A2770. Transformation and selection were performed as previously described (Frigaard et al., 2004). Full segregation of the deletion of SYNPCC7002_A2770 was verified by PCR by comparing the products of template DNAs from both the wild type and the mutant strains using primer set A2770D1-A2770D4.

2.4) Strains, growth conditions and culture preparation

All strains were maintained in liquid media A⁺ (Stevens et al., 1973) containing 10 mM nitrate and supplemented with desired antibiotics. Antibiotics were used in the

following concentrations when appropriate: spectinomycin ($50 \mu\text{g ml}^{-1}$), kanamycin ($100 \mu\text{g ml}^{-1}$), gentamycin ($20 \mu\text{g ml}^{-1}$) and erythromycin ($20 \mu\text{g ml}^{-1}$). Cultures were grown photoautotrophically at a standard condition: light intensity of $120 \mu\text{E}$, temperature at 38°C , and being sparged with 2% (v/v) CO_2 in air, except the two mutant strains of succinyl-CoA synthase (SucCD): ΔA9091 and $\Delta\text{A1094A7071A9091}$. We were unable to grow these two strains under high CO_2 environment by sparging 2% CO_2 . As a result, these two strains were grown by slowly bubbling with 1% CO_2 in air. Growth of *Synechococcus* 7002 was determined by measuring light scattering at 730 nm ($\text{OD}_{730 \text{ nm}}$) with a spectrophotometer.

To prepare cultures for central carbon metabolite analysis, all mutant strains were grown under the same photoautotrophic condition with WT until reaching an $\text{OD}_{730 \text{ nm}}$ of ~ 0.6 . Then, 2 mL of photoautotrophic cultures of all strains were harvested and extracted for metabolomic analysis following the previously described protocol (Bennette et al., 2011). After being sampled for the photoautotrophic metabolomic analysis, all cultures were quickly wrapped with foil paper and kept in a dark growth chamber for 3 hours. The temperature in the dark growth chamber temperature was 38°C . The caps on the culture flasks were left loose so that the cultures inside could stay aerobic. After the 3-hour dark aerobic incubation, cultures were sampled for dark aerobic metabolomic analysis following the same protocol (Bennette et al., 2011).

To prepare cultures for the ^{13}C labeling experiment under photoheterotrophic condition, WT strain was pre-acclimated to A^+ media supplemented with 5 mM glycerol. $^{13}\text{C}_3$ -labeled glycerol was used to conduct this experiment, as *Synechococcus* 7002 was reported capable of utilizing glycerol but not glucose as external reduced carbon source

(Shen et al., 1995). Before the experiment, 100 mL of WT culture was photoheterotrophically grown to an OD_{730nm} of ~ 1.0 . 500 μL of the $^{13}\text{C}_3$ -labeled glycerol stock (1 M) was added immediately after the T_0 sample ($t = 0$ s) was taken. Sampling continued for T_1 ($t = 30$ s), T_2 ($t = 1$ min), T_3 ($t = 10$ min), T_4 ($t = 20$ min), and T_5 ($t = 40$ min). Immediately after the T_5 sample was taken, the culture container was wrapped in foil paper and placed in a dark growth chamber. The purpose of this switch was to identify the carbon source used by *Synechococcus* 7002 at dark aerobic condition in the presence of an external reduced carbon source. Sampling at T_6 ($t = 45$ min), T_7 ($t = 60$ min), and T_8 ($t = 90$ min) took place under dark aerobic condition.

2.5) Intracellular metabolites analysis

Metabolite extraction and quantification was performed as previously described (Bennette et al., 2011). Briefly, 2 mL of cells were rapidly sampled and vacuum-filtered on a 0.45- μm membrane filter under dark conditions. Filtered cells were then quickly quenched in 1.8 mL of ice-cold quenching buffer (80:20 (v/v) MeOH/H₂O) in clean Petri dishes. Quenched samples were then incubated at -20 °C for 20 min. Cell materials was then scraped off from the membrane filters, and the solvent with cell materials was centrifuged at 14,000 x g at 4 °C for 5 min. The supernatant was removed and stored at -80 °C. 120 μL of solvent was vacuum-dried (Labconco Centri-Vap Concentrator), and the pellet was resuspended in 40 μL LC-MS grade water for analysis. The LC-MS analysis system and methods were described previously (Bennette et al., 2011). Extracellular metabolite profiles were analyzed by HPLC according to the protocol as previously described (Kumaraswamy et al., 2013).

2.6) Determination of intracellular SSA in *Synechococcus* 7002

Synechococcus 7002 WT cultures were grown to $OD_{730} \sim 0.6$, and then 15 mL of culture per sample was collected before and after incubation under dark aerobic condition for 3 hours. 15 mL of culture was spun down at 7500 rpm at 4 °C for 15 min, and then the supernatant was discarded. Cell pellets were then resuspended in 500 μ L of autoclaved ice-cold water, and sonicated for 15 times each over ice (with each pulse lasting 10 seconds) using a Fisher Scientific sonicator with an amplitude of 40%. The sonicated samples were then centrifuged at 14,000 $\times g$ at 4 °C for another 5 min. Supernatants (500 μ L per sample) were collected and transferred into new Eppendorf tubes. In order to detect SSA using LC-MS, SSA was derivated with 2,4-dinitrophenylhydrazine (DNPH) based a method adapted from Struys et al. (2005). Briefly, 50 μ L of DNPH (3.1 mg/mL in 2 mol/L hydrochloric acid) was added into 500 μ L of sample supernatant and SSA calibrators (concentrations at 0, 0.01, 0.05, 0.1, 0.5, and 1 mM), and the reaction mix was incubated for 15 min at room temperature. The SSA derivatives were extracted with 3 mL of ethyl acetate, with the organic fraction being transferred to new glass tubes and dried with a stream of nitrogen gas. The dry residue was dissolved in 125 μ L of methanol (100%), and 10 μ L liquid per sample was injected into the LC-MS/MS system for analysis. Mass transitions were set to be m/z -281.1 \rightarrow m/z -182.1 and m/z -285.1 \rightarrow m/z -182.1 for $^{13}C_0$ -SSA (M_0) and $^{13}C_4$ -SSA (M_4), respectively.

2.7) O₂ evolution rate, dark respiration rate, and Chlorophyll-a concentration measurement

Liquid cultures of WT and mutant strains were grown to OD_{730nm} at ~ 0.6, and harvested to measure their maximal O₂ evolution rates under saturating red light (~750 $\mu\text{E m}^{-2} \text{s}^{-1}$), and dark respiration rates. Both rates were measured using both O₂ rate and concentration type electrodes. 25 mM of bicarbonate was supplemented before each O₂ evolution rate measurement to provide sufficient inorganic carbon source as the electron sink of photo-reactions. Chlorophyll *a* concentrations were measured according to the colorimetric method previously described (Sakamoto et al., 1997).

3. Results

3.1) Determination of SSA-DNPH derivates

Because SSA is unstable in air (Wermuth et al., 1979), SSA extracts from cyanobacteria cannot be handled by previously described method (Bennette et al., 2011), which has an evaporation and concentration step in air. By adapting to a SSA derivatization method that was originally used to treat SSA in human urine fluid (Struys et al., 2005), we are now capable of quantifying intracellular SSA in the cyanobacterium *Synechococcus* 7002. On the chromatogram of 2.5 mM SSA standard, only one peak appeared at 14.1 min (Figure 3-3 A). However, on the chromatogram of WT extracts, other than the peak at 14.1 min, three additional peaks appeared at 12.7 min, 14.4 min and 14.9 min. The calibration curve was linear over the range 0-1.0 mM for SSA-DNPH derivates, with a linear regression (R^2) of 0.99 (Figure 3-3 B). Decomposition MS/MS spectra of SSA-DNPH shows an intense fragment of m/z -182.1, which corresponds to the loss of the DNPH group from SSA-DNPH. Therefore, some of these additional peaks may originate from several other metabolites that have similar molecular weight to SSA and are capable of forming derivates with DNPH in *Synechococcus* 7002.

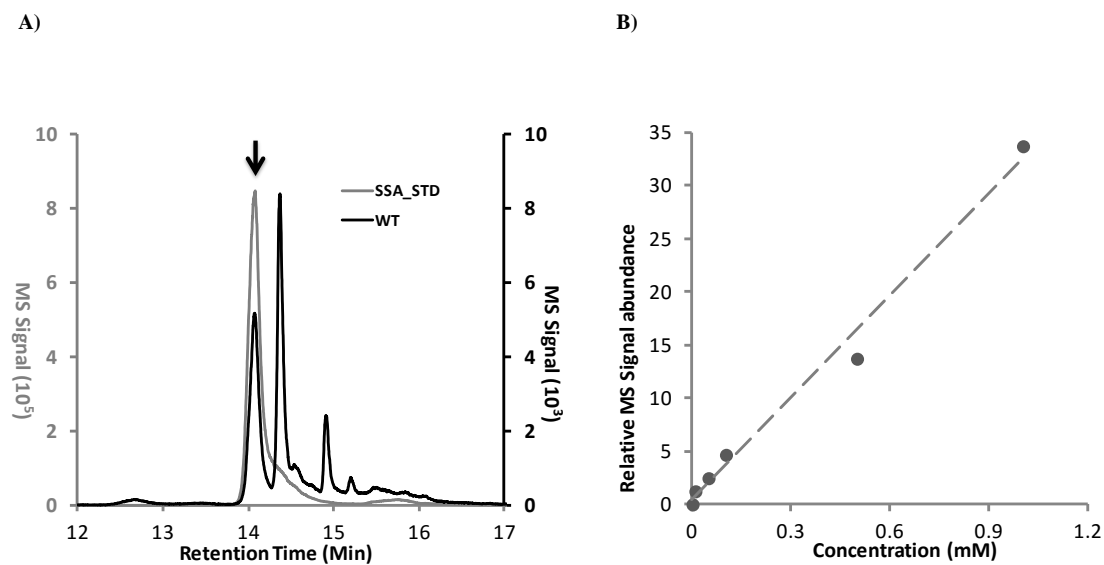


Figure 3-3 LC-MS method to determine intracellular SSA contents. A. Comparison of chromatograms of WT (black line) and 2.5 mM SSA standard (grey line). Black arrow indicates the peak of SSA. B. Standard curve of SSA within the concentration range of 0~1.0 mM, $R^2 = 0.99$.

3.2) ^{13}C labeling of SSA under light and dark conditions

The level of ^{13}C labeling of intracellular SSA was determined by the $[\text{}^{13}\text{C}_4\text{-SSA}] / [\text{}^{13}\text{C}_0\text{-SSA}]$ ratios (M_4 / M_0) over time (Figure 3-4 A). Other labeled forms (M_1 , M_2 and M_3) of SSA were not accounted because we observed a huge noise signal at the same retention time of the mass transition of $^{13}\text{C}_2\text{-SSA}$. To completely eliminate the noise effect, the mass spectra signals of $^{13}\text{C}_1\text{-SSA}$ and $^{13}\text{C}_3\text{-SSA}$ were also omitted, as these two transition forms have only 1 m/z value away from $^{13}\text{C}_2\text{-SSA}$, and might carry over some noise signals from $^{13}\text{C}_2\text{-SSA}$. M_4 / M_0 value started to increase immediately after the addition of ^{13}C -labeled glycerol (Figure 3-4 A). M_4 / M_0 value reached 0.25 before the culture was switched to dark aerobic incubation at the 40th minute. During dark aerobic incubation, the M_4/M_0 value slowly decreased, and dropped to 0.15, 50 minutes after the light-dark transition.

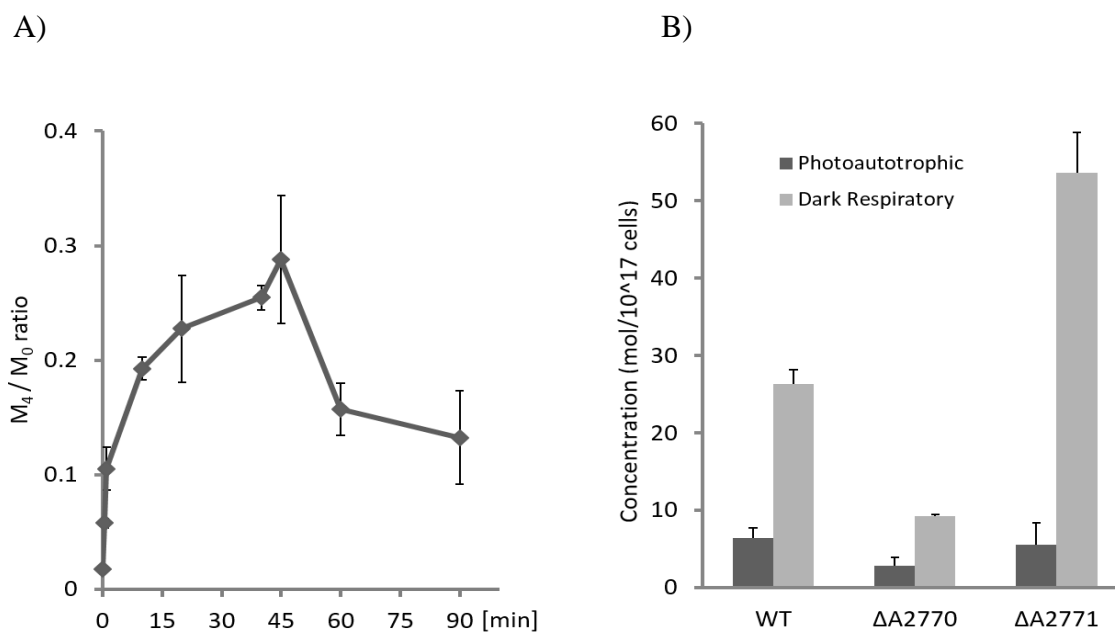


Figure 3-4 Quantification of intracellular SSA. **A.** ^{13}C labeling kinetics of SSA under photoheterotrophic condition. The arrow indicates the time point when culture was switched from light to dark. **B.** Intracellular SSA contents of WT, $\Delta A2770$, and $\Delta A2771$ under photoautotrophic and dark aerobic conditions. The results are mean values of three biological replicates and error bars represent standard deviations.

3.3) Intracellular metabolite analysis of TCA cycle mutants

The differences of SSA contents among WT and the two SSA route single-mutation strains ($\Delta A2770$ and $\Delta A2771$) were monitored under both photoautotrophic and dark aerobic conditions. Under photoautotrophic condition, WT had 2-fold more SSA than the $\Delta A2770$ strain, but had comparable SSA content to the $\Delta A2771$ strain. However, after 3 hours of dark aerobic incubation, compared to WT, the $\Delta A2771$ strain accumulated 2-fold more SSA, while the $\Delta A2770$ strain had a 2.5-fold decrease of SSA (Figure 3-4 B). These results confirm that 2-oxoglutarate decarboxylase (SynPCC7002_A2770) is functional under both photoautotrophic condition and dark aerobic condition. The increased accumulation of SSA under dark aerobic condition in each of these strains also suggested that a larger metabolic flux is carried through the complete TCA cycle under such conditions.

Intracellular contents of four key TCA carbon metabolites (citrate, 2-OG, succinate, and malate) in all mutants listed in the figure were compared to these of WT (Figure 3-5). Mutants were categorized into three “block side” groups: oxidative, reductive and both. The “block side” indicates the location(s) of the knocked-out enzyme(s) on the TCA cycle, using citrate-succinate as the dividing line (dashed line in Figure 1, right side: oxidative; left side: reductive). In the two “oxidative” group strains, $\Delta A2770$, and $\Delta A2771$, succinate contents were significantly reduced compared to WT levels, under both light and dark conditions. Under photoautotrophic condition, 2-OG content in the 2-OGDC knockout strain, $\Delta A2770$, accumulated by 2.3-fold, while remaining at a similar level in the $\Delta A2771$ strain, compared to WT. After 3-hour’s dark aerobic incubation, 2-OG contents in both mutant strains were 2-fold higher than in WT.

In the succinyl-CoA synthase (SucCD) knockout strain, $\Delta A9091$, succinate and malate contents reduced to ~60% of WT levels under photoautotrophic condition, and decreased further to ~40% of WT levels under dark aerobic condition.

In the two “reductive” group strains, $\Delta A1094$ and $\Delta A2569$, succinate contents were 2.2-fold and 2.6-fold higher than WT, respectively, under photoautotrophic condition. Succinate accumulation in these two strains was further exacerbated (9.4-fold and 13.0-fold higher than WT, respectively) under dark aerobic condition. Malate contents were significantly reduced in the $\Delta A2569$ strain under both conditions, while remaining at similar levels to WT in the $\Delta A1094$ strain. In one “both” group strain, $\Delta A2569A7071$, 2-OG and succinate remained at similar levels to WT, while malate contents decreased at both conditions. In another “both” group strain, $\Delta A1094A7071A9091$, 2-OG and succinate contents were 4.3-fold and 2.0-fold higher than WT, respectively, under photoautotrophic condition. Such increments in pool sizes diminished after the mutant strains were dark aerobically incubated.

		Photoautotrophic			
Strains	Block Side	Citrate	2-oxoglutarate	Succinate	Malate
WT	None	1	1	1	1
Δ A2771	Oxidative	0.8	1	0.5	0.7
Δ A2770	Oxidative	0.7	2.3	0.2	0.5
Δ A1094	Reductive	0.8	0.9	2.2	1.4
Δ A2569	Reductive	1	0.4	2.6	0.2
Δ A2569A7071	Both	0.6	0.8	1	0.3
Δ A9091	Oxidative	1	1.7	0.6	0.7
Δ A1094A7071A9091	Both	0.8	4.3	2	0.7

		Dark aerobic			
Strains	Block Side	Citrate	2-oxoglutarate	Succinate	Malate
WT	None	1	1	1	1
Δ A2771	Oxidative	0.8	2	0.2	0.7
Δ A2770	Oxidative	0.8	2.1	0.2	0.1
Δ A1094	Reductive	0.6	1.3	9.4	0.6
Δ A2569	Reductive	0.7	0.8	13	0.2
Δ A2569A7071	Both	0.5	1.4	1.3	0.2
Δ A9091	Oxidative	1.1	1.1	0.4	0.4
Δ A1094A7071A9091	Both	0.9	0.9	1.4	0.8

Figure 3-5 Metabolites profiling of TCA cycle metabolites in mutant strains. Category “block side” refers to the side of the TCA cycle (reductive side and oxidative side) that hypothetically prevent the synthesis of succinate due to the corresponding mutation(s). Grey bars indicate the fold changes of these metabolites compared to WT levels.

3.4) Growth phenotypes and succinate levels in mutant strains

All four single mutant strains ($\Delta A2770$, $\Delta A2771$, $\Delta A1094$, $\Delta A2569$) showed reduced photoautotrophic growth rates compared to WT (Table 3-2). Coincidentally, chlorophyll *a* contents and O₂ evolution rates of these mutant strains were lower than those of WT (Table 3-2). Dark respiration rates of $\Delta A1094$ and $\Delta A2569$, the two mutant strains lacking a complete succinate dehydrogenase (SDH) enzyme complex, were reduced more than 44% compared to WT. On contrary, disruptions in the SSA route caused less or no respiratory deficiency in the corresponding mutant strains ($\Delta A2770$ and $\Delta A2771$).

Under both photoautotrophic and dark aerobic conditions, succinate pool size increased when either SDH subunit was deleted, and decreased when the SSA route was disrupted (Figure 3-5). Such results indicate that, under photoautotrophic and dark aerobic conditions, 1) removal of either subunit of SDH complex abolishes the enzyme activity of SDH; 2) the SSA route is functional *in vivo*; and 3) oxidative TCA cycle (clock-wise direction of Figure 3-1) is dominant over the reductive TCA cycle in the biogenesis of succinate (counter clock-wise direction of Figure 3-1). Additionally, accumulation of succinate by 2~3-fold was observed in *Synechocystis* sp. PCC 6803 when 2-oxoglutarate (2-OG) was externally fed into the growth media of a *ΔsdhB* mutant (Cooley et al., 2000; Cooley et al., 2001), which corroborates well with our findings stated above.

Strain	Doubling Time (h)	Chl <i>a</i> content ($\mu\text{g} / 10^8$ cells)	O₂ Evolution Rate (nmol/μg Chl <i>a</i>/h)	O₂ Respiration Rate (nmol/10^8 cells/h)
WT	3.2 \pm 0.3	12.1 \pm 0.5	871 \pm 35	892 \pm 68
ΔA2770	3.8 \pm 0.2	10.2 \pm 0.3	654 \pm 15	685 \pm 2
ΔA2771	3.6 \pm 0.2	9.6 \pm 0.4	703 \pm 31	798 \pm 34
ΔA1094	3.9 \pm 0.1	9.0 \pm 0.3	689 \pm 29	537 \pm 3
ΔA2569	3.7 \pm 0.1	8.8 \pm 0.5	586 \pm 23	482 \pm 25

Table 3-2 Growth rates, Chl *a* contents, oxygen evolution and respiration rates of mutant strains.

3.5) GABA shunt enzymatic assays

The glutamate decarboxylase (sll1641) and N-acetylornithine aminotransferase (slr1022) of *Synechocystis* sp. PCC 6803, as well as the N-acetylornithine aminotransferase (SYNPCC7002_A0326) of *Synechococcus* sp. PCC 7002 were successfully expressed and purified from *E. coli* as an N-terminally poly-[His]₆-tagged protein. The purified proteins were positively immunoreactive with commercial antibodies to the poly-[His]₆ tag (Figure 3-6 A), and the purified proteins were further confirmed by tryptic peptide mass fingerprinting.

The enzyme activity of glutamate decarboxylase was firstly characterized. When the protein product from ORF sll1641 was incubated with glutamate, GABA was produced and glutamate was consumed (Figure 3-6 B). This biochemical result established that *sll1641* encodes glutamate decarboxylase and catalyzes the conversion of glutamate to GABA. The enzyme activity of N-acetylornithine aminotransferase was also assayed. When the protein product from ORF slr1022 or ORF SYNPCC7002_A0326 was incubated with L-ornithine and 2-OG, glutamate was produced (Figure 3-6 C), which validated the enzyme activity of N-acetylornithine aminotransferase. Because it was suggested that N-acetylornithine aminotransferase could also function as GABA aminotransferase, the potential activity for GABA aminotransferase was also characterized. When the protein product from ORF slr1022 or ORF SYNPCC7002_A0326 was incubated with GABA and 2-oxoglutarate, glutamate was also produced in the reaction mixture (Figure 3-6 D). These biochemical results established that N-acetylornithine aminotransferase is a bi-functional enzyme that has both N-acetylornithine aminotransferase and GABA aminotransferase activities.

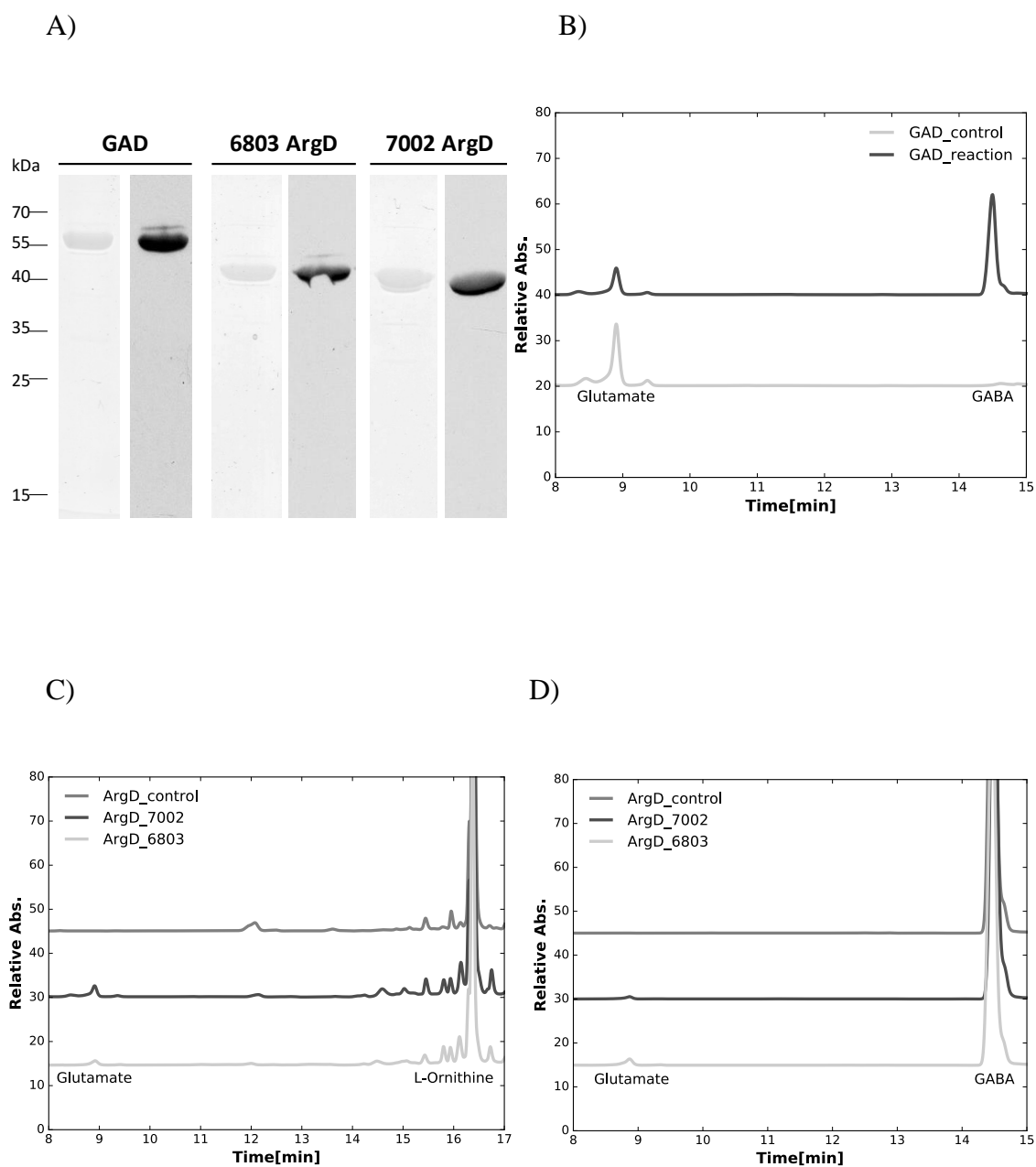


Figure 3-6 Characterizations of purified recombinant proteins. A: Purified recombinant proteins of the glutamate decarboxylase (GAD), and the acetylornithine aminotransferase from both *Synechocystis* sp. PCC 6803 (6803 ArgD) and *Synechococcus* sp. PCC 7002 (7002 ArgD) were analyzed. Left lanes for each enzyme were stained with Coomassie blue and right lanes were detected by immunoblotting with antibodies to the poly-[His]₆

tag. B: HPLC analysis showing the conversion of glutamate to GABA, catalyzed by the purified glutamate decarboxylase (GAD_reaction). C: HPLC analysis showing the formation of glutamate from L-ornithine catalyzed by the purified acetylornithine aminotransferase from both *Synechocystis* sp. PCC 6803 (ArgD_6803) and *Synechococcus* sp. PCC 7002 (ArgD_7002). D: HPLC analysis showing the formation of glutamate from GABA catalyzed by the purified acetylornithine aminotransferase from both *Synechocystis* sp. PCC 6803 (ArgD_6803) and *Synechococcus* sp. PCC 7002 (ArgD_7002), demonstrating that acetylornithine aminotransferase can also function as GABA aminotransferase. Control experiments in all these assays were performed the same way without recombinant proteins added.

3.6) Construction of glutamate decarboxylase expression strains

Our *in vitro* biochemical results validated the GABA shunt enzyme activities, and they are thus possibly functional in some cyanobacteria such as *Synechocystis* 6803. However, the apparent absence of glutamate decarboxylase in most cyanobacteria (e.g., *Synechococcus* 7002) suggested that the GABA shunt is not universally present in cyanobacteria. To investigate the possible role of the GABA shunt in the metabolic contents of cyanobacteria, a glutamate decarboxylase expression strain of *Synechococcus* 7002 was constructed, in which the glutamate decarboxylase (*sll1641*) from *Synechocystis* 6803 was expressed under the strong *cpcBA* promoter. The presence of the plasmid and the incorporation of the *sll1641* gene into *Synechococcus* 7002 was verified by PCR amplification of the *sll1641* operon (Figure 3-7 A) and was further confirmed by sequencing the amplicon. Successful expression of glutamate decarboxylase was also confirmed by immunoblotting using antibodies against His₁₀-tag, as shown in Figure S2B. Additionally, gene encoding 2-oxoglutarate decarboxylase (SYNPCC7002_A2770) was also deleted in the GAD-Ex strain. Complete deletion of SYNPCC7002_A2770 was validated using PCR with primer set A2770D1-A2770D4, as shown in Figure 3-7 C.

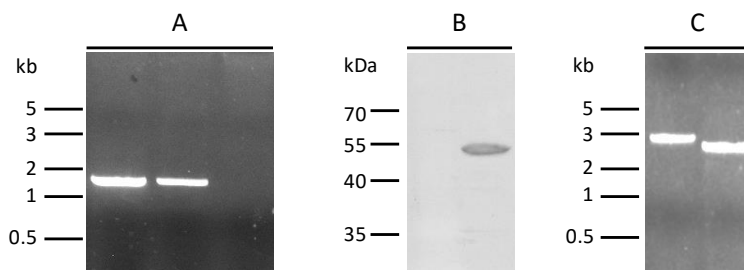


Figure 3-7 Verification of the constructed GABA shunt mutant strains. A: Verification of the presence of glutamate decarboxylase gene. The template DNA was derived from wild-type *Synechococcus* sp. PCC 7002 (right lane), from wild-type *Synechocystis* sp. PCC 6803 (middle lane), and from the recombinant strain GAD-Ex (left lane), which has the *sll1641* gene from *Synechocystis* sp. PCC 6803 inserted in plasmid pAQ1-Ex. B: Immunoblotting of whole cell extracts of *Synechococcus* sp. PCC 7002 wild type (left lane) as well as GAD-Ex strain (right lane) with antibodies to His₁₀-tag, demonstrating the successful expression of glutamate decarboxylase. C: Agarose gel electrophoretic analysis of amplicons from PCR reactions using primer set A2770D1-A2770D4, verifying the fully deletion of SYN-PCC7002_A2770, using DNA template from Δ 2770-GAD-Ex strain (right lane) or GAD-Ex strain (left lane)

3.7) Metabolic profiling of glutamate decarboxylase expression strains

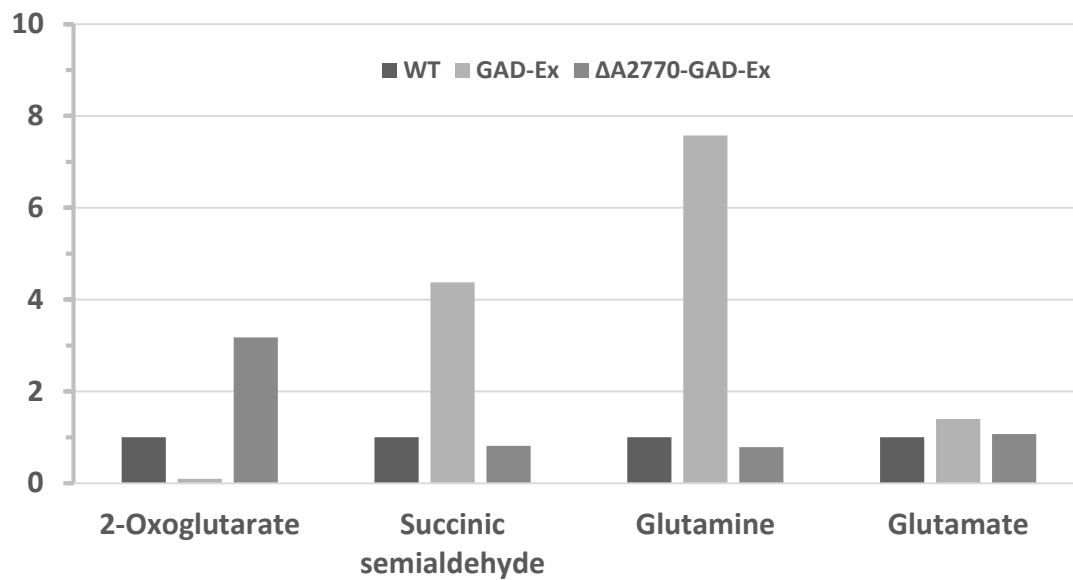
Metabolic profiling of the above constructed strains was performed as described in the Materials and Methods. In the GAD-Ex strain, 2-OG level reduced to about 10% of wild type (WT) level, while SSA pool is 4.4-fold higher than WT under photoautotrophic growth condition. In addition, glutamine and glutamate concentrations were also higher (7.8-fold, and 1.4-fold) in the GAD-Ex strain than WT. These results indicated that 2-OG was drained by both the TCA cycle and the GABA shunt, which could then lead to higher accumulation of SSA and glutamine/glutamate (Figure 3-6 A).

In the $\Delta A2770$ -GAD-Ex strain, 2-oxoglutarate accumulates to higher level (3.2-fold) while SSA, glutamine and glutamate remain at close levels when compared to WT under photoautotrophic conditions. Additionally, in the $\Delta A2770$ strain, it was shown that SSA content was 2-fold lower (Figure 3-4 B). Therefore, it is clearly that in the $\Delta A2770$ -GAD-Ex strain, where 2-oxoglutarate decarboxylase is absent, hetero-expressed GAD enables 2-oxoglutarate being converted to SSA, through the GABA shunt. However, 2-oxoglutarate still accumulated to higher level in the $\Delta A2770$ -GAD-Ex strain, indicating that the GABA shunt is less efficient in converting 2-oxoglutarate to SSA, compared with 2-oxoglutarate decarboxylase (Figure 3-8 A).

After these two strains were incubated in dark aerobic condition for 3 hours, SSA concentration in the GAD-Ex strain became similar to WT. However, higher (1.7-fold) amount of 2-oxoglutarate was still accumulated in the $\Delta A2770$ -GAD-Ex strain, while 2-oxoglutarate concentration was lower (0.7-fold) in the GAD-Ex strain, when compared to WT (Figure 3-8 B). These metabolite changes also suggest that GABA shunt is not as

efficient as 2-oxoglutarate decarboxylase in converting 2-OG to SSA in *Synechococcus* 7002. Interestingly, higher levels of glutamine and glutamate were still observed in the GAD-Ex strain under dark aerobic condition.

A)



B)

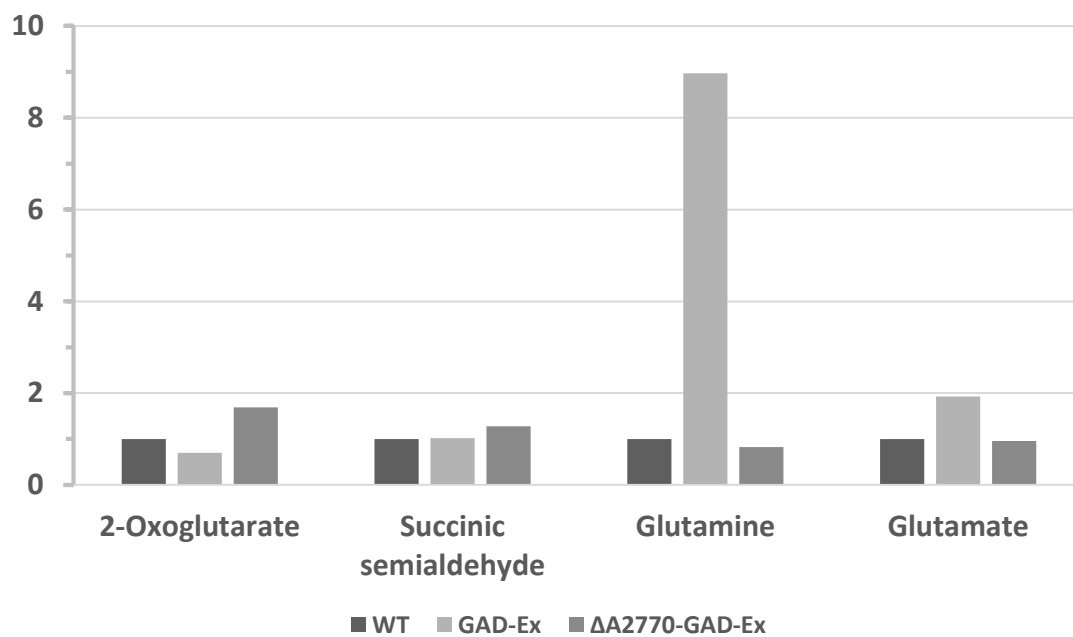


Figure 3-8 Metabolites profiling of GABA shunt mutant strains. Relative metabolites concentrations in GAD-Ex and $\Delta 2770$ -GAD-Ex strains, under photoautotrophic conditions (A) or dark aerobic conditions (B). Relative concentrations for each metabolite in wild type *Synechococcus* sp. PCC 7002 (WT) under these growth conditions were set to 1 unit for comparison.

4. Discussion

In this study, we measured and compared pool sizes of SSA in WT and the two SSA route single-knockout mutants ($\Delta A2770$ and $\Delta A2771$) under photoautotrophic and dark aerobic conditions. SSA accumulated when the efflux enzyme was removed ($\Delta A2771$), and depleted when the influx enzyme was removed ($\Delta A2770$), which indicates this SSA route is operating when cells respire in the dark. SSA did not accumulate in the $\Delta A2771$ strain under the photoautotrophic condition, which suggests the SSA route is less active under photoautotrophic conditions than dark aerobic conditions. 2-fold and 4-fold increments in the transcripts abundance of SynPCC7002_A2770 and SynPCC7002_A2771, respectively, under dark aerobic condition also suggest the metabolic importance of the SSA route at such growth condition (Ludwig et al., 2011). The finding that SSA route operates during dark aerobic respiration is further supported by the metabolomic data shown in Figure 3-5. When $\Delta A2770$ and $\Delta A2771$ were dark aerobically incubated for 3 hours, downstream metabolites of the SSA route (succinate and malate) further depleted compared to WT, while upstream metabolite (2-OG) further accumulated.

We also used ^{13}C -glycerol to study if SSA route operates under photoheterotrophic condition. ^{13}C -carbon rapidly incorporated into SSA after the ^{13}C -glycerol was fed to the WT culture under photoheterotrophic growth condition. Although we cannot fully uncover the labeling kinetics of SSA due to the contamination chromatogram peak of the M_2 transition, the M_4/M_0 ratio (Figure 3-4 A) indicates that at least 20% of the carbon molecules in SSA have been labeled within 40 min. This observation suggests that the SSA route is utilized as one major route to convert 2-OG

into the downstream metabolites, rather than what has been observed in a ^{13}C -metabolic flux analysis study in *Synechocystis* 6803 that carbon flux through SSA route is minimal under photoheterotrophic condition (You et al., 2014). M_4/M_0 ratio decreases after the onset of dark aerobic condition. Under dark aerobic condition, cells could oxidize the extracellular carbon source (glycerol), intracellular carbon storage (glycogen) or both carbon sources to generate ATP. The dropping M_4/M_0 ratio could be caused by a reduced glycerol catabolism or an increased glycogen catabolism, which leads to a reduced fraction of ^{13}C -carbons entering into the SSA route.

Based on previous flux balance analysis (FBA) simulation results, the SSA route was shown to operate at a negligible flux rate cyanobacteria under photoautotrophic condition (Knoop et al., 2013). However, reduced photoautotrophic growth of knockout mutants of SSA route ($\Delta A2770$ and $\Delta A2771$) were observed previously (Zhang & Bryant, 2011) and confirmed in this study (Table 3-2). Coincidentally, reduced chlorophyll *a* contents and oxygen evolution rates of these two knockout mutants were also observed, which appears to be responsible for the reduced photoautotrophic growth. Deletion of the SSA route may reduce the availability of some unknown metabolites that are essential for building effective photosynthetic machinery in *Synechococcus* 7002.

$\Delta A2569A7071$ had a similar pool size of succinate compared to WT, which contradicts to our expectation that this triple knockout strain does not produce any succinate, as the SDH and the SSA route are both blocked. Three TCA cycle variants would produce succinate as an intermediate metabolite: 1) the SSA route, 2) the GABA shunt, and 3) the glyoxylate cycle (Steinhauser et al., 2012). However, proteins required to complete the GABA shunt, glutamate decarboxylase (GAD), and the glyoxylate shunt,

isocitrate lyase (ICL) and malate synthase (MS), are all absent in *Synechococcus* 7002 (Zhang & Bryant, 2015). Thus, there must be an additional alternative route to produce succinate in *Synechococcus* 7002. Although it is well known that 2-OGDH is absent in all cyanobacteria, succinyl-CoA synthase (encoded by *A0890* and *A0891*) can still convert succinate-CoA into succinate. Succinyl-CoA can be potentially produced from the valine, leucine and isoleucine degradation pathway (KEGG database). Pool sizes of succinate and malate were significantly reduced in the $\Delta A9091$ strain (Figure 3-5), which supports this hypothesis. Nonetheless, even if we blocked all the reductive (SDH) and oxidative (2-OGDC + SSADH and SucCD) branches, intracellular succinate concentration in $\Delta A1094A7170A9091$ remained at a comparable amount to WT (Figure 3-5). After searching through the metabolic network of *Synechococcus* 7002, we find that L-Aspartate oxidase (Laspo, encoded by SYNPC7002_A0301) catalyzes the conversion of L-Aspartate to iminoaspartate, using O₂ or fumarate as the electron acceptor. This biochemical reaction yields H₂O₂ or succinate, depending on the choice of electron acceptor (Bossi et al., 2002). A more quantitative fluxomic analysis will be needed to identify the flux contributions of SucCD and Laspo routes to the succinate pool in *Synechococcus* 7002 under both photoautotrophic and dark aerobic conditions.

The biochemical and metabolic characterizations of the GABA shunt in this work clarified the mystery of the occurrence of this pathway in cyanobacteria. From the point of view of FBA, the GABA shunt is stoichiometrically identical to the recently discovered TCA cycle variant using 2-OGDC and SSADH, and thus both variants should result in identical biomass yields. Interestingly, however, FBA indicates that the biomass yield using these two variants is lower than for the conventional cycle using 2-OGDH

under respiratory metabolism conditions (Knoop et al., 2013; Shastri et al., 2005). In addition, FBA also suggests that autotrophic growth was similarly reduced when metabolites were forced through the 2-OGDH complex or the 2-OGDC/SSADH bypass, but not by forced flux through the GABA shunt. Based on these findings, it has been suggested that the GABA shunt may be an evolutionary favorable solution to completing the TCA cycle (Nogales et al., 2012). This may also be the reason for the existence of the GABA shunt but not the 2-OGDC/SSADH bypass in some *Prochlorococcus* and marine *Synechococcus* species. However, our metabolic study clearly demonstrated that GABA shunt is less efficient in converting 2-oxoglutarate to SSA in the GAD-Ex strain of *Synechococcus* 7002. One likely reason might be that enzyme activities of the expressed glutamate decarboxylase are not optimal in *Synechococcus* 7002.

Genes encoding enzymes for the GABA shunt can be found in the genomes of some cyanobacteria (e.g., *Synechocystis* sp. PCC 6803, *Nostoc* sp. PCC 7107, *Prochlorococcus marinus* str. MIT 9303 and *Synechococcus* sp. RCC307). However, *Prochlorococcus marinus* str. MIT 9303 and *Synechococcus* sp. RCC307 lack the 2-OGDC/SSADH bypass, and many other *Prochlorococcus* and marine *Synechococcus* species seemingly lack the GABA shunt as well as the 2-OGDC/SSADH bypass. Such organisms either have yet another alternative bypass or must have a branched TCA cycle. Similarly, many other cyanobacteria (e.g., *Synechococcus* 7002) apparently lack the glutamate decarboxylase needed to complete the GABA shunt. Thus, unlike the SSA route, the GABA shunt seems to be only present in a few cyanobacteria and does not appear to be universal (Xiong et al., 2014). Considering the mosaic distribution of TCA cycle, the GABA shunt as well as the glyoxylate cycle in cyanobacteria, it will also be

interesting to attempt to define the evolutionary events that produced this diversity in future research.

Chapter 4: Quantitative analysis of carbon flux distributions in the
cyanobacterium *Synechococcus* sp. PCC 7002

Coauthors: Yuan Zhang, Desmond S. Lun and G. Charles Dismukes

Summary

Microorganisms alter their metabolism in response to nutrient availability, which greatly influences their productivity as cell factories. Here we investigate the repartitioning of carbon fluxes upon nitrogen deprivation, a treatment that significantly increases glycogen content at the expense of growth rate. We present the first application of ^{13}C -based isotopically nonstationary metabolic flux analysis (INST-MFA) to photoautotrophic metabolism of a cyanobacterium, *Synechococcus* sp. PCC 7002. We illustrate a semi-quantitative method based on simple first-order kinetic modeling to identify 1) qualitative changes of carbon flux distributions at three major flux branches: G6P, 3PG and AKG under nitrogen deprivation and 2) a significant portion of MAL directly synthesized through the phosphoenolpyruvate synthase reaction. Then, we conducted quantitative INST-MFA and validated all discoveries generated by the semi-quantitative method. We discovered that increased glycogen synthesis under nitrogen deprivation is caused by increased carbon flux at the $3\text{PG} \rightarrow \text{GAP/DHAP}$ step as well as at the $\text{G6P} \rightarrow \text{ADPGLUC}$ step. Additionally, our INST-MFA results showed 1) the major role of the malic cyclic route ($\text{PEP} \rightarrow \text{OXA} \rightarrow \text{MAL} \rightarrow \text{PYR} \rightarrow \text{PEP}$) for generating PYR for photoautotrophic biosynthesis; 2) significant photoautotrophic fluxes going through the SSA route ($> 6\%$ of the RuBiSCO carboxylation activity) to support optimal photoautotrophic growth; and 3) a route change of fixed $\text{CO}_2 \rightarrow$ glycogen from conventional gluconeogenesis to a hybrid gluconeogenesis-pentose phosphate (hGPP) pathway. These findings bring the field multiple new concepts in the biology of photosynthetic growth in cyanobacteria.

1. Introduction

Cyanobacteria are currently being investigated as platforms for biotechnological applications, including cell factories for producing biochemicals, biomass for feedstocks, and wastewater treatment (Abed et al., 2009). A recently discovered fast growing cyanobacterium, *Synechococcus elongates* UTEX 2973, is particularly promising for biotechnological applications. This cyanobacterium has the fastest photoautotrophic doubling time on record (2.3 hours), and can be genetically modified with ease (Yu et al., 2015). However, cyanobacteria are a metabolically diverse group of microorganisms and their productivity for making desired products depends on understanding how to disrupt and control carbon flux distributions.

Measurements of the amounts of consumed initial substrates (CHNOPS elemental precursors, e.g. glucose, CO₂, etc.) and of the major terminal product yields (lipids, storage carbohydrates, proteins, pigments, etc.) gives steady-state pool sizes, but does not provide information on the instantaneous fluxes that dictate where rate-limiting kinetic bottlenecks are located. By feeding cultures with ¹³C-labeled substrates and analyzing the ¹³C metabolite labeling patterns under the steady intracellular condition, more useful information can be obtained, such as qualitative or semi-quantitative changes in pathway contributions under different growth conditions (Buescher et al, 2015; Hasunuma et al., 2013; Huege et al., 2011). However, in order to determine actual fluxes through individual metabolites, to identify the active pathways that control (regulate) the metabolic network, and thus identify enzymatic targets for control, we require more quantitative and comprehensive knowledge of carbon fluxes. Metabolic flux analysis (MFA) is a mathematical methodology that can provide such comprehensive quantitative

data (Wiechert 2001; Wittmann 2002; Tang et al., 2012). MFA associates several parameters with a biochemical network, and then computes the flux rates of all reactions in the metabolic map that are in best agreement with the measured data. MFA uses as input: steady-state ^{13}C labeling patterns, metabolite pool sizes and excretion rates, nutrients uptake rates, cellular growth rates, and cellular biomass compositions. MFA has been applied in microbial organisms to measure carbon flux distributions under heterotrophic or mixotrophic conditions (Beste et al., 2011; Alagesan et al., 2013). Photoautotrophs however assimilate carbon solely from CO_2 and yield a uniform steady-state ^{13}C -labeling pattern of all metabolites that cannot be used by conventional MFA to compute global carbon fluxes. Shastri & Morgan (2007) first proposed a theoretical design for ^{13}C MFA experiments applicable to photoautotrophic microorganisms that suggests using ^{13}C -labeling patterns during the isotopically transient period. Young et al. (2011) named the method isotopically nonstationary metabolic flux analysis (INST-MFA). The INST-MFA method uses the transient measurements of isotope incorporation following a step change from unlabeled to labeled CO_2 to map carbon fluxes under the photoautotrophic condition, which is different from the conventional MFA method that uses steady-state ^{13}C -labeling patterns of metabolites. Actual photoautotrophic ^{13}C flux data from a freshwater cyanobacterium, *Synechocystis* sp. PCC 6803 (hereby *Synechocystis* 6803), were first published by Young et al. (2011). Using the INST-MFA method, these authors discovered inefficiencies in photoautotrophic growth due to the oxidative pentose phosphate (OPP) pathway and malic enzyme activity. A second INST-MFA study on *Chlamydomonas reinhardtii* under photoautotrophic condition focused on demonstrating a controlled photo-bioreactor system rather than retrieving valuable carbon

fluxomics data (Martzolff et al., 2012). No other INST-MFA studies of microbial photoautotrophic growth have been published since then, although the need for this information has grown.

Nutrient deprivation under photoautotrophic conditions is commonly used to increase glycogen accumulation in cyanobacteria (Schwarz & Forchhammer, 2005) and lipid content in microalgae (Nigam et al., 2011). Such desired carbon products (glycogen, starch, lipids) can be later used as substrates for biofuel production (hydrogen, methane, alcohols, biodiesel etc.), either in a native system or in a heterotrophic feeding system (Melis et al., 2001; Montingelli et al., 2015; Gao et al., 2016; Taparia et al., 2015). However, using targeted transgenic methods to achieve similar accumulation effects in cells without the consequences of severely reduced growth is preferred to increase the productivity, which is defined as the product of biomass fractions and growth rates. Therefore, scientists need to map the global metabolic changes under nitrogen deprivation to locate and then modify the enzymes responsible at these metabolic regulation sites.

In a fast growing model cyanobacterium strain *Synechococcus* sp. PCC 7002 (hereby *Synechococcus* 7002), nitrogen deprived photoautotrophic cultures have shown increased and decreased biomass composition fractions of carbohydrates (12% → 60 %) and proteins (71% → 33%), respectively (Vu et al., 2013). These changes suggest a larger assimilated CO₂ partitioning into glycogen synthesis rather than protein precursors. *Synechococcus* 7002 has a well-studied genomic database and mature transformation protocol (Frigaard et al., 2004; Xu et al., 2011). Therefore, a quantitative interpretation of global carbon flux distribution favoring glycogen synthesis under nitrogen deprivation

would help more efficiently construct a strain potentially with high glycogen productivity. Such genetic modification can then be transferred into other biological systems to achieve even better glycogen productivity.

It is possible to use ^{13}C labeling data and metabolite concentration data to estimate qualitative changes of carbon flux distributions of certain metabolic pathways without computational capabilities to conduct INST-MFA. Herein we have used a computational approach to fit all ^{13}C fluxes to transient ^{13}C -labeling kinetics of mass isotopomers to obtain an accurate determination of each flux, implemented from the method by Young et al. (2011). We compare these quantitative results to those qualitative results that require less work and are quicker to obtain to show that ^{13}C -labeling data can be interpreted and utilized both with and without the computational capabilities for full INST-MFA analysis.

Previously, several labs have reported that the carbon pool distribution patterns of photosynthetically assimilated CO_2 into storage carbohydrates, proteins and lipids is affected by nitrogen source availabilities in microalgae (Belotti et al., 2013; Qian et al., 2015; Taikhao et al., 2014; Hasunuma et al., 2013; Nigam et al., 2011). In this INST-MFA study of the cyanobacterium *Synechococcus* 7002, we discovered that increased glycogen synthesis under nitrogen deprivation is caused by increased carbon flux at the $3\text{PG} \rightarrow \text{GAP/DHAP}$ step, as well as at the $\text{G6P} \rightarrow \text{ADPGLUC}$ step. In addition, we quantified three novel metabolic processes under photoautotrophic growth which serve critical or unknown functions: 1) a novel cyclic route, $\text{PEP} \rightarrow \text{OXA} \rightarrow \text{MAL} \rightarrow \text{PYR} \rightarrow \text{PEP}$ that potentially maintains the intracellular ATP/NAD(P)H ratio; 2) significant utilization of an alternative route in the TCA cycle that synthesizes important metabolic

intermediates for biosynthesis; and 3) change of assimilatory route of $\text{CO}_2 \rightarrow$ glycogen from the conventional gluconeogenesis pathway to a hybrid gluconeogenesis-PP (hGPP) pathway under nitrogen deprivation that serves an unknown purpose.

2. Experimental Procedures

2.1) Culture growth and experimental conditions.

Wild-type *Synechococcus* 7002 was photoautotrophically grown and maintained in A⁺ medium (A medium (Stevens et al., 1973) supplemented with 10 mM of NaNO₃). Growth was determined by measuring light scattering at 730 nm (OD_{730 nm}) with a spectrophotometer. 100 mL of cultures were first grown to OD_{730 nm} ~2.0, concentrated by centrifugation, and then resuspended in 400 mL of A or A⁺ medium supplemented with 25 mM of NaH¹²CO₃ in a photo-bioreactor (Photon System Instruments, Model FMT 150/400). This photo-bioreactor operates as turbidostat, maintaining a constant cell density, and therefore a constant light intensity per cell. Prior to ¹³C labeling experiments, cultures were acclimated to the actual experimental growth condition for 24 hours. There were two experimental growth conditions in this study: 1) with 10 mM of nitrate (+N), and 2) without a nitrogen source (-N). In both conditions, the culture density was maintained at OD_{730 nm} of 0.50 ± 0.05, growth light intensity at 60 μE/m²/s, growth temperature at 38 °C, and mixed by continuous air bubbling.

2.2) Intracellular metabolite extraction and analysis.

Different extraction protocols were used for determining metabolite pool sizes and transient ¹³C-labeling patterns. For pool size measurements, 2 mL of culture were collected by centrifugation at 7,500 X g and 2 °C for 5 min, followed by decanting the supernatant and re-suspending the pellet in 600 μL of extraction solution (80% methanol in water) at -20 °C for extraction. For transient ¹³C-labeling pattern analysis, we adapted the protocol from Young et al. (2011). In brief, 5 mL of culture was withdrawn and rapidly quenched by mixing with 10 mL of 30% methanol in water at -20 °C. Quenched

samples were then centrifuged for 15 min at 7500 X g and 2 °C. The supernatant was discarded and the cell pellet was then extracted with 600 µL of extraction solution (80% methanol in water) at -20 °C. The former method has a smaller loss of metabolites during the sample handling, while the latter method achieves faster quenching that is preferred for the time sensitive ^{13}C -labeling experiments. Samples were then analyzed by the LC-MS/MS method described in Bennette et al. (2011).

2.3) Intracellular steady state validation.

That the culture remains in steady state after the injection of $\text{NaH}^{13}\text{CO}_3$ to initiate the labeling experiment is critical and is the foundation of the flux calculations. To determine valid experimental conditions, pool sizes of 12 metabolites were measured at time points of 0, 1, 2, 4, 8, and 20 minutes after the injection of 25 mM of NaHCO_3 in both the batch culture and the bioreactor culture.

2.4) Carbon labeling experiment.

To quantify fluxes of all reactions in the map, 22 metabolites were measured at +N and -N conditions to quantify pool sizes, and 17 metabolites were analyzed for labeling dynamics. Before the introduction of $\text{NaH}^{13}\text{CO}_3$, 2 mL of culture was removed for the metabolite pool size measurement, and another 5 mL of culture was extracted for the T_0 time point. Then, 10 mL of 1 M $\text{NaH}^{13}\text{CO}_3$ was injected into the bioreactor culture with rapid mixing. Subsequently, 5 mL of culture was withdrawn and rapidly quenched and measured as described above at time points of 0, 0.17, 0.5, 1, 2, 4, 8, 12, 20 and 30 minutes.

2.5) Semi-quantitative analysis.

Total ^{13}C -enrichment dynamics of each metabolite were fitted to an exponential equation $y = A_0 (1 - e^{-kt})$ to get the turnover rate of the metabolite (k), where A_0 is the maximum ^{13}C -enrichment level, and t is the time (Huege et al., 2011). Turnover rates of all metabolites were normalized to the turnover rate of 3PG so that turnover rates of the same metabolite under different conditions can be compared. Metabolite pool sizes of each metabolite were also normalized to the pool size of 3PG. Such normalization produces two sets of parameters: relative turnover rates (k_r) and relative pool sizes (Q_r). Relative flux rates (f_r) of metabolites can be computed by the equation $f_r = k_r \times Q_r$. Relative flux rates of the same set of reactions at branching points under different conditions could provide qualitative information of changes of carbon flux distributions. For example, we have a branching point metabolite A, where A can be converted into metabolite B or C ($A \rightarrow B$ or $A \rightarrow C$). If f_r of $A \rightarrow B$ increases while f_r of $A \rightarrow C$ decreases under a different condition, then we qualitatively conclude that carbon flux distributions are changed in the way favoring larger fluxes towards the synthesis of metabolite B.

2.6) Isotopically nonstationary metabolic flux analysis (INST-MFA).

We implemented the INST-MFA approach described by Young et al. (2011) in this study. This approach estimates intracellular absolute metabolic fluxes based on the isotope labeling dynamics of intracellular metabolites and measured pool sizes. There are three additional parameters other than metabolic fluxes that are estimated: unmeasured pool sizes, as pool sizes were not measured for all metabolites in the map; the ratio of $^{12}\text{CO}_2$ and $^{13}\text{CO}_2$, as we assumed that the CO_2 uptake to the cell is a mixture of $^{12}\text{CO}_2$ and

$^{13}\text{CO}_2$ in an unknown proportion; and dilution parameters for each metabolite, which represent the fraction of the metabolite that does not become labeled, as described by Young et al. (2011). These four parameters were estimated by minimizing the lack-of-fit between experimentally measured and computationally simulated mass isotopomer distributions (MIDs) using least-squares regression that attempts to minimize the sum of squared residuals. The minimization was done using the interior point algorithm implemented by the function `fmincon` in Matlab R2015b (Mathworks, Natick, Mass.) with 100 randomly selected starting points. Confidence intervals for each parameter were estimated by Monte Carlo simulation, as described by Antoniewicz et al. (2006).

3. Results

3.1) Requirement for stable cultures for INST-MFA analysis.

Batch cultures and bioreactor cultures were injected with 25 mM of NaHCO_3 , and monitored for metabolite concentration stabilities. This dilution increases the total ionic strength of the growth medium from 2.350 M to 2.375 M, and therefore the additional energy burden on cells caused by such 1% increase in medium ionic strength should be small. To ensure that CO_2 saturation is maintained during NaHCO_3 injection, we compared cultures grown in a turbidostat bioreactor to those grown in batch cultures. The turbidostat was operated to control the concentration of medium before the injection of extra NaHCO_3 . The intracellular metabolite stability test was conducted on the bioreactor culture and metabolite concentrations were found to be more stable (mostly within $\pm 20\%$ variations from the mean values) (Figure 4-1). Pool sizes of the metabolites changed more significantly in the batch culture samples (Figure S4-1). Accordingly, we used only the bioreactor growth method to conduct our INST-MFA study.

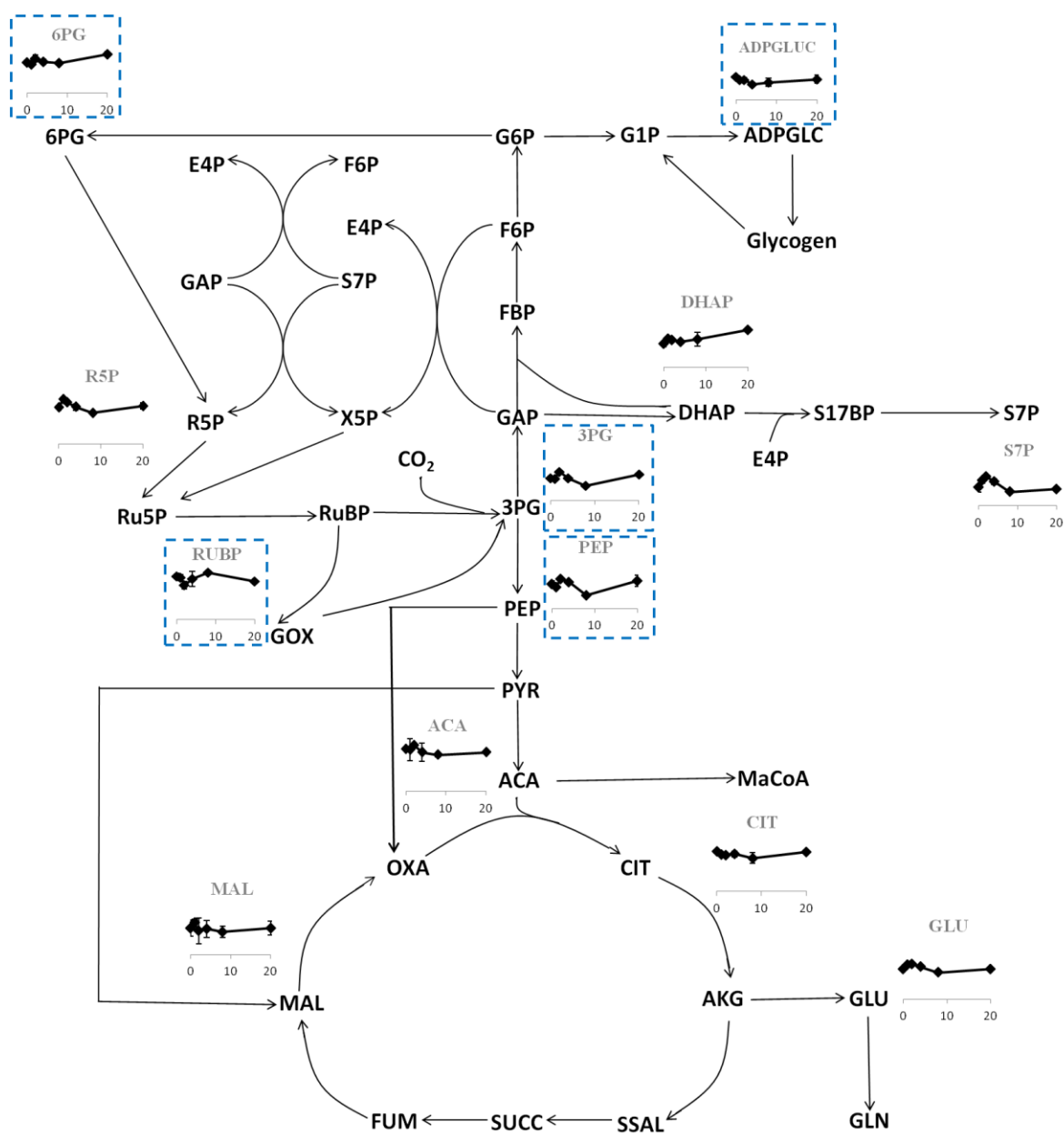


Figure 4-1 Pool size stability tests of 12 indicator metabolites of a bioreactor culture of *Synechococcus 7002*. Metabolites in semi-solid frames are ones significantly unstable in the batch culture (Figure S1) but more stable in the bioreactor culture. Cultures were supplemented with 25 mM NaHCO₃ at growth, and then spiked with 25 mM NaHCO₃ at onset of experiment. Growth light intensity was 60 $\mu\text{E}/\text{m}^2/\text{s}$. Error bars represent standard errors from 3 biological replicates.

3.2) How do carbon metabolite pool sizes change with growth conditions?

Pool sizes of 22 metabolites were measured at the beginning of each labeling experiment for both +N and -N cultures and are depicted as bar plots in Figure 4-2 and numerically tabulated in Table S4-1. These measurements provide additional fitting parameters for flux mappings, as described in the methods section. They also give a qualitative indication of altered carbon flux distributions at several particular metabolic branching points. For example, three metabolite loci drew immediate attention: 1) glycogen synthesis, 2) OPP gate, and 3) TCA-nitrogen assimilation (Figure 4-2). In the glycogen synthesis pathway, the ADPGLC pool was 10-fold higher in the -N culture. In the OPP pathway, the pool size of 6PG was 10-fold higher in the +N culture. In the TCA-nitrogen assimilation reactions, metabolites on the TCA cycle side (AKG, SUCC, and MAL) accumulated upon N deprivation, while ones on the nitrogen assimilation side (GLU and GLN) depleted (Figure 4-2).

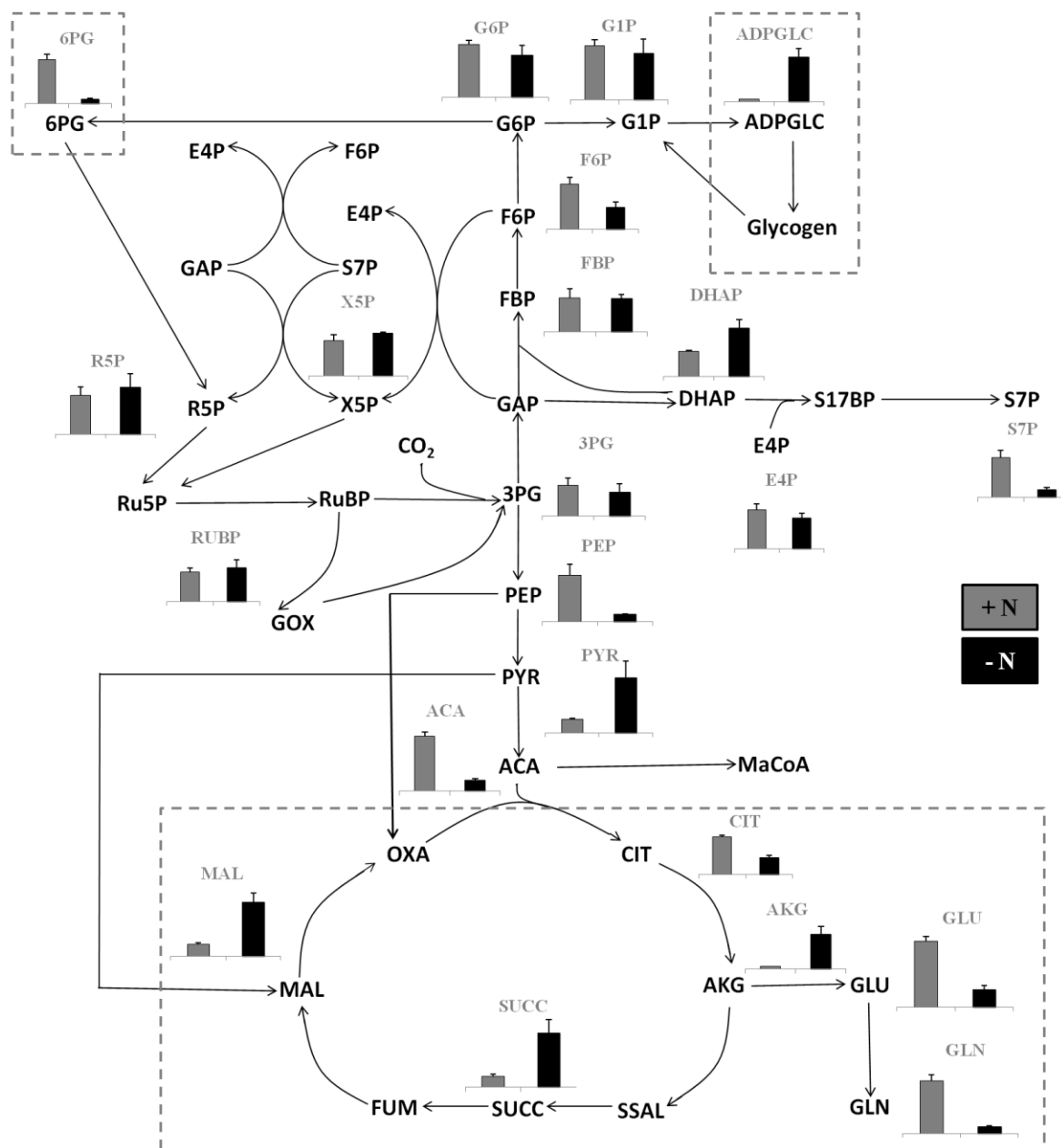


Figure 4-2 A comparison of metabolite pool sizes of photoautotrophic cultures grown with (+N) or without (-N) nitrate. Three loci are framed with grey semi-solid boxes: 1) glycogen synthesis; 2) OPP gate; and 3) TCA-nitrogen assimilation. The results are mean values of 3 biological replicates.

3.3) Semi-quantitative determination of carbon flux distributions.

The relative turnover rates and relative pool sizes in Figure 3 give a semi-quantitative representation of the changing amount of each metabolite for comparison at different conditions. Because ^{13}C -labeling occurred too slowly among some metabolites in the TCA cycle (CIT, AKG, SUCC, MAL, GLU) of the -N culture, their relative turnover rates could not be calculated by fitting to an exponential equation (Figure 4-3 B). Despite such slow labeling kinetics, the relative pool sizes of these metabolites in the -N culture were several fold larger than in the +N culture (Figure 4-3 C). This makes comparison of the TCA cycle fluxes between the two cultures not possible using the semi-quantitative estimation. Nonetheless, MAL was much faster ^{13}C -labeled than other metabolites in the TCA cycle (CIT, AKG, SUCC) under +N, while this fast labeling kinetic of MAL disappeared under -N. Relative turnover rates of ADPGLC and 6PG, respectively, at the two conditions are comparable. However, the +N culture had a 23-fold larger relative pool size of ADPGLC, and the -N culture had an 8-fold larger relative pool size of 6PG. Together these results indicate a large part of the carbon flux into the OPP pathway through 6PG was redirected into glycogen synthesis under -N. Finally, the changes of carbon flux distributions at 3PG were estimated based on the relative turnover rates and pool sizes of DHAP and PEP, which are direct downstream metabolites of 3PG. DHAP and PEP have similar relative turnover rates at the two conditions. By contrast, the +N culture had a 5-fold larger relative pool size of PEP, while the -N culture had a 2.6-fold larger relative pool size of DHAP. These findings indicate a larger part of the efflux of 3PG was directed to GAP/DHAP and the subsequent gluconeogenesis pathway and PP

pathway under -N. A summary of these qualitative interpretations of changed carbon flux distribution is shown in Table 4-1.

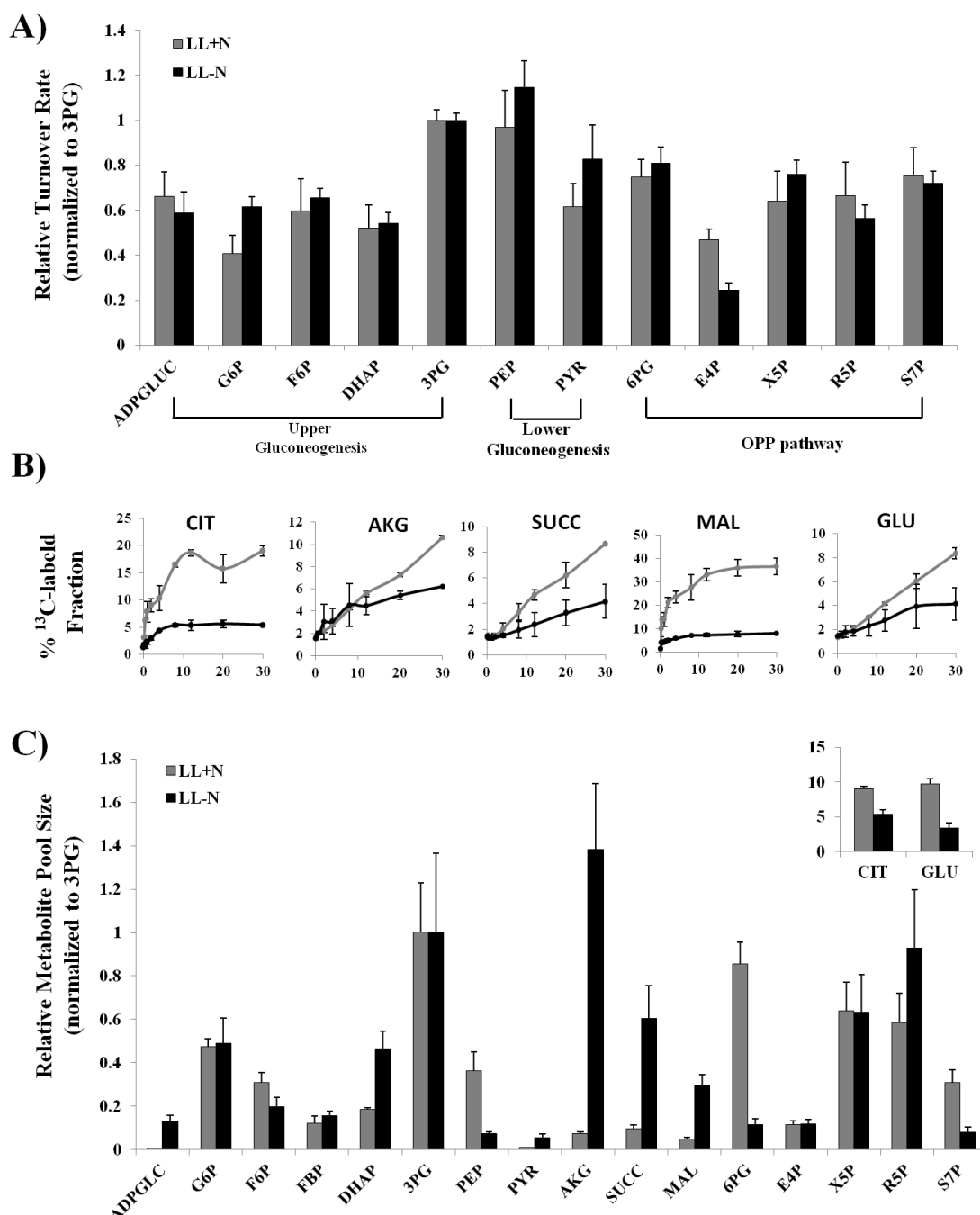


Figure 4-3 A) Relative turnover rates, B) Total ^{13}C -labeling abundance kinetics, and C) relative concentrations of carbon metabolites at nitrogen repleted (+N) and deprived (-N) conditions. Turnover rates and concentrations of all the metabolites have been normalized to 3PG turnover rates and concentrations, respectively, at each nitrogen condition.

Exceptions are CIT, AKG, SUCC, MAL and GLU, which showed such slow ^{13}C -labeling

kinetics under N deprivation that turnover rates of these five metabolites could not be calculated by equation fitting described in the methods section. Data points shown in B) represent average value of 2 biological replicates.

Gate Metabolite	Reaction	As Compared the +N Culture
G6P	G6P → 6PGL	↓
	G6P → ADPGLUC	↑
AKG	AKG → GLU	↓
	AKG → SSAL	↑
3PG	3PG → GAP/DHAP	↑
	3PG → PEP	↓

Table 4-1 Summary of the qualitative assessments of changed carbon flux distribution patterns under -N at the three decision points: G6P, 3PG and AKG. Arrow directions represent the increased (↑) or decreased (↓) carbon flux distribution towards the reaction product.

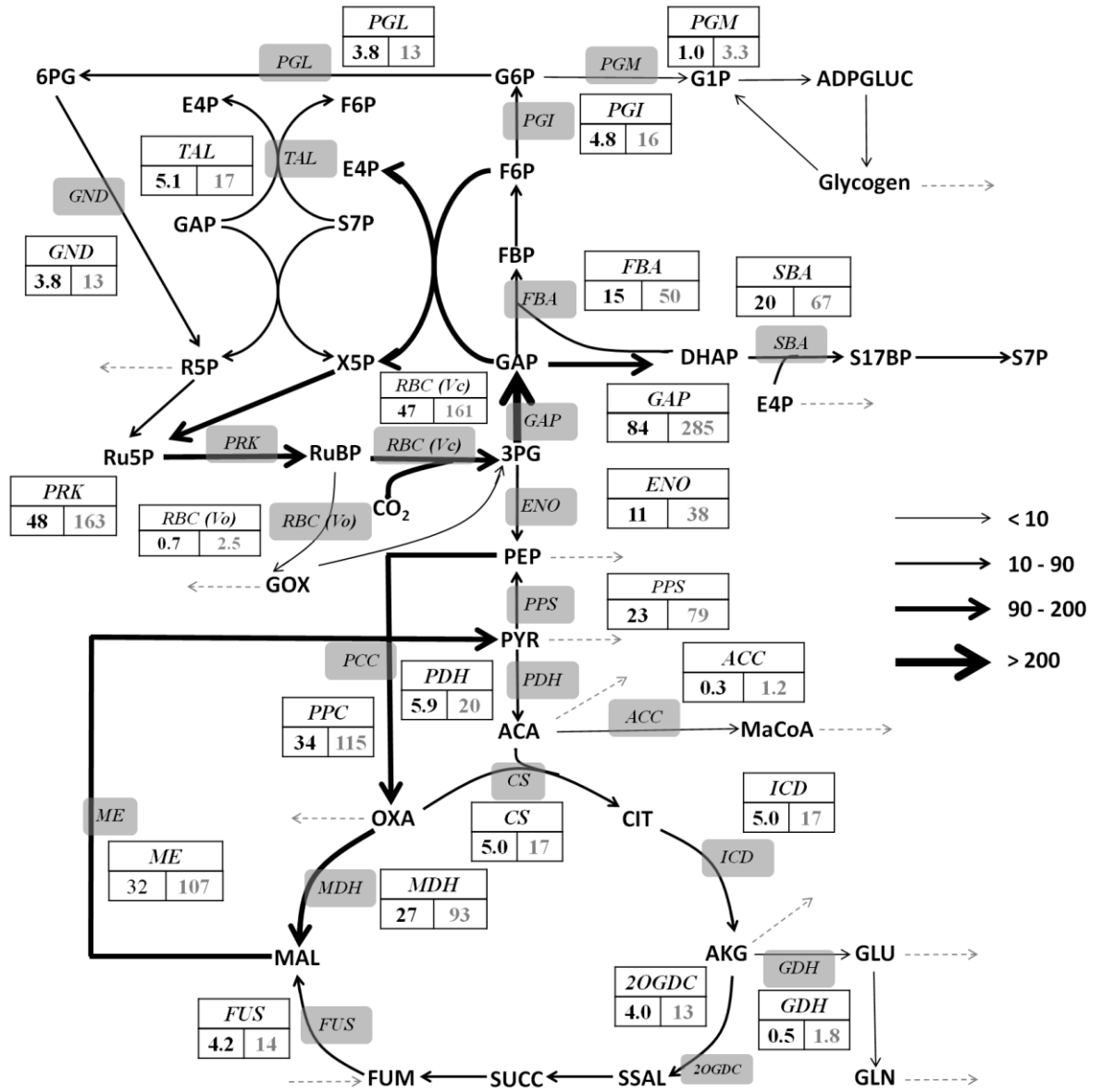
3.4) Quantitative analysis of carbon flux distribution.

Compared to the +N culture, the -N culture showed slower absolute metabolic flux rates of the RuBisCO reaction, lower glycolysis pathway (below *GAPDH*) and TCA cycle, but comparable absolute metabolic flux rates of reactions in the upper glycolysis pathway (above *GAPDH*), glycogen synthesis and OPP pathways (Figure 4-4). In order to compare the carbon flux distributions under the two different experimental conditions, we normalized all the flux rates to the corresponding net CO₂ fixation rate, and compared so-called relative metabolic flux rates.

Our INST-MFA results show negligible relative metabolic fluxes through oxygenation activity of RuBisCO at both experimental conditions (2.5% and 1.3% of net CO₂ fixation rate for the +N culture and the -N culture, respectively, as shown in Figure 4-4 A&B). The -N culture reveals an alternative CO₂-to-glycogen route that differs from the +N culture. Under nitrogen deprivation, an hGPP pathway was employed to convert fixed CO₂ into glycogen: GAP/DHAP → S17BP → S7P → F6P → G6P → glycogen (Figure 4-4 B). hGPP differs from the conventional gluconeogenesis pathway: GAP/DHAP → FBP → F6P → G6P → glycogen (Figure 4-4 A). The relative metabolic flux rate of glycogen synthesis of the +N culture was 63% slower than that of the -N culture. The calculated carbon flux distribution at the point of G6P shows that an increased fraction of total G6P efflux was directed toward glycogen synthesis (20% → 24%), rather than the OPP pathway under -N (Table 4-2). Relative metabolic flux rates of the OPP pathway under both conditions in our INST-MFA study were significant compared to the corresponding RuBisCO carboxylation activities (8% and 17% for +N and -N, respectively).

Relative metabolic flux rates of all the reactions involved in the lower glycolysis pathway and the TCA cycle were generally higher in the +N culture. 12% of 3PG efflux was funneled into lower glycolysis pathway under +N, while the percentage decreased to 8% under -N. Our results showed that during photosynthesis PYR is exclusively synthesized through the malic enzyme route: $PEP \rightarrow OXA \rightarrow MAL \rightarrow PYR$, which is followed by the phosphoenolpyruvate synthase (*PPS*) converts more PYR to PEP than pyruvate kinase (*PK*) converting PEP to PYR. We named this cyclic pathway as malic cyclic route in this paper. The relative metabolic flux rates of the malic cyclic route for the +N culture was 3-fold higher than those were of the -N culture. In addition, we observed substantial fluxes through the SSA route in the +N culture and the -N culture (8.1% and 6.5% of the corresponding RuBisCO carboxylation activities, respectively).

A)



reactions in the map are shown in Table S4-2. Arrow thickness represents the relative metabolic flux value of each metabolic reaction with the range shown in A).

Gate Metabolite (Relative Metabolic Influx Rate*)	Reaction	Relative Metabolic Flux Rate		Fraction of Total Influx	
		+ N	- N	+ N	- N
G6P (16, 38)	G6P → 6PGL	12.8	29	80%	76%
	G6P → ADPGLUC	3.3	9.0	20%	24%
AKG (17, 13)	AKG → GLU	1.8	1.0	11%	8%
	AKG → SSAL	13	11	76%	85%
3PG (322, 338)	3PG → GAP/DHAP	285	313	88%	92%
	3PG → PEP	38	26	12%	8%

Table 4-2. Photoautotrophic carbon distributions at different branching points. Relative flux rates are values normalized to per 100 unit CO₂ net fixation. Fraction of total influx represents the fractions of precursor metabolites funneled into each downstream product.

* Relative formation rates of precursor metabolites at +N (left) and -N (right) conditions, respectively. All values shown were normalized to per 100 unit CO₂ net fixation.

4. Discussion

In this study, we firstly used metabolic pool size and ^{13}C -labeling kinetics information to generate qualitative insights of carbon flux distribution changes at several key metabolic branches under $-N$. We then used INST-MFA method to quantitatively valid these insights and identify several new concepts in the biology of cyanobacterial photosynthetic growth. During photosynthesis, cyanobacteria accumulate glycogen while degrading proteins and chlorophylls in the cells under $-N$ (Guerra et al., 2013a). Simultaneously, external CO_2 is assimilated by cells and allocated into pathways that make precursors for glycogen or proteins, which is supported by the ^{13}C -labeling kinetics of the precursor metabolites in these pathways (Figure 4-3). Finding out changes of carbon flux distributions at important metabolic branches thus becomes the key to understand the global metabolic change upon N deprivation.

4.1) Changes of carbon flux distributions at metabolic branches under $-N$.

Our semi-quantitative analysis results suggest that increased glycogen synthesis under $-N$ was potentially caused by the combination of increased carbon flux distributions of $3\text{PG} \rightarrow \text{GAP/DHAP}$ and $\text{G6P} \rightarrow \text{ADPGLC}$ (Table 4-1). Our quantitative INST-MFA results further support this claim (Table 4-2). Under $-N$, 6% more of 3PG efflux was allocated towards GAP/DHAP, which contributed to a 1.4-fold increase of G6P influx. In addition, 4% more of G6P efflux was allocated towards ADPGLC, which ultimately led to a 1.7-fold increase of glycogen synthesis under $-N$. Interestingly, ADPGLC accumulated under $-N$ rather than G1P (Figure 4-2), which is the closer downstream metabolite of G6P. This finding suggests that glycogen synthase (encoded by *A1532* and *A2125*), which converts ADPGLC into glycogen, may be the enzymatic

bottleneck in the glycogen synthesis pathway. On the other hand, 4% less of 3PG efflux towards lower glycolysis pathway (3PG → PEP) as well as 3% less of AKG efflux towards GLU/GLN synthesis together contribute to the decreased GLU/GLN pool sizes shown in Figure 4-2.

4.2) The OPP pathway.

In cyanobacteria, the OPP pathway flux was thought to be minimal under light conditions. The gate enzyme of the OPP pathway, glucose-6-phosphate dehydrogenase (*G6PDH*), has been shown to be inhibited by light in the presence of a reduced carbon source due to the elevated ratio of NADPH/NADP⁺ and the intracellular RuBP concentration (Pelroy et al., 1972; Pelroy et al., 1976). Such regulation by light appears to happen at a post-translational stage (Knowles & Plaxton, 2003). Nonetheless, our results of the OPP pathway flux are significant compared to the corresponding RuBisCO carboxylation activities (8% and 17% for the +N culture and the –N culture, respectively). Such significant photoautotrophic OPP fluxes may be contributed by flux redirected from reductive pentose phosphate (RPP) pathway due to kinetic bottlenecks in this pathway. In *Synechococcus* 7002, nitrogen deprivation in photoautotrophic conditions strongly induces the expression of four genes in the OPP pathway: *G6PDH* (*zwf*, 3.7-fold), a positive regulator of *G6PDH* (*opcA*, 2.8-fold), 6-phosphogluconate dehydrogenase (*6PGDH*) (*gnd*, 2.9-fold), and transaldolase (*tal*, 2.4-fold) (Ludwig & Bryant, 2012). Our finding of a 2.2-fold increase in the relative metabolic flux rate through the OPP pathway agrees well with this transcriptomic transition upon N deprivation. Additionally, in another nitrogen deprivation study of *Synechocystis* 6803, the *in vitro* enzymatic activities of two OPP pathway key enzymes, *G6PDH* and *6PGDH*, were shown to

increase by 60% and 80%, respectively (Osanai et al., 2006). It was suggested by the authors that the elevated OPP pathway activity could function as a reducing power producer for cells to compensate for the reduced NADPH formation rate owing to shutdown of the photosynthetic system under nitrogen deprivation.

4.3) Metabolic channeling.

Under both +N and -N conditions, relative turnover rates of all metabolites were smaller or similar to those of 3PG, as they are downstream of 3PG (Figure 4-3 A). However, some downstream metabolites showed larger relative turnover rates than their upstream metabolites (e.g. ADPGLC and 6PG vs. G6P in the +N culture). This may have been caused by metabolic channeling: the formation of multienzyme complexes that directly convert intermediate metabolites into final products without releasing intermediates back to their pools (Winkel, 2004). Observation of metabolic channeling in another cyanobacterium, *Synechocystis* 6803, was reported by Young et al. (2011), where the authors found that the CBB cycle intermediates F6P, GAP, DHAP and R5P were significantly less labeled than their downstream products S7P, R5P and RUBP.

4.4) The hGPP pathway.

The special hGPP pathway under -N quantitatively illustrated in Figure 4B agrees well with our findings in a previous flux balance analysis study that suggested an alternative CO₂ → glycogen route (Qian et al., submitted). In *Synechococcus* 7002, GAP/DHAP is converted into either FBP or S17BP by the same set of bifunctional enzymes, fructose-bisphosphate aldolase class I and II (encoded by genes *A0010* and *A1352*). In our results, absolute metabolic flux rates of the *FBA* reaction (GAP/DHAP → FBP) and the *SBA* reaction (GAP/DHAP → S17BP) both doubled under -N, which agrees

well with the transcriptional changes of the two corresponding genes (*A0010*: 2.1-fold increment and *A1352*: 1.8-fold increment) when *Synechococcus* 7002 was grown under nitrogen deprivation (Ludwig & Bryant, 2012). However, directionality of the *FBA* reaction appeared to be reversed under -N. Thus, our results suggest that nitrogen availability serves as a trigger to determine the route of glycogen synthesis.

4.5) The malic cyclic route.

¹³C-labeling of MAL (Figure 3B) occurred much faster than its upstream TCA cycle metabolites (AKG and SUCC), suggesting that a large portion of the carbon influx to MAL was contributed by phosphoenolpyruvate carboxylase (*PCC*). Our INST-MFA results further support this indication (Figure 4-4). There are substantial *PCC* fluxes under both conditions (71% and 20% of the corresponding RuBiSCO carboxylation activities for +N and -N, respectively). Such *PCC* fluxes are much higher than the 10% of RuBiSCO carboxylation activity reported in Young et al. (2011). *PCC* catalyzes the irreversible carboxylation of PEP using HCO₃⁻ to form OXA (O’Leary, 1982). *PCC* isoforms widely exist in higher plants and cyanobacteria (Shylajanaciyar et al., 2015), while the carbon-fixation contribution of the C₄-like mechanism in cyanobacteria remains unclear. A recent study of the cyanobacterium *Anabaena* sp. PCC 7172 has shown that overexpression of the *pepc* gene increases photosynthetic oxygen evolution rate by ~22.5%, which suggests increased electron sink utilization in the overexpression strain (Jia et al., 2015). In this study, we discover that *PCC* acts as a key part of a malic cyclic route. One crucial role of this route was shown to be synthesizing PYR during photosynthesis. A *Synechocystis* 6803 knockout mutant of malic dehydrogenase photoautotrophically grew 15 times slower than wildtype (Bricker et al., 2004). This

growth deficiency can be reversed by supplementing PYR in the culture medium, which indicates malic dehydrogenase being utilized to produce PYR for biosynthesis. Utilization of the malic enzyme route has been suggested to be associated with the reduced pyruvate kinase (*PK*) activity in the light due to the intracellular pH increment when cells were switched from dark to light (Knowles et al., 2001).

Moreover, another important part of this malic cyclic route is the reaction producing PEP from PYR, which is catalyzed by the phosphoenolpyruvate synthase (*PPS*) reaction, encoded by *ppsA* (*A2050*). The complete reaction of phosphoenolpyruvate synthase is as follows:



PPS purified from the hyperthermophilic archaeon *Pyrococcus furiosus* was reported with a much higher catalytic efficiency with PYR than with PEP ($1.43 \times 10^4 \text{ mM}^{-1} \text{ s}^{-1}$ vs. $32 \text{ mM}^{-1} \text{ s}^{-1}$), which suggests a favored enzymatic direction toward PEP synthesis of this reaction (Hutchins et al., 2001). However, *PPS* towards PEP synthesis is wasteful of energy, as it consumes one ATP molecule to produce one PEP molecule. One possible explanation is that the malic cyclic route is needed not only for PYR synthesis but also for OXA synthesis that supports the continuous TCA cycle flow. Therefore, cells need to replenish the PEP pool through the *PPS* to support the active malic cyclic route. *PPS* purified from *Escherichia coli* (*E. coli*) is inhibited by PEP (Chulavatnatol & Atkinson, 1972). However, the PEP pool size of the +N culture was 6-fold larger than that of the -N culture (Figure 4-2), while the relative metabolic flux rate of *PPS* of 8-fold larger of the +N culture. This may be due to both 1) a reduced need for PYR in amino acid biosynthesis that turns down the entire malic cyclic pathway and 2) a decrease in ATP

and reductant generation rates in response to the shutdown of the photosynthetic machinery under N deprivation.

4.6) The SSA route.

The TCA cycle was once believed to be incomplete in cyanobacteria, since genes encoding 2-oxoglutarate dehydrogenase (*2-OGDH*), which converts AKG to SUCC-CoA, were absent (Smith et al., 1967; Perce et al., 1968, Ohashi et al., 2011). Recently, the succinic semialdehyde (SSA) route, which involves 2-oxoglutarate decarboxylase (*2-OGDC*) and succinic semialdehyde dehydrogenase (*SSADH*), and converts AKG to SUCC, was identified in the cyanobacterium *Synechococcus* 7002 (Zhang & Bryant, 2011). This route completes the truncated cyanobacterial TCA cycle. However, the physiological importance of this route under photoautotrophic growth remains unclear. Multiple FBA growth simulations of cyanobacteria *Synechococcus* 7002 and *Synechocystis* 6803 suggests negligible (<1% of RuBiSCO activities) fluxes go through the SSA route under photoautotrophic conditions (Vu et al., 2013; Knoop et al., 2013). Knockout mutants of the SSA route enzymes in *Synechococcus* 7002, however, show reduced photoautotrophic growth rates (Zhang & Bryant, 2011), which indicates that the SSA route is required for optimal photosynthetic growth. In this study, our INST-MFA results show substantial fluxes through the SSA route in the +N culture and the -N culture (8.1% and 6.5% of the corresponding RuBiSCO carboxylation activities, respectively) (Figure 4-4 A&B), which quantitatively supports the physiological importance of the SSA route for photoautotrophic growth in cyanobacteria.

5. Conclusion

In this study, we demonstrated how to analyze ^{13}C -labeling data of photoautotrophic growth in a cyanobacterium *Synechococcus* 7002 to identify changes of carbon flux distributions and discover new roles of existing metabolic pathways. We illustrated both semi-quantitative and quantitative methods for gaining this knowledge. Our strategy guides future scientists who wish to study physiological changes at the metabolic level under different nutrient conditions. In addition, the carbon flow patterns in photosynthetic growth with or without nitrogen source that we have discovered bring new insights that change our understanding of cyanobacterial photosynthesis. Finally, our findings of carbon flux distributions at different decision points and novel utilization of existing pathways will provide new bioengineering targets to further improve desired product yields.

Metabolite	Concentration ($\mu\text{mol} / \text{g DW}$)	
	+ N	- N
6PG	1.4 ± 0.2	0.14 ± 0.03
X5P	1.0 ± 0.2	0.8 ± 0.2
R5P	1.0 ± 0.2	1.2 ± 0.3
S7P	5.6 ± 1.1	1.1 ± 0.3
E4P	0.19 ± 0.03	0.15 ± 0.02
RUBP	0.38 ± 0.05	0.44 ± 0.1
ADPGLC	0.0095 ± 0.0009	0.16 ± 0.03
G6P	0.77 ± 0.06	0.61 ± 0.14
F6P	0.50 ± 0.08	0.25 ± 0.06
G1P	0.35 ± 0.04	0.30 ± 0.09
FBP	0.20 ± 0.05	0.20 ± 0.03
DHAP	0.30 ± 0.01	0.58 ± 0.10
3PG	1.6 ± 0.4	1.2 ± 0.5
PEP	0.59 ± 0.14	0.09 ± 0.01
PYR	0.017 ± 0.001	0.07 ± 0.02
ACA	0.031 ± 0.002	0.006 ± 0.001
CIT	14.7 ± 0.5	6.7 ± 0.8
AKG	0.12 ± 0.01	1.7 ± 0.4
SUCC	0.16 ± 0.03	0.75 ± 0.19
MAL	0.08 ± 0.01	0.37 ± 0.06
GLN	0.030 ± 0.003	0.0038 ± 0.0005
GLU	15.8 ± 1.2	4.2 ± 1.0

Table S4-1. Pool sizes of metabolites in cultures grown with or without nitrate in the growth medium. Error bars represent standard errors from 3 biological replicates.

Reaction	+ N			- N		
	Net flux	Net flux lb	Net flux ub	Net flux	Net flux lb	Net flux ub
1 G1P = 1 G6P	-0.96888	-0.96888	-0.96888	-0.86692	-0.86692	-0.86692
1 G1P -> 1 ADPGLC	6.82422	6.77591	7.47274	5.62051	4.97222	5.61719
1 ADPGLC -> 1 GLYC	6.82422	6.77591	7.47274	5.62051	4.97222	5.61719
1 GLYC -> 1 G1P	5.85534	5.80702	6.50386	4.75359	4.1053	4.75027
1 G6P = 1 F6P	-4.79122	-6.71656	-4.79123	-3.71853	-4.79007	-2.37869
1 G6P -> 1 6PGC	3.77786	3.77787	5.7032	2.8343	1.49446	3.90584
1 6PGC - > 1 RU5P + 1 CO2	3.77786	3.77787	5.7032	2.8343	1.49446	3.90584
1 F6P = 1 FBP	-14.7937	-16.4875	-14.7482	28.6141	27.6051	32.0369
1 FBP = 1 DHAP + 1 GAP	-14.7937	-16.4875	-14.7482	28.6141	27.6051	32.0369
1 DHAP = 1 GAP	-34.5677	-36.3475	-34.5548	-12.8419	-13.5902	-11.6158
1 GAP = 1 3PGA	-84.214	-87.7005	-84.0783	-30.2784	-31.6625	-27.7462
1 3PGA = 1	11.2143	10.9637	11.2382	2.49463	1.97974	2.71734

2PGA						
1 2PGA = 1 PEP	11.2143	10.9637	11.2382	2.49463	1.97974	2.71734
1 PEP = 1 PYR	-23.3634	-23.6517	-22.5432	-0.95513	-8.36403	-0.96372
1 RU5P = 1 X5P	-29.7765	-29.8244	-29.2754	-9.12341	-9.56884	-8.09363
1 RU5P = 1 R5P	-14.5218	-14.5458	-14.2713	-4.49368	-4.71639	-3.97879
1 RU5P - > 1 RUBP	48.0762	47.9689	49.7825	16.4514	14.9616	17.1687
1 CO2 + 1 RUBP - > 2 3PGA	47.352	47.2447	49.0583	16.3216	14.8319	17.039
1 X5P = 1 GAP + 1 EC2	-29.7765	-29.8244	-29.2754	-9.12341	-9.56884	-8.09363
1 F6P = 1 EC2 + 1 E4P	15.0785	14.8279	15.1024	4.59452	4.07963	4.81723
1 S7P = 1 R5P + 1 EC2	14.6981	14.4475	14.722	4.52889	4.014	4.75161
1 F6P = 1 GAP + 1 EC3	-5.07601	-5.47105	-4.86637	-36.9271	-39.9811	-35.4926
1 S7P = 1 E4P + 1 EC3	5.07601	4.86637	5.47105	36.9271	35.4926	39.9811
1 DHAP	19.7741	19.5406	20.182	41.456	40.0684	44.3333

+ 1 E4P - > 1 SBP						
1 SBP -> 1 S7P	19.7741	19.5406	20.182	41.456	40.0684	44.3333
1 PYR -> 1 CO2 + 1 ACA	5.86429	5.61371	5.88822	1.5645	1.04961	1.78721
1 ACA + 1 OAA - > 1 CIT	5.00768	4.7571	5.03161	1.28934	0.77445	1.51205
1 CIT = 1 ICI	5.00768	4.7571	5.03161	1.28934	0.77445	1.51205
1 ICI = 1 CO2 + 1 AKG	5.00768	4.7571	5.03161	1.28934	0.77445	1.51205
1 AKG - > 1 CO2 + 1 SUCSAL	3.97362	3.72304	3.99755	1.10377	0.588875	1.32648
1 SUCSAL -> 1 SUCC	3.97362	3.72304	3.99755	1.10377	0.588875	1.32648
1 SUCC = 1 FUM	3.97362	3.72304	3.99755	1.10377	0.588875	1.32648
1 FUM = 1 MAL	4.23135	3.98077	4.25528	1.15304	0.638154	1.37576
1 MAL = 1 OAA	-27.3966	-27.6849	-26.5763	-1.78065	-9.18955	-1.78924
1 MAL - > 1 CO2 + 1 PYR	31.6279	30.8206	31.7106	2.9337	2.94275	9.96677

1 CO2 + 1 PEP -> 1 OAA	33.8802	33.0729	33.963	3.32944	3.3385	10.3625
1 RUBP - > 1 3PGA + 1 2PG	0.724194	0.724194	0.724196	0.129749	0.129749	0.130624
1 2PG -> 1 GLC	0.724194	0.724194	0.724196	0.129749	0.129749	0.130624
1 GLC -> 1 GOX	0.724194	0.724194	0.724196	0.129749	0.129749	0.130624
2 GOX - > 1 CO2 + 1 GA	4.46E-07	4.44E-07	1.76E-06	1.11E-09	1.11E-09	0.000438
1 GA = 1 2PGA	4.46E-07	4.44E-07	1.76E-06	1.11E-09	1.11E-09	0.000438
1 AKG = 1 GLU	0.534397	0.534397	0.534397	0.092189	0.092189	0.092189
1 GLU -> 1 GLN	0.258141	0.258141	0.258141	0.044532	0.044532	0.044532
1 ACA - > 1 LIPID	0.349385	0.349385	0.349385	0.187659	0.187659	0.187659
1 G6P + 0.5 R5P + 0.5 OAA + 0.745 AKG + 0.5 GOX -> 0.5 FUM + 1 DNA	0.039636	0.039636	0.039636	0.015833	0.015833	0.015833

1 G6P + 0.498 R5P + 0.502 OAA + 0.757 AKG + 0.498 GOX -> 0.498 FUM + 1 RNA	0.004844	0.004844	0.004844	0.001479	0.001479	0.001479
0.154 PEP + 0.53 PYR + 0.034 R5P + 0.084 E4P + 0.112 ACA + 0.321 OAA + 0.103 AKG + 0.155 GOX + 0.061 GLU + 0.057 GLN -> 0.327 CO2 + 0.052 FUM + 1 Protein	4.52879	4.52879	4.52879	0.781264	0.781264	0.781264
3.34 GLYC + 0.723	0.734001	0.734001	0.734001	0.259556	0.259556	0.259556

LIPID + 0.061 DNA + 0.0057 RNA + 3.01 Protein - > 1 Biomass						
1 Biomass ->	0.734001	0.734001	0.734001	0.259556	0.259556	0.259556
-> 1 CO2	29.5	29.5	29.5	9.67	9.67	9.67

Table S4-2 Absolute metabolic fluxes of all metabolic reactions in the map in Figure 4-4.

Unit is $\mu\text{mol g}^{-1} \text{DW min}^{-1}$.

Chapter 5: Inactivation of nitrate reductase alters metabolic
branching of carbohydrate fermentation in the cyanobacterium
Synechococcus sp. strain PCC 7002

Coauthors: G. Kenchappa Kumaraswamy, Shuyi Zhang, Colin Gates,
Gennady M. Ananyev, Donald A. Bryant and G. Charles Dismukes

This article is similar to the peer-reviewed article:

Qian X, Kumaraswamy GK, Zhang S, Gates C, Ananyev GM, Bryant DA
and Dismukes GC (2015) Inactivation of nitrate reductase alters metabolic
branching of carbohydrate fermentation in the cyanobacterium
Synechococcus sp. strain PCC 7002. *Biotechnol Bioeng*.

Used with permission by Wiley

Summary

To produce cellular energy, cyanobacteria reduce nitrate as the preferred pathway over proton reduction (H_2 evolution) by catabolizing glycogen under dark anaerobic conditions. This competition lowers H_2 production by consuming a large fraction of the reducing equivalents (NADPH and NADH). To eliminate this competition, we constructed a knockout mutant of nitrate reductase, encoded by *narB*, in *Synechococcus* sp. PCC 7002. As expected, $\Delta narB$ was able to take up intracellular nitrate but was unable to reduce it to nitrite or ammonia, and was unable to grow photoautotrophically on nitrate. During photoautotrophic growth on urea, $\Delta narB$ significantly redirects biomass accumulation into glycogen at the expense of protein accumulation. During subsequent dark fermentation, metabolite concentrations - both the adenylate cellular energy charge (\sim ATP) and the redox poise (NAD(P)H/NAD(P)) - were independent of nitrate availability in $\Delta narB$, in contrast to the wild type (WT) control. The $\Delta narB$ strain diverted more reducing equivalents from glycogen catabolism into reduced products, mainly H_2 and D-lactate, by 6-fold (2.8% yield) and 2-fold (82.3% yield), respectively, than WT. Continuous removal of H_2 from the fermentation medium (milking) further boosted net H_2 production by 7-fold in $\Delta narB$, at the expense of less excreted lactate, resulting in a 49-fold combined increase in the net H_2 evolution rate during 2 days of fermentation compared to the WT. The absence of nitrate reductase eliminated the inductive effect of nitrate addition on rerouting carbohydrate catabolism from glycolysis to the oxidative pentose phosphate (OPP) pathway, indicating that intracellular redox poise and not nitrate itself acts as the control switch for carbon flux branching between pathways.

1. Introduction

Aquatic microbial oxygenic photoautotrophs (AMOPs) are the most abundant naturally photosynthetic microbes on Earth and include ecologically diverse classes of cyanobacteria, algae and diatoms. Their global productivity in biomass production exceeds that of terrestrial photosynthesis and benefits from their higher intrinsic photosynthetic efficiency in light to biomass conversion (Ducat & Silver, 2012; Dismukes et al., 2008). For these reasons, they are widely investigated as feedstocks for conversion into biofuels in the form of hydrogen, diesel or alcohol through biological, physical or chemical processes (Parmar et al., 2011; Jones & Mayfield, 2012; Roeselers et al., 2008; Romagnoli et al., 2010). Their utility as cell factories for production of fuel precursors, including hydrogen, is also widely acknowledged and studied (Gressel, 2008; Mathews & Tan, 2009; Radakovits et al., 2010; Ducat et al., 2011a; Ducat et al., 2011b; Hays & Ducat, 2015). *Synechococcus* sp. strain PCC 7002 (hereafter *Synechococcus* 7002) is a model cyanobacterium with well characterized genomic and transcriptomic databases, mature protocols for transformation and other genetic manipulations, and a relatively fast photoautotrophic growth rate (3 to 4 h / generation) (Frigaard et al., 2004; Xu et al., 2011). Like many other cyanobacteria, *Synechococcus* 7002 harbors a bidirectional [NiFe]-hydrogenase belonging to the pentameric Hox class, which catalyzes reversible hydrogen (H₂) production using NAD(P)H and in some strains reduced flavodoxin and ferredoxin as the electron sources (Aubert-Jousset et al., 2011; Cournac et al., 2004; Carrieri et al., 2011; Ghirardi et al., 2007; Gutekunst et al., 2014). These features make *Synechococcus* 7002 an excellent model for studying and modifying the metabolic circuits that affect biohydrogen production.

The cyanobacterial Hox hydrogenase is inactivated by O₂, even at atmospheric concentrations, but is reversibly reactivated by NADH and NADPH under anoxic conditions (Cournac et al, 2004). When oxygen is absent, the production rate and yield of H₂ by the Hox hydrogenase are heavily dependent on the intracellular level of reduced NAD(P)H owing to the reversible nature of this enzyme (Ananyev et al., 2012). Reducing equivalents can be generated in two ways. During photosynthesis, NADP⁺ can be reduced to NADPH by ferredoxin:NADP⁺ oxidoreductase (FNR) via photosystem I-dependent ferredoxin reduction. Alternatively, NADPH can be used to reduce NAD⁺ to NADH through the transhydrogenase (TH) activity (Jackson, 2003; Zhao et al., 2008). NADH is generated during glycolysis of glycogen, while NADPH can be generated if glucose 6-phosphate (G6P) is metabolized through the oxidative pentose phosphate (OPP) pathway. NAD(P)H generated under dark anoxic conditions is freely available for dark-H₂ production in cyanobacteria. H₂ production under dark anaerobic conditions by autofermentation of photosynthetically accumulated glycogen is a slow process occurring over days and has a non-ideal conversion efficiency (<39%) that is limited by unfavorable thermodynamics (Ananyev et al., 2012). However, this conversion rate can be accelerated by genetic rewiring.

Multiple genetic engineering strategies have been applied to increase the intracellular NAD(P)H or reduced ferredoxin availability, aiming to achieve higher H₂ yields. In *Synechococcus* 7002, knocking out the *ldhA* gene, which encodes D-lactate dehydrogenase, an enzyme that competes with the Hox hydrogenase for NADH, led to 5-fold higher H₂ yield and a faster hydrogen production rate (McNeely et al., 2010). Another successful approach was demonstrated by overexpression and knockout strains

of the glyceraldehyde 3-phosphate dehydrogenase (*gap1*) gene, which both caused up to 3-fold stimulation of H₂ yields that result from different consequences on carbon accumulation via gluconeogenesis and carbon catabolism via partitioning between glycolysis and the oxidative pentose phosphate (OPP) pathway (Kumaraswamy et al., 2013). Rerouting glucose catabolism through the OPP pathway to increase H₂ yield was also demonstrated in an *E. coli* over-expression strain of glucose-6-phosphate dehydrogenase (*zwf*) and fructose 1, 6-bisphosphatase II (*glpX*). This overexpression mutant produces 2.3-fold more H₂ than the control WT strain (Kim et al., 2011). On the photo-biological H₂ side, genetic engineering to improve H₂ production was achieved by reducing electron competition by cyclic electron transfer. *Chlamydomonas reinhardtii* strain *Stm6*, which is blocked in transition state 1 and has its cyclic electron transfer inhibited, is capable of producing ~5 to 13 times more H₂ than the control WT strain over a range of photo-conditions (Kruse et al., 2005).

Nitrate reduction competes directly with NAD(P)H utilization by the Hox hydrogenase in cyanobacteria. Once nitrate is transported into the cell by nitrate permease (NrtP), two reduced ferredoxin molecules reduce one nitrate to one nitrite, catalyzed by nitrate reductase (encoded by *narB*) (Srivastava et al., 2015). Nitrite will be further reduced to ammonia using 6 electrons from ferredoxin, catalyzed by nitrite reductase (encoded by *nirA*) for use in biosynthesis, or excreted out of the cell (Flores et al., 2005). In *Synechococcus* 7002 the high reductant utilization for acquisition and fixing of nitrate results in a metabolic switch that accelerates and redirects glycogen catabolism from glycolysis to the OPP pathway, which has a 3-fold greater reductant yield (McNeely et al., 2014). This study concluded that autofermentative H₂ production is

controlled by reductant availability. Based on this study, elimination of nitrate reduction activity is predicted to improve the dark H₂ yield in the presence of nitrate. This hypothesis was previously tested in cyanobacterium *Synechocystis* sp. PCC 6803 (hereafter *Synechocystis* 6803) by construction of the *narB* knockout mutant, which was found to have similar or lower H₂-evolving capacity compared to WT in the presence of nitrate (Baebprasert et al., 2011). To reconcile this unexpected result, in the present study we generated a knockout mutant with *narB* inactivated in *Synechococcus* 7002 and examined its autofermentative metabolism in the presence and absence of nitrate. We conducted a quantitative inventory as a function of time of the glycogen catabolic conversion, yields of H₂, NAD(P)H, excreted organic acids and CO₂. Additionally, we used quantitative mass spectrometry (LC-tandem-MS/MS) at selected time points to determine the metabolite pool sizes for selected pathways that are active during glycogen autofermentation, including intracellular energy and redox balance (concentrations of adenylates and pyridine nucleotides, respectively). Our findings show that the *narB* knockout of *Synechococcus* 7002 is sufficient to redirect the dominant flux of electrons from nitrate reduction to other fermentative metabolites, including a 6-fold higher H₂ yield than the WT strain.

2. Experimental Procedures

2.1) Mutant construction and segregation.

Wild-type *Synechococcus* 7002 was first adapted to medium A containing 5 mM urea without nitrate (Stevens et al., 1973), and then the corresponding *narB* coding sequence (SynPCC7002_A1314) was deleted and replaced by using the homologous recombination strategy shown in Figure 5-1A, in which the *narB* gene is replaced by a DNA fragment encoding aminoglycoside phosphotransferase II (*aphAII*), which confers kanamycin resistance. Transformation and selection were performed as previously described (Frigaard et al., 2004). Complete segregation of the *narB* and *narB::aphAII* alleles was verified by PCR with template DNAs derived from the wild type and transformant strains (Figure 5-1B). The primers used are listed in Table 4-1. The $\Delta narB$ strain was additionally phenotypically confirmed by its inability to grow photoautotrophically (Figure 5-2) when nitrate was the only nitrogen source.

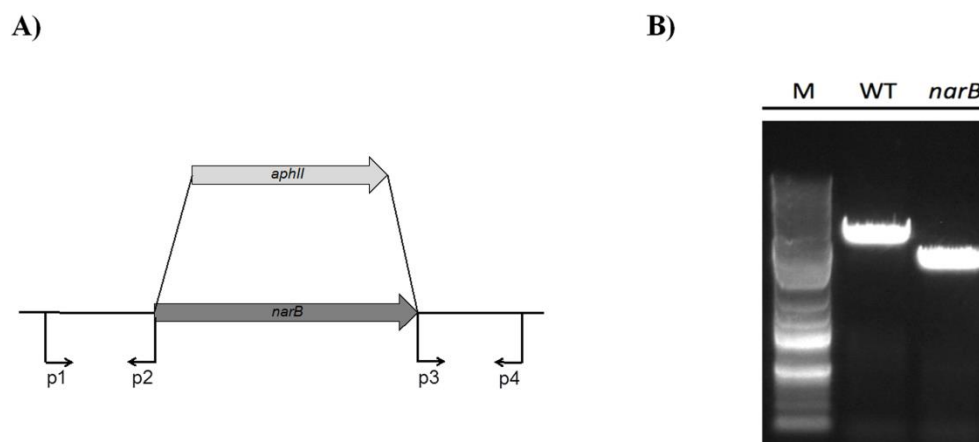


Figure 5-1 A: Schematic representation of the homologous recombination methods. The upstream and downstream flanking regions for the gene of interest (*narB*) were amplified by PCR, using primer pairs P1-P2 and P3P; and these fragments were ligated to the antibiotic cassette (*aphII*). The resulting construction was transformed into *Synechococcus* 7002 to generate fully segregated deletion strain. B: The $\Delta narB$ deletion mutant was verified by PCR amplification with primers P1 and P4 (Fig. 1), using template DNA derived from WT or transformed cells. M: DNA ladder. Lane WT, contained template DNA from the WT strain. Lane *narB* contained template DNA from antibiotic-resistant strain in which *narB* had been replaced by *aphII* as described above. Size difference indicates the deletion of *narB*.

Name	Sequences
P1	GTTGGTTATCTCCTGATGAGTTCG
P2	TCCATTTCTAGACCGCTAACTTA
P3	TTAGGAGGTACCGAAACCTGGGTT
P4	GGGGATCGTGACCAACAAGGACAA

Table 5-1 Primers used to generate *narB* deletion mutant.

2.2) Strains, growth conditions and culture preparation.

The *AnarB* strain was maintained in liquid medium supplemented with 100 μg kanamycin mL^{-1} . Two types of modified medium A, A^{+NO_3} and $\text{A}^{+\text{UREA}}$, were used to compare the photoautotrophic growth of the *AnarB* to that of the WT. Medium A contains no nitrogen source; for clarity, the subscript indicates the nitrogen source in the medium, (e. g. A^{+NO_3} or $\text{A}^{+\text{UREA}}$). Media A and A^{+NO_3} were used to study the fermentative metabolism of the two strains. The concentration of NaNO_3 or urea in the medium was always 5 mM. Cultures were grown photoautotrophically at 38 °C and were sparged with 2% (v/v) CO_2 in air. To measure the growth, cultures were grown photoautotrophically under a light intensity of 200 $\mu\text{E m}^{-2} \text{s}^{-1}$. Growth of *Synechococcus* 7002 was determined by measuring light scattering at 730 nm ($\text{OD}_{730 \text{ nm}}$) with a spectrophotometer. To prepare cells for autofermentation, $\text{A}^{+\text{UREA}}$ medium supplemented with 2 μM NiCl_2 was used to grow both strains. Cells were grown to $\text{OD}_{730 \text{ nm}}$ of 1.5 ± 0.2 with a light intensity of 200 $\mu\text{E m}^{-2} \text{s}^{-1}$. Cultures were then transferred into different fermentation media (A^{+NO_3} and A) and switched to dark anoxic conditions to induce fermentative metabolism.

Prior to onset of autofermentation, we added an incubation step to fully activate the nitrate reductase in WT, using the procedure of Sakamoto et al. (1999). Photoautotrophic growth of both strains was continued for 1 h following transfer to nitrogen-free medium A. This step results in activation of NarB, NirA and NrtP activities in *Synechococcus* 7002 cells grown on urea (Sakamoto et al, 1999; Sakamoto et al, 2008). Nitrogen starvation was reported to result in the accumulation of 2-OG, which leads to the induction of nitrate assimilatory genes in cyanobacteria (Muro-Pastor et al, 2001). The purpose for using nitrogen-free medium A in the activation step was to reduce

differences in glycogen accumulation between the two strains. Glycogen content increased during the activation step by 132 ± 6 mol / 10^{17} cells and 142 ± 40 mol / 10^{17} cells in WT and the *ΔnarB* strain, respectively.

2.3) Fermentative conditions.

The WT and the *ΔnarB* strains were allowed to autoferment in the dark in anoxic media with or without nitrate for 2 days to analyze electron distribution quantitatively and determine metabolic changes in the two strains. In addition, the WT and the *ΔnarB* strain were autofermented on nitrate and sampled in a time-dependent manner for 4 days. The purpose of this part of the experiment was to compare quantitatively the kinetics of nitrate uptake, nitrite excretion and ammonia excretion of the two strains in the presence of nitrate. Cultures were harvested by centrifugation, and cells were resuspended in the same volume of A⁻ medium. The resuspended cultures were treated to activate the nitrate reductase NarB in WT. Expression of the *narB* gene showed to decrease 5-fold when *Synechococcus* 7002 WT cells were grown on urea rather than nitrate (Ludwig & Bryant, 2012). Cells were then harvested by centrifugation and were washed once with medium A. Cell pellets were then resuspended in medium A or A^{+NO₃}. The final OD_{730 nm} readings for all cultures were 1.5. Aliquots (5 mL) of cells were then dark fermented in 10 mL vials as described in McNeely et al. (2014).

2.4) Analytical assays.

H₂ in the headspace was measured by gas chromatography (GC) as described in Guerra et al. (2013a). After the headspace H₂ was measured, 1 mL of culture in each vial was centrifuged to separate the supernatant from the cell pellet. The cell pellet was saved

for intracellular quantification of total carbohydrates. The supernatant was collected for HPLC (Perkin Elmer) analysis of lactate, acetate and succinate as was described in Kumaraswamy et al. (2013). Frozen cell pellets were used to quantify total reducing carbohydrates by an adapted anthrone method (Trevelyan & Harrison, 1952). Briefly, cells were boiled in 12 N sulfuric acid for 1 h, and then rapidly mixed with the anthrone reagent and placed in an ice bath. The mixture samples were then boiled for several minutes until a clear gradient in color developed in the standards. Samples and standards were measured at the absorbance of 620 nm – 820 nm. The total carbohydrate concentration in the biological samples was quantified based on the plotted standard curve. Nitrate, nitrite and ammonium concentrations in the supernatants were measured by assays described in McNeely et al. (2014). Intracellular metabolite extraction and quantification was performed as described by Bennette et al. (2011). 120 μ L of extracts was vacuum-dried (Labconco Centri-Vap Concentrator), and the pellet was resuspended in 40 μ L LC-MS grade water for analysis. This LC-MS method measures central carbon metabolites in glycolysis, OPP, TCA, and nitrogen assimilation pathways, as well as adenylated nucleotides (ATP, ADP, and AMP) and pyridine nucleotides (NAD(P)H and NAD(P)⁺). The LC-MS analysis system and methods were described in Kumaraswamy et al. (2013).

2.5) Measurements of instantaneous H₂ production rate and pyridine nucleotide concentrations.

A home-built electrochemical cell described elsewhere (Ananyev et al., 2012) was used to measure the current from oxidation of dissolved H₂ in the cell culture that is in contact with a membrane-covered electrode (Clark cell). H₂ rate is represented as

electrical current (I , nA), which can be converted to gas volume using Faraday's second law (Korotcenkov et al., 2009) after integration of the current. In addition, an optical fluorescence unit combined to this electrochemical cell apparatus was used to monitor intrinsic fluorescence emission from reduced pyridine nucleotides, NADPH + NADH, at 420 nm. This emission was shown to be linearly proportional to the concentration *in vivo* (Harbig et al., 1976).

Samples for electrochemical and fluorescence measurements were prepared by centrifugation of 28 mL of cultures grown to 1.5 ± 0.2 OD_{730nm}, and washed twice in A⁻ media. Washed cells were resuspended in fresh A⁻ media and incubated under the same photoautotrophic condition for 1 h to reactivate nitrate reductase. After this incubation, cells were concentrated by centrifugation and resuspended in 500 μ L of A media with or without 5 mM nitrate. 50 μ L of the resuspended sample was loaded onto the electrochemical cell for H₂ rate and fluorescence measurements.

3. Results

The *AnarB* strain could not grow photoautotrophically on nitrate, but did grow on urea or ammonia (Figure 5-2). The WT strain grew at a similar growth rate on ammonia or urea, but rapid cell loss was very frequently observed in cultures grown on ammonia when they reached an $OD_{730\text{ nm}} \sim 1.2$. This rapid death was due to the alkalization of the medium that did not contain additional buffering (Sakamoto et al., 1998). Therefore, we chose urea as the nitrogen source for the growth of both strains prior to harvesting them for fermentation trials. The *AnarB* and WT strains produced very different biomass compositions when grown on urea (Table 4-2). The *AnarB* strain had a significantly higher total reducing sugar content (1.8-fold) but lower protein (0.7-fold) and chlorophyll *a* (0.6-fold) contents compared to WT in the early exponential “EE” phase ($OD_{730\text{ nm}}$ of ~ 0.5). When cultures reached $OD_{730\text{ nm}}$ of ~ 1.5 , cells were harvested for fermentation, denoted “HF”. “HF” cells, both WT and the *AnarB* exhibited increased reduced sugar contents (2.3-fold and 2.5-fold, respectively) and slightly lower protein contents (0.9-fold and 0.8-fold, respectively) compared to the “EE” phase. These numbers show that WT accumulates protein first followed by glycogen later in growth, while the *AnarB strain* significantly redirects biomass accumulation into glycogen reserves at the expense of protein accumulation throughout growth.

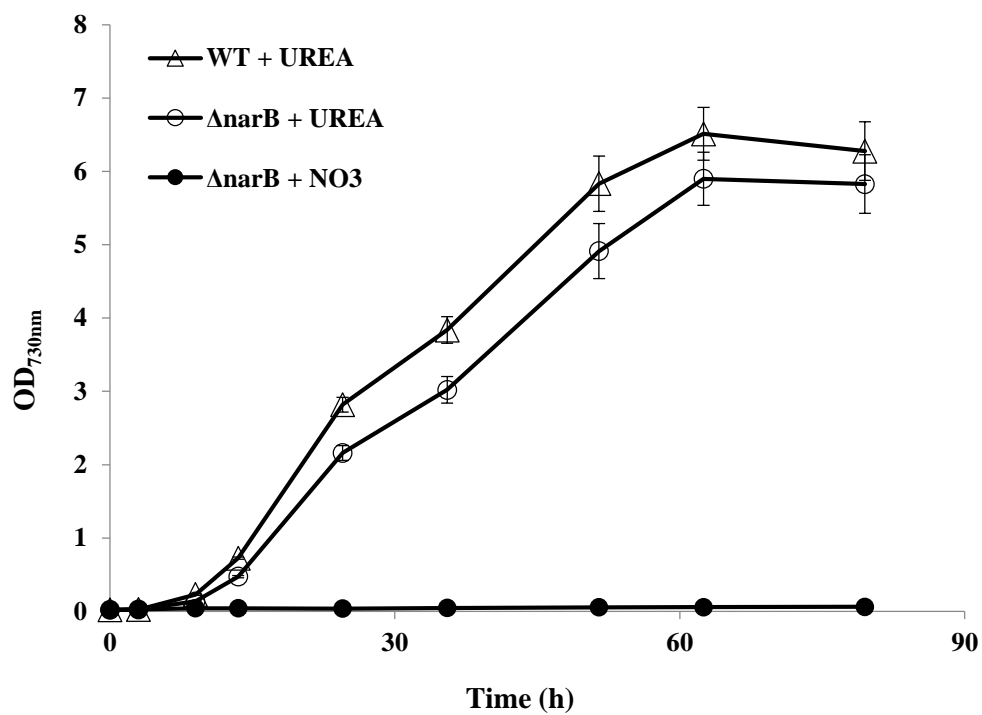


Figure 5-2 Growth curves of WT and the $\Delta narB$ strain photoautotrophically grown on 5 mM of urea or nitrate. The results are mean values of three biological replicates.

Strain	Chlorophyll a content (kg / 10 ¹⁷ cells)	Total reduced sugar content (mol / 10 ¹⁷ cells)				Total protein content (kg / 10 ¹⁷ cells)	
		HF	OF	AF	% change		
WT(+NO ₃) (EE)	11.3 ± 0.1	197 ± 7				353 ± 3	
WT (EE)	13.3 ± 0.2	212 ± 19				384 ± 9	
<i>AnarB</i> (EE)	8.2 ± 0.2	382 ± 24				294 ± 16	
		HF	OF	AF	% change	HF	
WT (HF)	N.A.	486 ± 2	618 ± 4	+NO ₃	464 ± 3	24.9	352 ± 6
				- NO ₃	464 ± 9	24.9	
<i>AnarB</i> (HF)	N.A.	937 ± 17	1079 ± 23	+NO ₃	847 ± 12	21.5	239 ± 6
				- NO ₃	832 ± 15	22.9	

Table 5-2 Chlorophyll-a, total reduced sugar content and total protein content of photoautotrophic cultures of WT and the *AnarB* strains grown on urea as the sole nitrogen source, except the one indicated by “+NO₃” that was grown on nitrate as the sole nitrogen source. “EE” refers to early exponential cultures measured at OD₇₃₀ of ~ 0.5. “HF” refers to cultures harvested for fermentation measured at OD₇₃₀ of ~1.5. “OF” refers to cultures at the onset of fermentation. “AF” refers to cultures right after the 2-day-fermentation was over. “% change” is the change of total reduced sugar content throughout the fermentation. “N.A.” means not available. The results are the mean values of three biological replicates.

During the autofermentation phase following the activation step, nitrate uptake, nitrite excretion and ammonia excretion by the WT and $\Delta narB$ strains were monitored daily for an extended time period (4 days) to visualize the kinetics of these processes better (Figure 5-3 A&B). Nitrate uptake was observed by both the WT and $\Delta narB$ cells, and overall the WT took up twice as much nitrate as the $\Delta narB$ strain over 4 days. For WT cells, 90% of the nitrate uptake occurred within the first day of fermentation, while nitrite was excreted at a similar rate on each day over the 4-day-autofermentation period. Overall, 51% of the nitrate taken up was excreted in the form of nitrite by the WT strain over 4 days. In contrast, less uptake of nitrate was observed in the $\Delta narB$ culture, and no nitrite was excreted. No ammonia excretion was observed in either strain within the 4 days. Nitrate uptake and nitrite excretion rates by WT cells fermented in the presence of nitrate were comparable to the rates previously reported by McNeely et al. (2014), confirming that the activation step induced nitrate reductase activity in WT cells (Figure 5-3 A&B). The $\Delta narB$ strain took up some nitrate but much less than WT. This is presumably because the nitrate permease is still active in this mutant. Nitrate uptake can occur by an unidentified low-efficiency transport mechanism, as the permease knockout mutant of *Synechococcus* 7002 was able to grow photoautotrophically on 12 mM nitrate (Sakamoto et al., 1999).

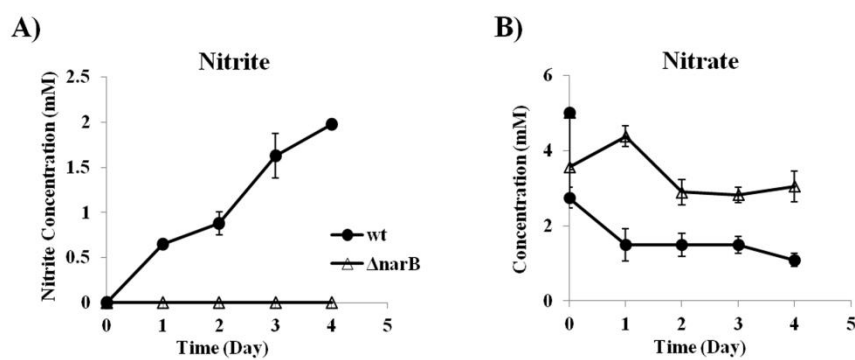


Figure 5-3 A) Nitrite excretion and B) nitrate uptake by the WT (dark circle) and $\Delta narB$ (open delta) of *Synechococcus 7002* under auto-fermentative condition in the presence of 5 mM nitrate. The results are mean values of four biological replicates.

After 2 days of dark anaerobic fermentation in sealed vials, WT cells catabolized the same amount of glycogen irrespective of the presence or absence of nitrate in the media. The *AnarB* strain, which contained significantly more glycogen following photoautotrophic growth, also catabolized ~50% more glycogen than WT during the same 2 day period of dark anoxia, and this was independent of the presence or absence of nitrate in the media (Table 4-3). This higher glycogen catabolic rate of *AnarB* led to a greater rate of fermentative product excretion (2.5-fold more lactate), independent of the presence or absence of nitrate. When the fermentation was conducted in the presence of nitrate, the *AnarB* strain produced 7 times more H₂ than WT after 2 days of fermentation, while in the absence of nitrate, both *AnarB* and WT produced the same amount of H₂, as expected (Figure 5-4A). We also measured CO₂ in the headspace (Figure 5-4B). The WT strain produced 2-fold more CO₂ in the headspace when fermented in the presence of nitrate than without nitrate, similar to our previous report and consistent with catabolic flux through the OPP pathway (McNeely et al., 2014). Such increase in the CO₂ level in the presence of nitrate was not observed with the *AnarB* strain (Figure 5-4B). After 2-days of fermentation in nitrate media, nitrite was the main product excreted by the WT culture (Table 4-4), consistent with a previous report (McNeely et al., 2014). Of the 3.7 ± 0.1 mM of nitrate taken up by cells from the media, one-fourth (0.9 ± 0.1 mM) was excreted as nitrite. No nitrite was produced by the *AnarB* strain (Figure 5-4C). No ammonia excretion was observed from either strain, regardless of the presence of nitrate.

Category	R.S.C.	H ₂	Acetate	Lactate	Alanine ^b	Nitrite
WT + NO ₃	154 ± 5	2 ± 0.5	0	167 ± 7	6	748 ± 113
WT – NO ₃	154 ± 10	15 ± 3	56 ± 2	321 ± 14	25	0
<i>AnarB</i> + NO ₃	232 ± 26	14 ± 3	33 ± 15	409 ± 41	37	0
<i>AnarB</i> – NO ₃	246 ± 27	12 ± 2	36 ± 2	382 ± 13	42	0
reductant eq. per molecule (100% Glycolysis)	2	-1	1	-1	-1	-1
reductant eq. per molecule (100% OPP)	7	-1	1	-1	-1	-1
WT + NO ₃ reductant eq. (100% Glycolysis)	308	-2 (0.6%)	0	-167 (54.2%)	-6 (1.9%)	-748 (243%)
WT + NO ₃ reductant eq. (100% OPP)	1078	-2 (0.2%)	0	-167 (15.5%)	-11 (1.0%)	-748 (69.4%)
WT – NO ₃ reductant eq. (100% Glycolysis)	308	-15 (4.1%)	56	-321 (88.2%)	-25 (6.9%)	0 (0%)
<i>AnarB</i> + NO ₃ reductant eq. (100% Glycolysis)	464	-14 (2.8%)	33	-409 (82.3%)	-37 (7.4%)	0 (0%)
<i>AnarB</i> – NO ₃ reductant eq. (100% Glycolysis)	492	-12 (2.3%)	36	-382 (72.3%)	-42 (8.0%)	0 (0%)

Table 5-3 Measured reduced sugars catabolized (RSC, or glucose equivalents) and measured excreted metabolite yields after 2 days of dark anaerobiosis in the presence or absence of 5 mM NO₃⁻. The units are mol / 10¹⁷ cells. The results are the mean values of four biological replicates. The amount of excreted alanine was estimated based on percentages (8% and 2% of total theoretical carbon equivalents in the absence and presence of nitrate, respectively) given in McNeely et al. (2010, 2014). % numbers in the brackets represent the fraction of RSC reducing equivalents that go into each of the

products. Starting from row 6, a positive number means “produce NAD(P)H equivalent”, and a negative number means “consume NAD(P)H equivalent”.

Strain + Fermentation Condition	Reductant equivalent catabolized ^a		Total reductant equivalent excreted ^b	Pathway utilized based on reductant equivalent yield/consumpti on analysis
	100% Glycolysis	100% OPP		
WT + NO₃	308	1078	752	Glycolysis + OPP
WT – NO₃	308	1078	305	Glycolysis
<i>ΔnarB</i> + NO₃	464	1624	397	Glycolysis
<i>ΔnarB</i> – NO₃	492	1722	412	Glycolysis

Table 5-4 Reductant balance calculations after 2 days of fermentation in the presence or absence of 5 mM NO₃⁻. Units are mol/10¹⁷ cells. Actual quantities of consumed glucose equivalents and excreted metabolites are shown in Table 4-3.

^a Calculated yield of reductant (as NAD(P)H) expected from the measured carbohydrate catabolized assuming 2 equivalent per glucose (formed solely by the reactions of glycolysis) or 7 per glucose (formed via OPP and glycolysis).

^b Calculated yield of reductant (as NADH) expected from the measured yields of excreted acetate, H₂, lactate, alanine and nitrite assuming carbon flux via glycolysis.

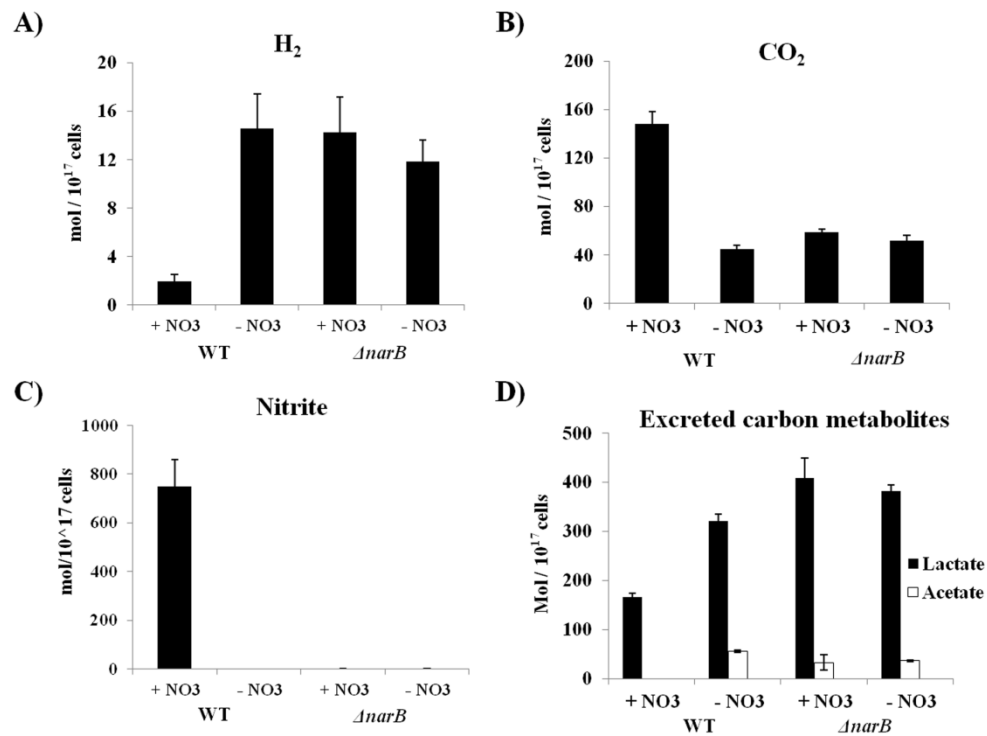


Figure 5-4 Excretion of fermentative end products by the WT and $\Delta narB$ strains of *Synechococcus 7002* after 2 days of autofermentation. “+NO₃” or “-NO₃” indicates presence and absence of nitrate respectively in the fermentative medium. A) H₂ evolved; B) CO₂ accumulated in the headspace without acidification of the medium; C) Extracellular nitrite excretion; D) organic carbon metabolites. The results are mean values of four biological replicates.

When fermented in the absence of nitrate, WT produced more D-lactate and acetate than when cells were fermented in the presence of nitrate. However, the *ΔnarB* strain produced similar amounts of D-lactate and acetate when fermented with and without nitrate (Figure 5-4D). D-Lactate production by the *ΔnarB* strain was ~20% higher than WT, when fermented without nitrate. These different patterns of excreted metabolites in the two strains were accompanied by large differences in the intracellular adenylate nucleotides and pyridine nucleotide levels (Figure 5-5 and Figure 5-6B). The cellular energy charge (CEC) and NAD(P)H/NAD(P)⁺ ratio reveal the intracellular adenylate energy status and redox status, respectively. For the WT strain a 25% decrease in CEC and a 75% decrease in redox poise were observed when fermented in the presence of nitrate, consistent with expectations for adenylate-dependent nitrate uptake and reduction to nitrite. By contrast in the *ΔnarB* strain, these two parameters did not change in the presence or absence of nitrate (Figure 5-5).

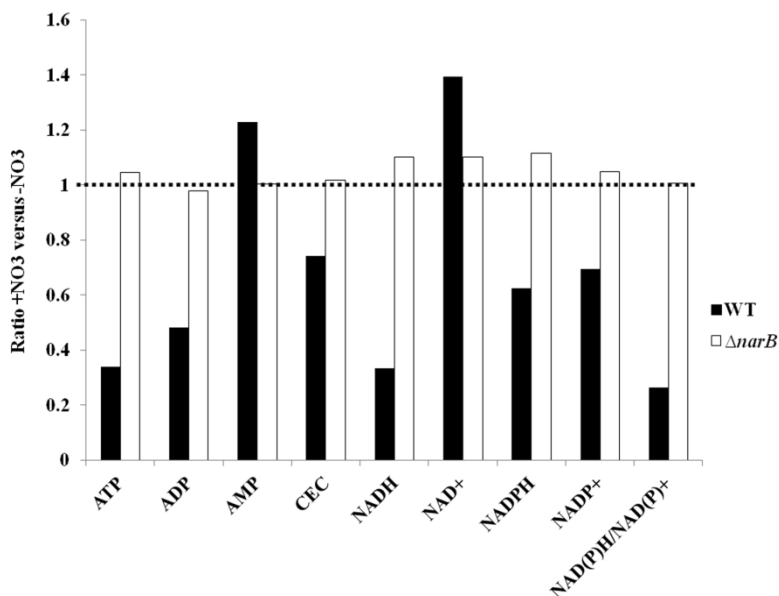


Figure 5-5 The ratio of intracellular metabolite concentrations in the presence vs. absence of nitrate in the fermentation media after 2 days of fermentation. Concentration ratios for adenosine phosphates (AXP) and pyridine nucleotides (NADPH, NADH, NADP⁺, NAD⁺) are given, as well as the derived quantity cellular energy charges: $CEC = ([ATP] + 1/2 [ADP]) / ([ATP] + [ADP] + [AMP])$, and the redox poise: $NAD(P)H / NAD(P)$. The unratiod concentrations are given in Table 4-5.

Strain Condition	Concentration (mM / 10^{12} cells)						
	ATP	ADP	AMP	NADH	NAD ⁺	NADPH	NADP ⁺
WT + NO ₃	140 ± 31	72 ± 6	108 ± 39	500 ± 58	116 ± 12	1.7 ± 0.5	13 ± 1.2
WT - NO ₃	410 ± 29	149 ± 16	88 ± 7	1504 ± 161	83 ± 9	2.7 ± 0.3	19 ± 0.6
<i>AnarB</i> + NO ₃	293 ± 11	96 ± 6	169 ± 11	825 ± 162	96 ± 10	2.1 ± 0.5	15 ± 0.5
<i>AnarB</i> - NO ₃	280 ± 17	98 ± 6	159 ± 8	749 ± 104	87 ± 15	1.8 ± 0.2	14 ± 1.4

Table 5-5 Concentrations of adenosine phosphates (AXP) and pyridine nucleotides (NADH, NAD⁺, NADPH, NADP⁺) in the presence vs. absence of nitrate in the fermentation media at day 2. The results are the mean values of four biological replicates.

To eliminate H₂ uptake by cells, which was previously shown to lower the net H₂ production rate and is in thermodynamic equilibrium with cellular utilization of pyridine nucleotides (Ananyev et al., 2012), we used electrochemical removal of dissolved H₂, so-called H₂ “milking conditions. We monitored the H₂ production rate from the current, while simultaneously monitoring the concentration of total NAD(P)H by fluorescence (Figure 5-6). Under H₂ milking in the absence of nitrate, WT produced H₂ at an average rate of 37 ± 4 mol/10¹⁷ cells/day (Table 4-6), which is 4.9 times faster than in sealed vials. As shown in Figure 5-6A, the initial rate rose to a plateau at 12 h and remained approximately constant until 20 h when the experiment was stopped. During this same period the NAD(P)H concentration rises continuously in multiple phases (Figure 5-6B). In the presence of nitrate, the H₂ production kinetics of WT showed a lag phase during the initial 7 hours, which coincides with the reduction of nitrate (or excretion of nitrite). The sharp transition is the time when nitrate is eliminated from the medium, and reductant is then available to produce more H₂ and other fermentative metabolites, as previously seen (Ananyev et al., 2012; McNeely et al., 2014). Consistent with the lower H₂ flux in the presence of nitrate, the concentration of NAD(P)H is significantly lower than observed in the absence of nitrate (Figure 5-6B). By contrast, the *AnarB* strain has no such difference in the NAD(P)H concentration over 20 h between cells fermented with or without nitrate (Figure 5-6D), and both have similar rate and no lag phase in H₂ production (Figure 5-6C). The *AnarB* strain produced H₂ at 49 ± 2 mol/10¹⁷ cells/day and 44 ± 3 mol/10¹⁷ cells/day, with and without nitrate, respectively. This rate is 30% faster than WT in the absence of nitrate on the electrode and is consistent with the larger glycogen content of the deletion strain. Overall, deletion of the *narB* gene combined with

the H₂ “milking” strategy increased the H₂ evolution rate for 49-fold compared to the rate in WT in the presence of nitrate.

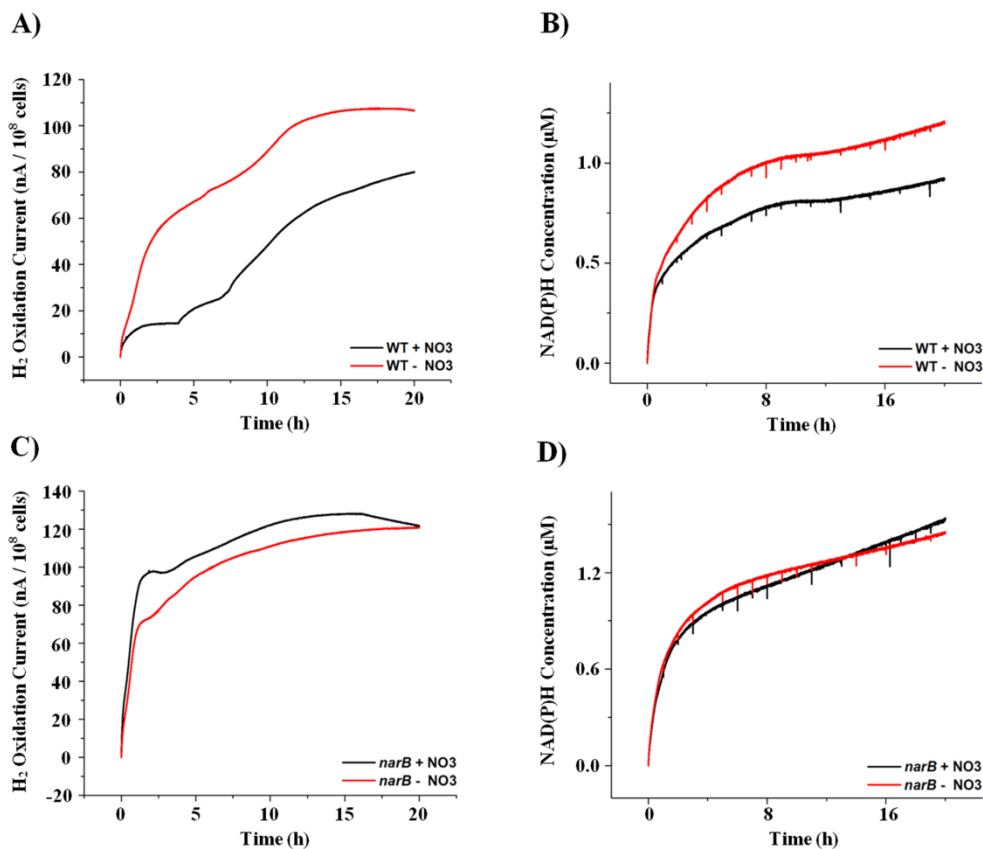
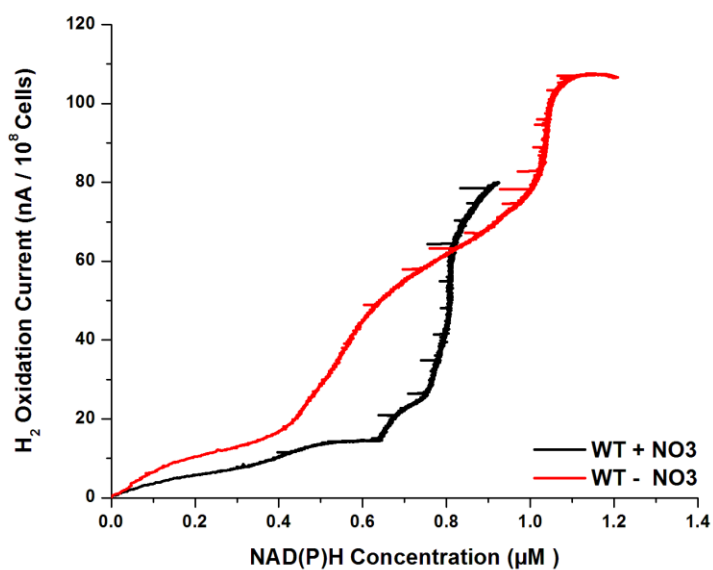


Figure 5-6 Autofermentative H₂ evolution rates (A & C) measured via H₂ rate electrode, and NAD(P)H concentrations (B&D) measured by fluorescence of WT and $\Delta narB$ strains during dark anaerobiosis with or without nitrate (“+ NO₃” and “- NO₃”) on the H₂ electrode (milking conditions). The results are the mean of three biological replicates. Integrated yields of H₂ from A) and C) are listed in Table 4-6. Plot of the H₂ evolution rate vs. the NAD(P)H concentration for WT and $\Delta narB$ strains were given in Figure 5-7.

A)



B)

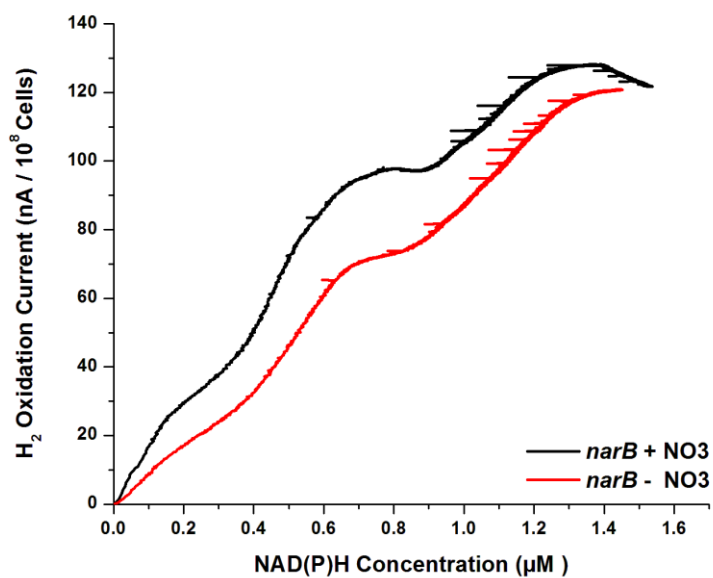


Figure 5-7 Plot of autofermentative H₂ evolution rate against intracellular NAD(P)H concentration of WT (A) and $\Delta narB$ strains (B) during dark anaerobiosis with or without nitrate (“+ NO₃” and “- NO₃”) on the H₂ electrode (milking condition).

Category	H₂ (Vial)	H₂ (Milking)
WT + NO₃	1 ± 0.3	Non-comparable
WT – NO₃	7.5 ± 1.5	37 ± 4
<i>ΔnarB</i> + NO₃	7 ± 1.5	49 ± 2
<i>ΔnarB</i> – NO₃	6 ± 1	44 ± 3

Table 5-6 Comparison of H₂ evolution rates in the vial experiments and “milking”

experiments. Units are mol / 10¹⁷ cells / day. H₂ evolution rate of WT in the presence of nitrate under milking condition is non-comparable with other results in the table, as nitrate was completely consumed within the first 7 hours (Figure 5-6).

4. Discussion

Nitrogen is essential for cellular synthesis of proteins, which accounts for up to 60% of the total biomass in *Synechococcus* 7002 (Vu et al, 2013). Reducing nitrate to ammonia to support amino acid synthesis costs eight electrons. Nitrate assimilation could account for more than 30% of the total electron consumption in *Anacystis nidulans* under photoautotrophic conditions (Flores et al., 1983). Uptake of ammonia or urea instead of nitrate can therefore save eight electrons per nitrogen atom assimilated. These saved electrons can be redirected to fix inorganic carbon and to produce more biomass. During the early exponential growth phase on urea, the extra fixed inorganic carbon was found to be directed to the synthesis of proteins rather than reduced sugars in WT strain of *Synechococcus* 7002 (Table 4-2). By contrast, for the $\Delta narB$ strain photoautotrophic growth on urea results in substantially less protein and chlorophyll and more glycogen at all phases of growth (Table 4-2), indicating that carbon partitioning changes in response to the identity of the nitrogen precursor.

During autofermentation with nitrate, CO₂ gas accumulated in the headspace of sealed vials was 2-fold higher in WT than the $\Delta narB$ strain (Figure 5-4B). This elevated CO₂ production in the presence of nitrate was previously shown to be caused by a higher carbon flux through the OPP pathway in *Synechococcus* 7002 (McNeely et al., 2014). During fermentation, when one glucose molecule is catabolized through the glycolysis pathway, it yields two molecules each of acetyl-CoA and CO₂ (Figure 5-9). By contrast, maximally four molecules of CO₂ and one acetyl-CoA molecule per glucose are produced per glucose molecule catabolized through the OPP pathway. Even though 50% more glycogen was catabolized during 2 days fermentation of the $\Delta narB$ strain than WT

fermented on nitrate (Table 4-3), WT still excreted significantly more CO₂ than the *AnarB* strain. This indicates that nitrate did not induce a higher carbon flux through the OPP pathway in the *AnarB* strain, in contrast to WT. This conclusion is further supported by the observation for the *AnarB* strain that similar levels of CO₂ were observed regardless of the presence or absence of nitrate in the fermentation medium (Figure 5-4B). WT fermented on nitrate had significantly lower cellular ATP content and CEC and significantly lower NAD(P)H and redox poise compared to WT fermented without nitrate (Figures 4.5 and 4.7). These observations are also consistent with redirection of carbon flux from glycolysis to OPP, as explained next.

During autofermentation, the theoretical maximum yield is 5 ATP per glucose equivalent catabolized through the glycolytic pathway, starting with glucose-6-phosphate and if all the pyruvate is converted into acetate. The calculation is shown in Table 4-7. The theoretical maximum number of ATP molecules produced from catabolism of glycogen through the OPP pathway is 0 or 3 ATP per glucose equivalent, depending on whether zero or one glyceraldehyde-3-phosphate (GAP) molecules produced are catabolized by the lower branch of glycolysis (steps 3, 4 and 5 in Table 4-7). The same two routes produce about 3-fold different reductant yields, 7 (OPP) vs. 2 (glycolysis) NAD(P)H molecules per glucose equivalents. For absolute redox poise measurements, we rely more upon the *in vivo* fluorescence data (Figure 5-6) than the mass spec data (Figure 5-5), owing to chemical instability of the pyridine nucleotide ratio following cell rupture and workup. We see that during autofermentation for the WT, the presence of nitrate produces a lower redox poise and less NAD(P)H than without nitrate, consistent with consumption to form nitrite. This difference disappears for the *AnarB* strain. Neither

decreased CEC (Figure 5-5) nor decreased intracellular NAD(P)H concentration (Figure 5-6D) was observed in the *AnarB* strain fermented with nitrate compared to without nitrate. We interpret this to suggest that nitrate is not itself an effector of any enzymes or genes involved in fermentative metabolism in *Synechococcus* 7002. Because there was no metabolism of nitrate in the *AnarB* strain, nitrate could not act as a strong terminal electron acceptor to lower the cellular redox poise, which is known to inhibit glucose-6-phosphate dehydrogenase (G6PDH) activity. This enzyme functions in the first step of the OPP pathway. G6PDH has been shown to be redox-regulated in multiple microorganisms (Gleason, 1996; Luzzatto, 1980).

Step #	Reaction	ATP yield (ATP / glucose equivalent)
1	glycogen \rightarrow glucose-6-phosphate	0
2	fructose-6-phosphate \rightarrow fructose-1,6-biphosphate	-1
3	2 (1,3-biphosphoglycerate) \rightarrow 2 (3-phospho-glycerate)	2
4	2 phospho-enol-pyruvate \rightarrow 2 pyruvate	2
5	2 acetyl-coA \rightarrow 2 acetate	2
	Total ATP yield	5

Table 5-7 The calculation of theoretical maximum ATP yield per glucose equivalent catabolized through the glycolytic pathway during autofermentation.

We conducted a quantitative inventory to compare the theoretical yield of reducing equivalents to the actual experimental yield based on the known amount of glycogen catabolized (Table 4-4 & Figure 5-8). The theoretical reducing equivalent yields ranged between values calculated based on either glycolysis only pathway or OPP + lower glycolysis pathways for both strains fermented with or without nitrate. The total actual reducing equivalent requirement of WT fermented with nitrate was within this theoretical range, which indicated that both glycolysis and OPP pathways were used when WT was fermented with nitrate. For WT fermented without nitrate, the theoretical yield of reducing equivalents utilizing only the glycolytic pathway matched the observed yield, which suggested that the culture exclusively used glycolysis to breakdown its glycogen in the absence of nitrate. The *ΔnarB* strain catabolized its glycogen at the same rate in the presence and absence of nitrate and ~50% faster than WT. This elevated catabolic rate is likely due to the increased initial glycogen content in the *ΔnarB* strain compared to WT (Table 4-2), consistent with similar previous results (Guerra et al., 2013a). The *ΔnarB* strain produced excess reducing equivalent during fermentation relative to WT as seen by pyridine nucleotide fluorescence *in vivo* (Figure 5-6) and by mass spectrometry both with and without nitrate (Figure 5-5). The majority of the reducing equivalents in the *ΔnarB* strain were directed to synthesize lactate (Figure 5-8). The excess amount of reducing equivalents may be accounted for by some carbon metabolites that we did not monitor, such as 2-OG, fumarate and citrate. Although more glycogen was catabolized, the *ΔnarB* strain did not produce more H₂ compared to WT fermented without nitrate. In summary, inactivation of the *narB* gene redirected carbon flux from the OPP pathway to glycolysis (Figure 5-9).

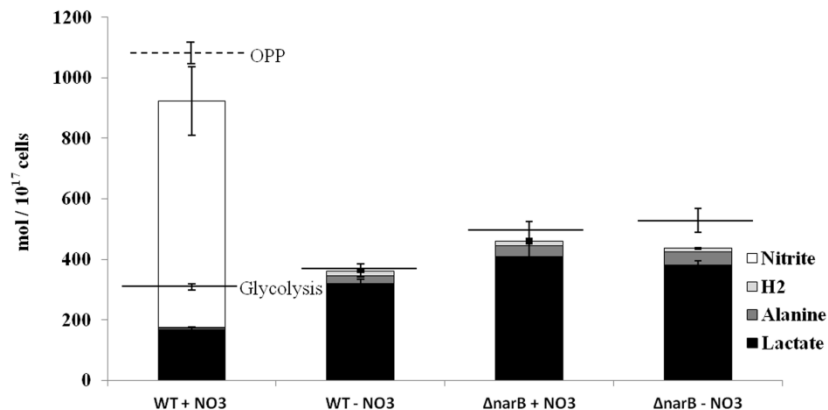


Figure 5-8 Autofermentative reductant balances for the WT and *AnarB* strains with or without nitrate (“+ NO₃” and “- NO₃”) in the fermentation medium using seal vials. The bar graph gives the yield of lactate (black), H₂ (gray) and nitrite (white), the sum of which is the total excreted reductant. The solid horizontal line gives the calculated yield of NAD(P)H equivalents that would have formed from the amount of catabolized carbohydrate and excreted acetate, assuming carbon flux through the upper and lower branches of glycolysis (EMP pathway). The semi-solid horizontal line gives the yield of NAD(P)H calculated from the catabolized carbohydrate and excreted acetate assuming carbon flux through the oxidative pentose phosphate pathway (OPP) with lower glycolysis pathway. All results are the mean of four biological replicates.

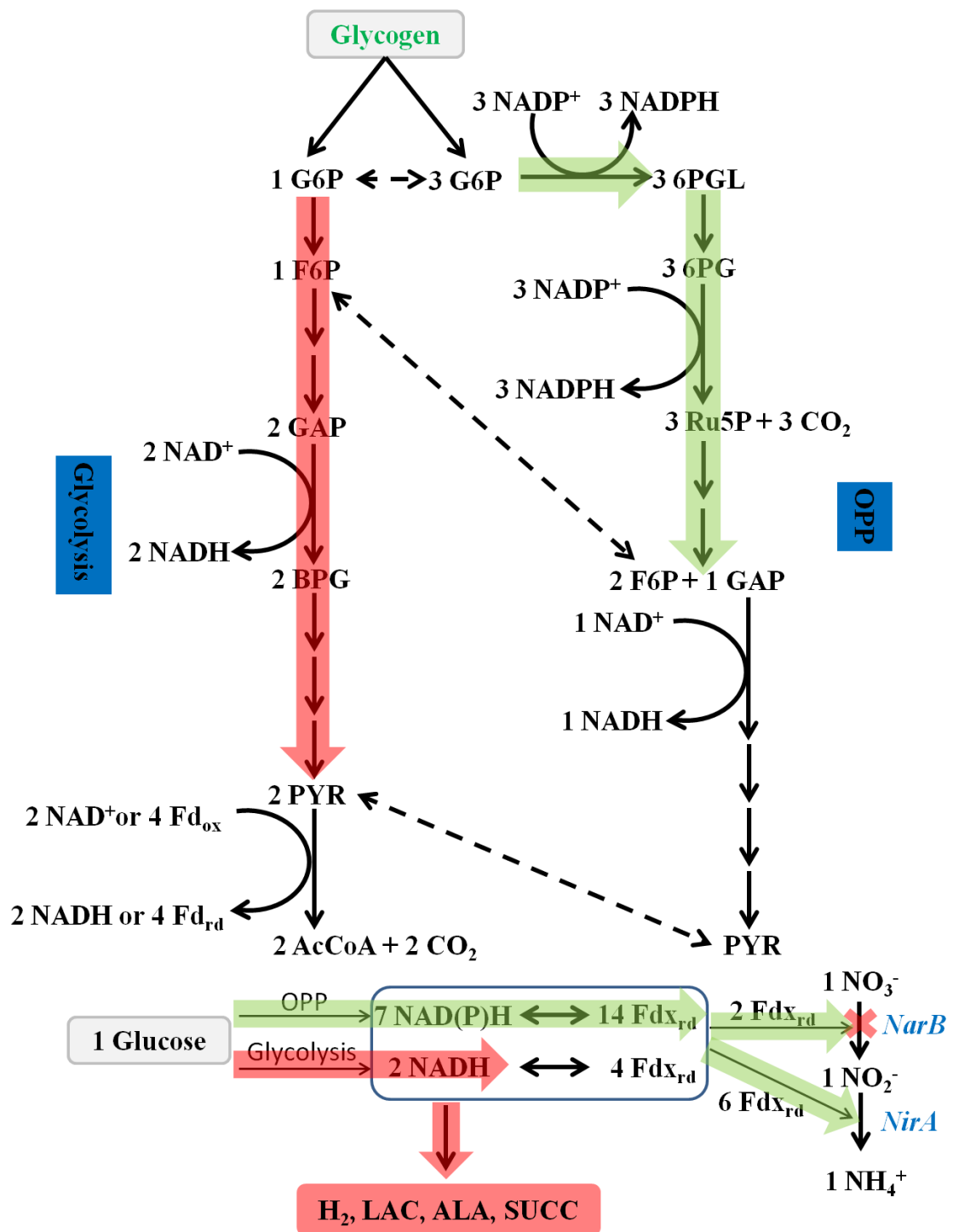


Figure 5-9 A quantitative schematic representation of overall effects of deleting the *narB* gene in *Synechococcus* 7002 when cultures are fermented with nitrate. Green color

shaded areas represent the major carbon flux and reductant flux routes for WT, and red color shaded areas represent the major carbon flux and reductant flux routes for the *narB* strain. Metabolites: G6P = glucose-6-phosphate; F6P = fructose-6-phosphate; GAP = glyceraldehyde-3-phosphate; BPG = 1, 3-bisphosphoglycerate; PYR = pyruvate; 6PGL = 6-phosphogluconolactone; 6PG = 6-phosphogluconate; Ru5P = ribulose-5-phosphate; AcCoA = Acetyl-CoA; Fdx_{rd} = reduced ferredoxin; LAC = D-lactate; ALA = alanine; SUCC = succinate. Enzyme: NarB = nitrate reductase; NirA = nitrite reductase.

In 2 days, in total, 180 mol/10¹⁷ cells and 361 mol/10¹⁷ cells of reducing equivalents were consumed to synthesize H₂, lactate and alanine in WT fermented with or without nitrate, respectively. Accordingly, nitrate consumes ~50% of the reducing equivalents generated in WT cells fermented with nitrate. Because almost all the reducing equivalents were used to synthesize fermentative products in the form of organic acids and H₂ in the *ΔnarB* strain, it is then reasonable to conclude that inactivation of the *narB* gene redirected ~50% of the reducing equivalents back to the generation of fermentative products. On the H₂ electrode which continuously “milks” H₂ from cells, the *ΔnarB* strain fermented with or without nitrate produced H₂ at a 1.3-times faster rate than WT fermented without nitrate. This result indicates that continuous removal of H₂ from the *ΔnarB* strain successfully redirects a portion of NAD(P)H from lactate dehydrogenase to the Hox hydrogenase.

Unlike the *narB* strain of *Synechocystis* 6803 that showed similar or lower H₂ evolving capacity compared to WT in the presence of nitrate (Baebprasert et al, 2011), the *ΔnarB* strain of *Synechococcus* 7002 in this study, showed a 6-fold higher H₂ yield than WT in the presence of nitrate when fermented in vials. NarB is the only known nitrate reductase in *Synechocystis* 6803 and *Synechococcus* 7002. Previously, Appels’ group (Gutthann et al., 2007) has reported that inhibition of nitrate reductase in *Synechocystis* 6803 by replacing molybdate with tungstate resulted in an increased fermentative hydrogen production. Interestingly, inactivation of *narB* in *Synechocystis* 6803 did not result in an increase in H₂ production compared to the WT strain when 5 mM nitrate was present in the fermentation medium. However, a significant increase in H₂ production was achieved when both *narB* and *nirA* were knocked out in *Synechocystis*

6803 (Baebprasert et al., 2011). This raises several questions: In a $\Delta narB$ strain of *Synechocystis* 6803, without consuming significant amount of reducing equivalents due to absence of nitrate/nitrite reduction, how were reducing equivalents distributed? Why was there no increase in total H₂ yield? Why were more reducing equivalents redirected to produce more H₂ in the *narB* + *nirA* double mutant? In further confusing results, the authors observed that H₂ production was generally higher in the absence of nitrate, compared to presence of nitrate even for the *narB* + *nirA* double mutant, but authors did not give any explanations. To reconcile these inconsistencies, firstly the authors should carefully check to verify that their *narB* and *narB/nirA* strains are properly segregated. If both strains have been well segregated, then it would be helpful to perform the same quantitative analysis of the reducing equivalents generated from catabolized glycogen and consumed by the terminal products, as well as a detailed metabolomic study to identify any metabolite changes upon the supplementation of nitrate during fermentation. In the present study we conducted such experiments to examine fully these key aspects using the $\Delta narB$ strain of *Synechococcus* 7002 and obtained very different results.

5. Conclusion

Elimination of the *narB*-encoded nitrate reductase in *Synechococcus* 7002 resulted in significantly elevated fermentative H₂ yields in the presence of nitrate. Eliminating nitrate reductase activity could help reduce the cost of biomass pretreatment prior to fermentation by eliminating nitrate reduction, which can compete for reducing equivalents and reduce the yields of desired fermentative products. Nonetheless, H₂ production only accounted for a fraction of the total reductant pool in the $\Delta narB$ strain. To re-route the majority of reducing equivalents effectively to the bidirectional NiFe-hydrogenase and produce more H₂, the *narB* mutation will have to be combined with other mutations that are known to enhance H₂ yields during fermentation in addition to the “milking” strategy. The combination of these effects should lead to significantly enhanced H₂ yields.

Chapter 6: Conclusions

A quantitative understanding of carbon flux distributions under different photoautotrophic conditions is a key factor in identifying metabolic bottlenecks that will help construct productive cyanobacterial strains for biofuels. The object of this thesis was to generate quantitative insights into carbon distributions under photoautotrophic conditions and reductant equivalent distributions under fermentative conditions in a model cyanobacterium *Synechococcus* sp. PCC 7002. In chapter 2, I constructed and employed a mathematical FBA model to predict photoautotrophic carbon flux distributions under different light and nitrogen conditions. Then, in chapter 3 and 4, I described experiments feeding cultures with ^{13}C -substrates that generated more experimental fluxomic results to support predictions made in chapter 2, and further enhance our knowledge of cyanobacterial carbon assimilatory routes under light. Chapter 5 took advantage of our previous knowledge of fermentative nitrate metabolism to create a strain that allocated electrons towards fermentative metabolites including H_2 production rather than nitrate reduction.

In chapter 2, we constructed a comprehensive genome-scale model of photoautotrophic growth, denoted *iSyp821*, for the cyanobacterium *Synechococcus* 7002, which incorporated a variable biomass objective function (*vBOF*) that was constrained to fit the measured cellular carbohydrate/protein content under different light intensities. *iSyp821* provided rigorous agreement with experimentally measured cell growth rates and inorganic carbon uptake rates as a function of light intensity. In addition, *iSyp821* simulated two observed metabolic transitions that occurred as light intensity increased: 1)

from cyclic to linear electron flow through PSI, and 2) from active carbon allocation (growth) to carbon and energy storage mode. *iSyp821* predicted significant flux through a hybrid gluconeogenesis-pentose phosphate (PP) pathway that partitions fixed CO₂ intermediates into glycogen by an alternative pathway rather than through conventional gluconeogenesis, which was verified experimentally by following the kinetics of ¹³C metabolite formation from ¹³CO₂ fixation. *iSyp821* can also utilize experimentally measured transcriptomic data to estimate changes in concentrations of gene products (enzymes) under nutrient stress. We found that by using this strategy, *iSyp821* correctly predicted the observed redistribution pattern of carbon products under nitrogen depletion, including decreased rates of CO₂ uptake, amino acid synthesis, and increased rates of glycogen and lipid synthesis.

In chapter 3, glutamate decarboxylase and N-acetylornithine aminotransferase were biochemically characterized and our results demonstrated that N-acetylornithine aminotransferase could also function as a GABA aminotransferase. Furthermore, the glutamate decarboxylase from *Synechocystis* sp. PCC 6803 was expressed in *Synechococcus* sp. PCC 7002, which originally lacked the enzyme, to study the metabolic correlations between the SSA route and the GABA shunt. *In vivo* metabolite profiling studies of 7 *Synechococcus* sp. PCC 7002 mutant strains relating to these two routes were also conducted to further examine their physiological importance and connections. Our results showed that all SSA route mutants suffered reduced rates of photoautotrophic growth and oxygen evolution, and had lower chlorophyll *a* contents. Metabolite profiling also indicated that, compared to 2-oxoglutarate decarboxylase, the GABA shunt was less efficient in converting 2-oxoglutarate to succinic semialdehyde in *Synechococcus* sp.

PCC 7002. The metabolic profiling study of these two TCA variants will provide new insights to carbon and nitrogen metabolism as well as pathway evolution of the TCA cycle in cyanobacteria.

In chapter 4, we investigated the repartitioning of carbon fluxes upon nitrogen deprivation, a treatment that significantly increased glycogen content at the expense of growth rate. We presented the first application of ^{13}C -based isotopically nonstationary metabolic flux analysis (INST-MFA) to photoautotrophic metabolism of a cyanobacterium, *Synechococcus* sp. PCC 7002. We illustrated a semi-quantitative method based on simple first-order kinetic modeling to identify 1) qualitative changes of carbon flux distributions at three major flux branches: G6P, 3PG and AKG under nitrogen deprivation and 2) a significant portion of MAL directly synthesized through the phosphoenolpyruvate synthase reaction. Then, we conducted quantitative INST-MFA and validated all discoveries generated by the semi-quantitative method. We discovered that increased glycogen synthesis under nitrogen deprivation was caused by increased carbon flux at the $3\text{PG} \rightarrow \text{GAP/DHAP}$ step as well as at the $\text{G6P} \rightarrow \text{ADPGLUC}$ step. Additionally, our INST-MFA results showed 1) the major role of the malic cyclic route ($\text{PEP} \rightarrow \text{OXA} \rightarrow \text{MAL} \rightarrow \text{PYR} \rightarrow \text{PEP}$) for generating PYR for photoautotrophic biosynthesis and maintaining the ATP/NAD(P)H ratio during photosynthesis; 2) significant photoautotrophic fluxes going through the SSA route ($> 6\%$ of the RuBiSCO carboxylation activity) to support optimal photoautotrophic growth; and 3) a route change of fixed $\text{CO}_2 \rightarrow$ glycogen from conventional gluconeogenesis to a hybrid gluconeogenesis-pentose phosphate (hGPP) pathway. These findings bring the field multiple new concepts in the biology of photosynthetic growth in cyanobacteria.

In chapter 5, we constructed a knockout mutant of nitrate reductase, encoded by *narB* in order to eliminate the electron competition by nitrate reduction, in *Synechococcus* sp. PCC 7002. As expected, $\Delta narB$ was able to take up intracellular nitrate but was unable to reduce it to nitrite or ammonia, and was unable to grow photoautotrophically on nitrate. During photoautotrophic growth on urea, $\Delta narB$ significantly redirected biomass accumulation into glycogen at the expense of protein accumulation. During subsequent dark fermentation, metabolite concentrations - both the adenylate cellular energy charge (\sim ATP) and the redox poise (NAD(P)H/NAD(P)) - were independent of nitrate availability in $\Delta narB$, in contrast to the wild type (WT) control. The $\Delta narB$ strain diverted more reducing equivalents from glycogen catabolism into reduced products, mainly H₂ and D-lactate, by 6-fold (2.8% yield) and 2-fold (82.3% yield), respectively, than in WT. Continuous removal of H₂ from the fermentation medium (milking) further boosted net H₂ production by 7-fold in $\Delta narB$, at the expense of less excreted lactate, resulting in a 49-fold combined increase in the net H₂ evolution rate over the course of 2 days of fermentation compared to the WT. The absence of nitrate reductase eliminated the inductive effect of nitrate addition on rerouting carbohydrate catabolism from glycolysis to the oxidative pentose phosphate (OPP) pathway, indicating that intracellular redox poise and not nitrate itself acts as the control switch for carbon flux branching between pathways.

The results from my thesis enhance our understanding of cyanobacterial metabolisms at different growth and survival stages. Carbon flux distribution patterns quantitatively presented in chapter 4 provide valuable guidance for metabolic engineering to achieve higher biomass productivity and therefore more substrates for the

consequential fermentative productions. The new roles of existing carbon anabolism pathways illustrated in chapter 2 and 4 are worth further exploring so that the new biological insights brought by these discoveries can benefit the world in a more applicable way.

References

- Abed, R.M., Dobretsov, S., & Sudesh, K.** (2009) Applications of cyanobacteria in biotechnology. *J Appl Microbiol.* 106:1-12.
- Adebiyi, A.Q., Jazmin, L.J., & Young, J.D.** (2015) ¹³C flux analysis of cyanobacterial metabolism. *Photosynth Res.* 126:19-32.
- Alagesan, S., Gaudana, S.B., Sinha, A., & Wangikar, P.P.** (2013) Metabolic flux analysis of *Cyanothece* sp. ATCC 51142 under mixotrophic conditions. *Photosynth Res.* 118:191-198.
- Allen, J.F.** (2003) Cyclic, pseudocyclic and noncyclic photophosphorylation: New links in the chain. *Trends Plant Sci.*, 8:15–9.
- Ananyev, G.M., Skizim, N.J., & Dismukes G.C.** (2012) Enhancing biological hydrogen production from cyanobacteria by removal of excreted products. *J Biotechnol.* 162:97-104.
- Antoniewicz, M.R., Kraynie, D.F., Laffend, L.A., Gonzalez-Lergier, J., Kelleher, J.K., & Stephanopoulos, G.** (2007) Metabolic flux analysis in a nonstationary system: fed-batch fermentation of a high yielding strain of *E. coli* producing 1,3-propanediol. *Metab Eng.* 9:277–292.
- Anfelt, J., Kaczmarzyk, D., Shabestary, K., Renberg, B., Rockberg, J., Nielsen, J., Uhlén, M., & Hudson, E.P.** (2015) Genetic and nutrient modulation of acetyl-CoA levels in *Synechocystis* for n-butanol production. *Microb Cell Fact.* 14:167.
- Antal, T.K. & Lindblad, P.** (2005) Production of H₂ by sulphur-deprived cells of the unicellular cyanobacteria *Gloeocapsa alpicola* and *Synechocystis* sp. PCC 6803 during dark incubation with methane or at various extracellular pH. *J Appl Microbiol.* 98:114-120.
- Antoniewicz, M.R., Kelleher, J.K., & Stephanopoulos, G.** (2006) Determination of confidence intervals of metabolic fluxes estimated from stable isotope measurements. *Metab Eng.* 8(4):324-337.
- Atsumi, S., Higashide, W., & Liao, J.C.** (2009) Direct photosynthetic recycling of carbon dioxide to isobutyraldehyde. *Nat Biotechnol.* 27:1177-1180.
- Aubert-Jousset, E., Cano, M., Guedeney, G., Richaud, P., & Cournac, L.** (2011) Role of HoxE subunit in *Synechocystis* PCC 6803 hydrogenase. *FEBS J.* 278:4035-4043.
- Baebprasert, W., Jantaro, S., Khetkorn, W., Lindblad, P., & Incharoensakdi, A.** (2011) Increased H₂ production in the cyanobacterium *Synechocystis* sp. strain 6803 by redirecting the electron supply via genetic engineering of the nitrate assimilation pathway. *Metabolic Eng.* 13:610-616.

- Bandyopadhyay, A., Stockel, J., Min, H., Sherman, L.A., & Pakrasi, H.B.** (2010) High rates of photobiological H₂ production by a cyanobacterium under aerobic conditions. *Nat Commun.* 1:139.
- Becker, E.W.** (2007) Micro-algae as a source of protein. *Biotechnol Adv.* 25:207-210.
- Beggins, J.** (1969) Respiration in blue-green algae. *J Bacteriol.* 99:570-575.
- Belotti, G., Bravi, M., de Caprariis, B., de Filippis, P., & Scarsella, M.** (2013) Effect of nitrogen and phosphorus starvations on *Chlorella vulgaris* lipids productivity and quality under different trophic regimens for biodiesel production. *Am J Plant Sci.* 4:44-51.
- Bennette, N.B., Eng, J.E., and Dismukes, G.** (2011) An LC-MS-based chemical and analytical method for targeted metabolite quantification in the model cyanobacterium *Synechococcus* sp. PCC 7002. *Anal Chem.* 83:3808-3816.
- Berto, P., Adamo, S.D., Bergantino, E., Vallese, F., Giacometti, G.M. & Costantini, P.** (2011) The Cyanobacterium *Synechocystis* sp. PCC 6803 is able to express an active [FeFe] hydrogenase without additional maturation proteins. *Biochem Biophys Res Commun.* 405:678–683.
- Beste, D.J.V., Bonde, B., Hawkins, N., Ward, J.L., Beale, M.H., Noack, S., Nöh, K., Kruger, N.J., Ratcliffe, R.G., & McFadden, J.** (2011) ¹³C metabolic flux analysis identifies an unusual route for pyruvate dissimilation in *Mycobacteria* which requires isocitrate lyase and carbon dioxide fixation. *PLoS Pathog.* 7:e1002091.
- Bossi, R.T., Negri, A., Tedeschi, G., & Mattevi, A.** (2002) Structure of FAD-bound L-Aspartate oxidase: insight into substrate specificity and catalysis. *Biochemistry.* 41:3018-3024.
- Bothe, H., Schmitz, O., Yates, M.G., & Newton, W.E.** (2010) Nitrogen fixation and hydrogen metabolism in cyanobacteria. *Microbiol Mol Biol Rev.* 74:529-551.
- BPstats.** *BP Statistical Review of World Energy.* 64th ed. 2015. Print.
- Brentner, L.B., Peccia, J., & Zimmerman, J.B.** (2010) Challenges in developing biohydrogen as a sustainable energy source: implications for a research agenda. *Environ Sci Technol.* 44:2243-2254.
- Bricker T.M., Zhang S., Laborde S.M., Mayer P.R. 3rd, Frankel L.K., Moroney J.V.** (2004) The malic enzyme is required for optimal photoautotrophic growth of *Synechocystis* sp. strain PCC 6803 under continuous light but not under a diurnal light regimen. *J Bacteriol.* 186:8144–8148.
- Buescher, J.M., Antoniewicz, M.R., Boros, L.G., Burgess, S.C., Brunengraber, H., Clish, C.B., DeBerardinis, R.J., Feron, O., Frezza, C., Ghesquiere, B., Gottlieb, E., Hiller, K., Jones, R.G., Kamphorst, J.J., Kibbey, R.G., Kimmelman, A.C., Locasale, J.W., Lunt, S.Y., Maddocks, O.D., Malloy, C., Metallo, C.M., Meuillet, E.J., Munger, J., Nöh, K., Rabinowitz, J.D., Ralser, M., Sauer, U., Stephanopoulos, G., St-Pierre, J., Tennant, D.A., Wittmann, C., Vander Heiden, M.G., Vazquez, A., Vousden, K.,**

Young, J.D., Zamboni, N., & Fendt, S.M. (2015) A roadmap for interpreting (13)C metabolite labeling patterns from cells. *Curr Opin Biotechnol.* 34:189-201.

Cardol, P., Forti, G. & Finazzi, G. (2011) Regulation of electron transport in microalgae. *Bba-Bioenergetics.* 1807:912-918.

Carrieri, D., Momot, D., Brasg, I.A., Ananyev, G., Lenz, O., Bryant, D.A., & Dismukes, G.C. (2010) Boosting autofermtation rates and product yields with sodium stress cycling: application to production of renewable fuels by cyanobacteria. *Appl Environ Microbiol.* 76:6455-6462.

Carrieri, D., Wawrousek, K., Eckert, C., Yu, J., & Maness P.C. (2011) The role of the bidirectional hydrogenase in cyanobacteria. *Bioresour Technol.* 102:8368-8377.

Castielli, O., De la Cerda, B., Navarro, J.A., Hervás, M., & De la Rosa, M.A. (2009) Proteomic analyses of the response of cyanobacteria to different stress conditions. *FEBS Lett.* 583:1753-1758.

Chollet R, Vidal J, O'Leary MH (1996) Phosphoenolpyruvate carboxylase: a ubiquitous, highly regulated enzyme in plants. *Annu Rev Plant Physiol Plant Mol Biol.* 47:273–298.

Chow, T.J., Su, H.Y., Tsai, T.Y., Chou, H.H., Lee, T.M. & Chang, J.S. (2015) Using recombinant cyanobacterium (*Synechococcus elongates*) with increased carbohydrate productivity as feedstock for bioethanol via separate hydrolysis and fermentation process. *Bioresour Technol.* 184:33-41.

Chulavatnatol, M., & Atkinson, D.E. (1972) Phosphoenolpyruvate synthetase from *Escherichia coli*. *J Biol Chem.* 248:2712-2715.

Cooley, J.W., Howitt, C.A., & Vermaas, W.F.J. (2000) Succinate:quinol oxidoreductases in the cyanobacterium *Synechocystis* sp. strain 6803: presence and function in metabolism and electron transport. *J. Bacteriol.*182: 714-722.

Cooley, J.W. & Vermaas, W.F.J. (2001) Succinate Dehydrogenase and Other Respiratory Pathways in Thylakoid Membranes of *Synechocystis* sp. Strain PCC 6803: Capacity Comparisons and Physiological Function. *J Bacteriol.* 183:4251-4258.

Cornet, J.F., Dussap, C.G., and Gros, J.B. (1998) Kinetics and energetic of photosynthetic microorganisms in photobioreactors. *Biochem Eng Biotechnol.* 59:153-224.

Cournac, L., Guedeney, G., Peltier, G., & Vignais, P.M. (2004) Sustained photoevolution of molecular hydrogen in a mutant of *Synechocystis* sp. strain PCC 6803 deficient in the type I NADPH-dehydrogenase complex. *J Bacteriol.* 186:1737-1746.

Deng, M. & Coleman, J.R. (1999) Ethanol synthesis by genetic engineering in cyanobacteria. *Appl Eviron Microbiol.* 65: 523-528.

- Dismukes, G.C., Carrieri, D., Bennette, N., Ananyev, G.M., & Posewitz, M.C.** (2008) Aquatic phototrophs: efficient alternatives to land-based crops for biofuels. *Curr Opin Biotechnol.* 19:235-240.
- Du, W., Liang, F., Duan, Y., Tan, X. & Lu, X.** (2013) Exploring the photosynthetic production capacity of sucrose by cyanobacteria. *Metab Eng.* 19:17–25.
- Ducat, D.C., Way, J.C., & Silver, P.A.** (2011a) Engineering cyanobacteria to generate high-value products. *Trends Biotechnol.* 29:95-103.
- Ducat, D.C., Sachdeva, G., & Silver, P.A.** (2011b) Rewiring hydrogenase-dependent redox circuits in cyanobacteria. *Proc Natl Acad Sci USA.* 108:3941-3946.
- Ducat D.C. & Silver P.A.** (2012) Improving carbon fixation pathways. *Curr Opin Chem Biol.* 16:337-344.
- Ducat, D.C., Avelar-Rivas, J.A., Way, J.C. & Silver, P.A.** (2012) Rerouting carbon flux to enhance photosynthetic productivity. *Appl Environ Microbiol.* 78:2660–2668.
- Duke, S.C. and Allen, M.M.** (1990) Effect of nitrogen starvation on polypeptide composition, ribulose-1,5-bisphosphate carboxylase/oxygenase, and thylakoid carotenoprotein content of *Synechocystis* sp. Strain PCC 6308. *Plant Physiol.* 94:752-759.
- Dutta, D., De, D., Chaudhuri, S., & Bhattacharya, S.K.** (2005) Hydrogen production by cyanobacteria. *Microb Cell Fact.* 4:36.
- Elanskaya, I.V., Karandashova, I.V., Bogachev, A.V., & Hagemann, M.** (2002) Functional analysis of the Na⁺/H⁺ antiporter encoding genes of the cyanobacterium *Synechocystis* PCC 6803. *Biochemistry (Mosc).* 67:432-440.
- Falkowski, G. Paul & Raven A. John.** Aquatic Photosynthesis. 2nd ed. Princeton, NJ: Princeton University Press, 2007.
- Feist, A.M., Herrgard, J., Thiele, I., Reed, J.L. and Palsson, B.Ø.** (2009) Reconstruction of biochemical networks in microbial organism. *Nat Rev Microbiol.* 7:129-143.
- Flores, E., Frías, J.E., Rubio, L.M., & Herrero, A.** (2005) Photosynthetic nitrate assimilation in cyanobacteria. *Photosynth Res.* 83:117-133.
- Flores, E., Guerrero, M.G., & Losada, M.** (1983) Photosynthetic nature of nitrate uptake and reduction in the cyanobacterium *Anacystis nidulans*. *Biochim biophys Acta.* 722:408-416.
- Fu, P.** (2009) Genome-scale modeling of *Synechocystis* sp. PCC 6803 and prediction of pathway insertion. *J. Chem Technol Biotechnol.* 84:473-483.
- Frigaard, N.L., Sakuragi, Y. and Bryant, D.A.** (2004) Gene inactivation in the cyanobacterium *Synechococcus* sp. PCC 7002 and the green sulfur bacterium

Chlorobium tepidum using in vitro-made DNA constructs and natural transformation. *Photos. Res. Prot. Method Mol Biol.* 274:325-340.

Gao, K., Orr, V., & Rehm, L. (2016) Butanol fermentation from microalgae-derived carbohydrates after ionic liquid extraction. *Bioresour Technol.* 206:77-85.

Gao, X., Sun, T., Pei, G., Chen, L. & Zhang, W. (2016) Cyanobacterial chassis engineering for enhancing production of biofuels and chemicals. *Appl Microbiol Biotechnol.* Epub.

Gao, Z., Zhao, H., Li, Z., Tan, X. & Lu, X. (2012) Photosynthetic production of ethanol from carbon dioxide in genetically engineered cyanobacteria. *Energy Environ Sci.* 5:9857-9865.

Gartner, K., Lechno-Yossef, S., Cornish, A.J., Wolk, P.C., Hegg, E.C. (2012) Expression of *Shewanella Oneidensis* MR-1 [FeFe] hydrogenase genes in *Anabaena* Sp. strain PCC 7120. *Appl Environ Microbiol.* 78:8579–8586.

Ghirardi, M., Posewitz, M., Maness, P.C., Dubini, A., Yu, J., & Seibert, M. (2007) Hydrogenases and hydrogen photoproduction in oxygenic photosynthetic organisms. *Annu Rev Plant Biol.* 58:71-91.

Gleason, F.K. (1996) Glucose-6-phosphate dehydrogenase from the cyanobacterium *Anabaena* sp. PCC 7120: Purification and kinetics of redox modulation. *Arch Biochim Biophys.* 334:277-283.

Green, L.S., Li, Y., Emerich, D.W., Bergersen, F.J., & Day, D.A. (2000) Catabolism of alpha-ketoglutarate by a *sucA* mutant of *Bradyrhizobium japonicum*: evidence for an alternative tricarboxylic acid cycle. *J Bacteriol.* 182:2838-44.

Gressel, J. (2008) Transgenics are imperative for biofuel crops. *Plant Sci.* 174:246-263.

Griffiths, M.J. and Harrison, T.L. (2009) Lipid productivity as a key characteristic for choosing algal species for biodiesel production. *J Appl Phycol.* 21:493-507.

Guerra, L.T., Xu, Y., Bennette, N., McNeely, K., Bryant, D.A. and Dismukes, G.C. (2013a) Natural osmolytes are much less effective substrates than glycogen for catabolic energy production in the marine cyanobacterium *Synechococcus* sp. strain PCC 7002. *J Biotechnol.* 166:65-75.

Guerra, L.T., Levitan, O., Frada, M.J., Sun, J.S., Falkowski, P.G. and Dismukes, G.C. (2013b) Regulatory branch points affecting protein and lipid biosynthesis in the diatom *Phaeodactylum tricornutum*. *Biomass Bioenergy.* 59:306-315.

Gutthann, F., Egert, M., Marques, A. & Appel, J. (2007) Inhibition of respiration and nitrate assimilation enhances photohydrogen evolution under low oxygen concentrations in *Synechocystis* sp. PCC 6803. *Biochim Biophys Acta.* 1767:161-169.

Gutekunst, K., Chen, X., Schreiber, K., Kspar, U., Makam, S., & Appel, J. (2014) The bidirectional NiFe-hydrogenase in *Synechocystis* sp. PCC 6803 is reduced by

flavodoxin and ferredoxin and is essential under mixotrophic, nitrate-limiting conditions. *J Biol Chem.* 289:1930-1937.

Harbig, K., Chance, B., Kovách, A.G., & Reivich, M. (1976) *In vivo* measurement of pyridine nucleotide fluorescence from cat brain cortex. *J Appl Physiol.* 41:480-488.

Hays, S.G. & Ducat, D.C. (2015) Engineering cyanobacteria as photosynthetic feedstock factories. *Photosynth Res.* 123:285-295.

Hamilton, J.J. and Reed, J.L. (2012) Identification of functional differences in metabolic networks using comparative genomics and constraint-based models. *PLoS ONE.* 7:e34670.

Hasunuma, T., Kikuyama, F., Matsuda, M., Aikawa, S., Izumi, Y. and Kondo, A. (2013) Dynamic metabolic profiling of cyanobacterial glycogen biosynthesis under conditions of nitrate depletion. *J Exp Bot.* 64:2943-2954.

Heavner, B.D. and Price, N.D. (2015) Transparency in metabolic network reconstruction enables scalable biological discovery. *Curr Opin Biotechnol.* 34:105-109.

Henry, C.S., Dejongh, M., Best, A.A., Frybarger, P.M., Linsay, B. and Stevens, R.L. (2010) High-throughput generation, optimization and analysis of genome-scale metabolic models. *Nat Biotechnol.* 28:977-982.

Herrmann, K.M. and Weaver, L.M. (1999) The shikimate pathway. *Annu. Rev. Plant Physiol. Plant Mol Biol.* 50:473-503.

Heyer, H. & Krumbein, W.E. (1991) Excretion of fermentation products in dark and anaerobically incubated cyanobacteria. *Arch Microbiol.* 155:284-287.

Howitt, C.A., Udall, P.K., & Vermaas, W.F. (1999) Type 2 NADH dehydrogenases in the cyanobacterium *Synechocystis* sp. strain PCC 6803 are involved in regulation rather than respiration. *J Bacteriol.* 181:3994-4003.

Huege, J., Goetze, J., Schwarz, D., Bauwe, H., Hagemann, M. and Kopka, J. (2011) Modulation of the major paths of carbon in photorespiratory mutants of *Synechocystis*. *PLoS ONE.* 6:e16278.

Hutchins, A.M., Holden, J.F., & Adams, M.W.W. (2001) Phosphoenolpyruvate synthetase from the hyperthermophilic archaeon *Pyrococcus furiosus*. *J Bacteriol.* 183:709-715.

Jackson, J.B. (2003) Proton translocation by transhydrogenase. *FEBS Lett.* 545:18-24

Jia, X.H., Zhang, P.P., Shi, D.J., Mi, H.L., hu, J.C., Huang, X.W., & He, P.M. (2015) Regulation of *pepc* gene expression in *Anabaena* sp. PCC 7120 and its effects on cyclic electron flow around photosystem I and tolerances to environmental stresses. *J Integr Plant Biol.* 57:468-76.

- Jones, C.S. & Mayfield, S.P.** (2012) Algae biofuels: versatility for the future of bioenergy. *Curr Opin Biotechnol.* 23:346-351.
- Joseph, A., Aikawa, S., Sasaki, K., Matsuda, F., Hasunuma, T. & Kondo, A.** (2014) Increased biomass production and glycogen accumulation in *apcE* gene deleted *Synechocystis* sp. PCC 6803. *AMB Express.* 4:17.
- Kelley, J.J., Li, X., Mutthoju, B., Maor, S., Egen, D. and Lun, D.S.** (2015) MOST: A software environment for constraint-based metabolic modeling and strain design. *Bioinformatics.* 31:610-611.
- Kim, Y.M., Cho, H., Jung, G.Y., & Park, J.M.** (2011) Engineering the pentose phosphate pathway to improve hydrogen yield in recombinant *Escherichia coli*. *Biotechnol Bioeng.* 108:2941-2946.
- Kim, M.K., Lane, A., Kelly, J. and Lun, D.S.** E-Flux2 and SPOT: Validation methods for inferring intracellular metabolic flux distributions from transcriptomic data. *Submitted.*
- King, P.W., Posewitz, M.C., Ghirardi, M.L., & Seibert, M.** (2006) Functional studies of [FeFe] hydrogenase maturation in an *Escherichia coli* biosynthetic system. *J Bacteriol.* 188:2163-2172.
- Knies, D., Wittmüß, P., Appel, S., Sawodny, O., Ederer, M., & Feuer, R.** (2015) Modeling and simulation of optimal resource management during the diurnal cycle in *Emiliana huxleyi* by genome-scaled reconstruction and an extended flux balance analysis approach. *Metabolites.* 5:659-676.
- Knoop, H., Zilliges, Y., Lockau, W. and Steuer, R.** (2010) The metabolic network of *Synechococystis* sp. PCC 6803: systemic properties of autotrophic growth. *Plant Physiol.*, 154, 410-422.
- Knoop, H., Gründel, M., Zilliges, Y., Lehmann, R., Hoffmann, S., Lockau, W. and Steuer, R.** (2013) Flux balance analysis of cyanobacterial metabolism: the metabolic network of *Synechocystis* sp. PCC 6803. *PLoS ONE.* 9:e1003081.
- Knoop, H. & Steuer, R.** (2015) A computational analysis of stoichiometric constraints and trade-offs in cyanobacterial biofuel production. *Front Bioeng Biotechnol.* 3:47.
- Knowles, V.L., Smith, C.S., Smith, C.R., & Plaxton, W.C.** (2001) Structural and regulatory properties of pyruvate kinase from the cyanobacterium *Synechococcus* PCC 6301. *J Biol Chem.* 276:20966-20972.
- Knowles, V.L., & Plaxton, W.C.** (2003) From genome to enzyme: Analysis of key glycolytic and oxidative pentose phosphate pathway enzymes in the cyanobacterium *Synechocystis* sp. PCC 6803. *Plant Cell Physiol.* 44:758-763.
- Konopka, A. and Schnur, M.** (1980) Effect of light intensity on macromolecular synthesis in cyanobacteria. *Microb Ecol.* 6: 291-301.

Korotcenkov, G., Han, G., & Stetter, J.R. (2009) Review of electrochemical hydrogen sensor. *Chem Rev.* 109:1402-1433.

Kothari, A., Parameswaran, P., & Garcia-Pichel, F. (2014) Powerful fermentative hydrogen evolution of photosynthate in the cyanobacterium *Lyngbya aestuarii* BL J mediated by a bidirectional hydrogenase. *Front Microbial.* 5:680.

Kramer, D.M., Avenson, T., & Edwards, G.E. (2004) Dynamic flexibility in the light reactions of photosynthesis governed by both electron and proton transfer reactions. *Trends Plant Sci.* 9:349-357.

Kramer, D.M., & Evans, J.R. (2011) The importance of energy balance in improving photosynthetic productivity. *Plant Physiol.* 155:70-78.

Krishnan, A., Gu, H., Kumaraswamy, G.K., Ananyev, G., Posewitz, M., & Dismukes, G.C. The carbon decision tree of *Chlamydomonas reinhardtii*: How starchless mutant strains redirect carbon metabolism. *Submitted.*

Krishnan, A., Zhang, S., Liu, Y., Tadmori, K.A., Bryant, D.A., & Dismukes, G.C. (2015) Consequences of ccmR deletion on respiration, fermentation and H metabolism in cyanobacterium *Synechococcus* sp. PCC 7002. *Biotechnol Bioeng.* Epub. doi: 10.1002/bit.25913.

Kruse, O., Rupprecht, J., Bader, K., Thomas-Hall, S., Schenk, P.M., Finazzi, G., & Hankamer, B. (2005) Improved photobiological H₂ production in engineered green algal cells. *J Biol Chem.* 280:34170-34177.

Kumaraswamy, G.K., Guerra, T., Qian, X., Zhang, S., Bryant, D.A. and Dismukes, G.C. (2013) Reprogramming the glycolytic pathway for increased hydrogen production in cyanobacteria: metabolic engineering of NAD⁺-dependent GAPDH. *Energy Environ Sci.* 6:3722–3731.

Lan, E.I. & Liao, J.C. (2012) ATP drives direct photosynthetic production of 1-butanol in cyanobacteria. *Proc Natl Acad Sci USA.* 109:6018-6023.

Laurent, S., Chen, H., Bédu, S., Ziarelli, F., Peng, F., & Zhang, C.C. (2005) Nomentabolizable analogue of 2-oxoglutarate elicits heterocyst differentiation under repressive conditions in *Anabaena* sp. PCC 7120. *Proc Natl Acad Sci USA.* 102:9970-9912.

Liu, X., Fallon, S., Sheng, J. and Crutiss, III R. (2011) CO₂-limitation-inducible green recovery of fatty acids from cyanobacterial biomass. *Proc. Natl Aca. Sci. USA.* 108:6905-6908.

Liu, X., Saydah, B., Eranki, P., Colosi, L.M., Greg, M.B., Rhodes, J., & Clarens, A.F. (2013) Pilot-scale data provide enhanced estimates of the life cycle energy and emissions profile of algae biofuels produced via hydrothermal liquefactions. *Bioresour Technol.* 148:163-171.

- Luque, I. & Forchhammer, K.**, Nitrogen assimilation and C/N balance sensing, in: Herrero, A. & E. Flores (Eds.), *The cyanobacteria molecular biology, genomics and evolution*, Caister Academic Press, Norfolk, UK, 2008, pp.335-382.
- Ludwig, M., & Bryant, D.A.** (2011) Transcription profiling of the model cyanobacterium *Synechococcus* sp. strain PCC 7002 by next-gen (SOLiD™) sequencing of cDNA. *Front Microbiol.* 2:41.
- Ludwig, M. and Bryant, D.A.** (2012) Acclimation of the global transcriptome of the cyanobacterium *Synechococcus* sp. strain PCC 7002 to nutrient limitations and different nitrogen sources. *Front Microbiol.* 3:145.
- Lun, D.S., Rockwell, G., Guido, N.J., Kelner, J.A., Berger, B., Galagan, J.E. and Church, G.M.** (2009) Large-scale identification of genetic design strategies using local search. *Mol Syst Biol.* 5:296.
- Luzzatto, L.** (1967) Regulation of the activity of glucose-6-phosphate dehydrogenase by NADP⁺ and NADPH. *Biochim biophys Acta.* 146:18-25.
- Machado, I.M.P., & Atsumi, S.** (2012) Cyanobacterial biofuel production. *J Biotechnol.* 162:50-56.
- Mahadevan, R. and Schilling, C.H.** (2003) The effects of alternate optimal solutions in constraint-based genome-scale metabolic models. *Metab Eng.* 5:264-276. doi:10.1016/j.ymben.2003.09.002
- Martzolff, A., Cahoreau E., Cogne, G., Peyriga, L., Portais, J., Dechandol, E., Grand, F.L., Massou, S., Gonçalves, O., Pruvost, J., & Legrand, J.** (2012) Photobioreactor design for isotopic non-stationary ¹³C-metabolic flux analysis (INST ¹³C-MFA) under photoautotrophic conditions. *Biotechnol Bioeng.* 109:3030-3040.
- Mathews, J.A. & Tan, H.** (2009) Biofuels and indirect land use change effects: the debate continues. *Biofuels Bioprod Bioref.* 3:305-317.
- Melis, A., Happe, T.** (2001) Hydrogen production. Green algae as a source of energy. *Plant Physiol.* 127:740-748.
- Melis, A.** (2009) Solar energy conversion efficiencies in photosynthesis: Minimizing the chlorophyll antennae to maximize efficiency. *Plant Sci.* 177:272-280.
- McIntosh, C.L., Germer, F., Schulz, R., Appel, J., & Jones, A.K.** (2011) The [NiFe]-hydrogenase of the cyanobacterium *Synechocystis* sp. PCC 6803 works bidirectionally with a bias to H₂ production. *J Am Chem Soc.* 133:11308-11319.
- McNeely, K., Xu, Y., Bennette, N., Bryant, D.A. and Dismukes, G.C.** (2010) Redirecting reductant flux into hydrogen production via metabolic engineering of fermentative carbon metabolism in a cyanobacterium. *Appl Environ Microbiol.* 76:5032 – 5038.

- McNeely, K., Kumaraswamy, G.K., Guerra, T., Bennette, N., Ananyev, G., Dismukes, G.C.** (2014) Metabolic switching of central carbon metabolism in response to nitrate: application to autofermentative hydrogen production in cyanobacteria. *J Biotechnol.* 182-183:83-91.
- Miller, S.R., Martin, M., Touchton, J., & Castenholz, R.W.** (2002) Effects of nitrogen availability on pigmentation and carbon assimilation in the cyanobacterium *Synechococcus* sp. Strain SH-94-5. *Arch Microbiol.* 177:392-400.
- Monk, J., Nogales, J. and Palsson, B.O.** (2014) Optimizing genome-scale network reconstructions. *Nat Biotechnol.* 32:447-452.
- Montingelli, M.E., Tedesco, S., & Olabi, A.G.** (2015) Biogas production from algal biomass: A review. *Renew Sust Energy Rev.* 43:961-972.
- Muro-Pastor, M.I., Reyes, J.C., Florencio, F.J.** (2001) Cyanobacteria perceive nitrogen status by sensing intracellular 2-oxoglutarate levels. *J Biol Chem.* 276:38320-38328.
- Nakajima, T., Kajihata, S., Yoshikawa, K., Matsuda, F., Furusawa, C., Hirasawa, T., Shimizu, H.** (2014) Integrated Metabolic flux and omics analysis of *Synechocystis* sp. PCC 6803 under mixotrophic and photoheterotrophic conditions. *Plant cell physiol.* 55:1605-1612.
- Niederholtmeyer, H., Wolfstädter, B.T., Savage, D.F., Silver, P.A. & Way, J.C.** (2010) Engineering cyanobacteria to synthesize and export hydrophilic products. *Appl Environ Microbiol.* 76:3462–3466.
- Nigam, S., Rai, M.P. and Sharma, R.** (2011) Effect of nitrogen on growth and lipid content of *Chlorella pyrenoidosa*. *Am J Biochem Biotechnol.* 7:124-129.
- Nomura, C.T., Persson, S., Shen, G., Inoue-Sakamoto, K. and Donald, A.B.** (2006) Characterization of two cytochrome oxidase operons in the marine cyanobacterium *Synechococcus* sp. PCC 7002: inactivation of *ctaDI* affects the PS I:PS II ratio. *Photosynth Res.* 87:215-228.
- Nogales, J., Gudmundsson, S., Knight, E.M., Palsson, B.O. and Thiele, I.** (2012) Detailing the optimality of photosynthesis in cyanobacteria through systems biology analysis. *Proc Natl Aca Sci USA.* 109:2678-2683.
- Nozzi, N.E., Oliver, J.W.K. & Atsumi, S.** (2013) Cyanobacteria as a platform for biofuel production. *Front Bioeng Biotechnol.* 1:7.
- Nyberg, M., Heidorn, T., & Lindblad, P.** (2015) Hydrogen production by the engineered cyanobacterial strain *Nostoc* PCC 7120 $\Delta hupW$ examined in a flat panel. *J Biotechnol.* 215:35-43.
- Ohashi, Y., Shi, W., Takatani, N., Aichi, M., Maeda, S., Watanabe, S., Yoshikawa, H., & O'Leary, M.H.** (1982) Phosphoenolpyruvate carboxylase: An enzymologist's view. *Annu Rev Plant Physiol.* 33:294–131.

- Olguín, E.J., Galicia, S., Angulo-Guerrero, O. and Hernández, E.** (2001) The effect of low light flux and nitrogen deficiency on the chemical composition of *Spirulina* sp. (*Arthrospira*) grown on digested pig waste. *Bioresour Technol.* 77:19-24.
- Omata, T.** (2011) Regulation of nitrate assimilation in cyanobacteria. *J Exp Bot.* 62:1411-1424.
- Ooyabu, J., Ohtsuka, M., Kashino, Y., Koike, H., & Satoh, K.** (2008) The expression pattern of NAD(P)H oxidases and the cyclic electron transport pathway around photosystem I of *Synechocystis* sp. PCC6803 depend on growth conditions. *Biosci Biotechnol Biochem.* 72:3180-3188.
- Ortega-Ramos, M., Jittawuttipoka, T., Saenkham, P., Czarnecka-Kwasiborski, A., Bottin, H., Cassier-Chauvat, C., & Chauvat, F.** (2014) Engineering *Synechocystis* PCC 6803 for hydrogen production: Influence on the tolerance to oxidative and sugar stresses. *Plos One.* 9:e89372.
- Orth, J.D. ., Thiele, I. and Palsson, B.O.** (2010) What is flux balance analysis? *Nat Biotechnol.* 28:245-248.
- Osanai, T., Imamura, S., Asayama, M., Shirai, M., Suzuki, I., Murata, N., & Tanaka, K.** (2006) Nitrogen induction of sugar catabolic gene expression in *Synechocystis* sp. PCC 6803. *DNA Res.* 13(5):185-195.
- Parmar, A., Singh, N.K., Pandey, A., Gnansounou, E. and Madamwar, D.** (2011) Cyanobacteria and microalgae: a positive prospect for biofuels. *Bioresour Technol.* 102:10163-10172.
- Pearce, J., & Carr, N.G.** (1967) The metabolism of acetate by the blue-green algae, *Anabaena variabilis* and *Anacystis nidulans*. *J Gen Microbiol.* 49:301–313.
- Pelroy, R.A., Rippka, R., & Stanier, R.Y.** (1972) Metabolism of glucose by unicellular blue-green algae. *Arch Mikrobiol.* 87:303-322.
- Pelroy, R.A., Kirk, MR., & Bassham, J.A.** (1976) Photosystem II regulation of macromolecule synthesis in the blue-green alga *Aphanocapsa* 6714. *J Bacteriol.* 128(2):623-632.
- Qi, F., Yao, L., Tan, X. and Lu, X.** Construction, characterization and application of molecular tools for metabolic engineering of *Synechocystis* sp. *Biotechnol Lett.* 35:1655-1661.
- Qian, X., Kim, M.K., Kumaraswamy, G.K., Agarwal, A., Lun, D.S., & Dismukes, G.C.** Beyond conventional flux balance analysis of photoautotrophic metabolism: light intensity dependent partitioning of carbon into cellular products. *Plant J. submitted*
- Qian, X., Kumaraswamy, G.K., Zhang, S., Gates, C., Ananyev, G.M. and Dismukes, G.C.** (2015) Inactivation of nitrate reductase alters metabolic branching of carbohydrate fermentation in the cyanobacterium *Synechococcus* sp. strain PCC 7002. *Biotechnol Bioeng.* Epub. doi: 10.1002/bit.25862.

Quintana, N., Van der Kooy, F., Van de Rhee, MD., Voshol, G.P. and Verpoorte, R. (2011) Renewable energy from cyanobacteria: energy production optimization by metabolic pathway engineering. *Appl Microbiol Biotechnol.* 91:471-490.

Radakovits, R., Jinkerson, R.E., Darzins, A. and Posewitz, M.C. (2010) Genetic engineering of algae for enhanced biofuel production. *Eukaryot Cell.* 9:486-501.

Raman, K. and Chandra, N. (2009) Flux balance analysis of biological systems: applications and challenges. *Brief Bioinform.* 10:435-449.

Raven, J. A. (1982) The Energetics of Fresh-Water Algae - Energy-Requirements for Biosynthesis and Volume Regulation. *New Phytol.* 92:1-20.

Ravikrishnan, A. and Raman, K. (2015) Critical assessment of genome-scale metabolic networks: the need for unified standard. *Brief Bioinform.*, 2015; Epub. doi: 10.1093/bib/bbv003

Roselers, G., van Loosdrecht, M.C.M., & Muyzer, G. (2008) Phototropic biofilms and their potential applications. *J Appl Phycol.* 20:227-235.

Romagnoli, F., Blumberga, D., & Gigli, E. (2010) Biogas from marine macroalgae: a new environmental technology – life cycle inventory for a further LCA. *Environ Climate Technol.* 4:97-108.

Rügen, M., Bockmayr, A., & Steuer, R. (2015) Elucidating temporal resource allocation and diurnal dynamics in phototrophic metabolism using conditional FBA. *Sci Rep.* 5:15247.

Sakamoto, T., Inoue-Sakamoto, K., & Bryant, D.A. (1999) A novel nitrate/nitrite permease in the marine cyanobacterium *Synechococcus* sp. Strain PCC 7002. *J Bacteriol.* 181:7363-7372.

Sakamoto, T., Delgaizo, V.B., & Bryant, D.A. (1998) Growth on urea can trigger death and peroxidation of the cyanobacterium *Synechococcus* sp. strain PCC 7002. *Appl Environ Microbiol.* 64:2361-2366.

Sakamoto, T., Inoue-Sakamoto, K., Persson, S., & Bryant, D.A. (2008) Transcription factor NtcB specifically controls the nitrate assimilation genes in the marine cyanobacterium *Synechococcus* sp. strain PCC 7002. *Phycol Res.* 56:223-237.

Sakamoto, T. & Bryant, D.A. (1997) Growth at low temperature causes nitrogen limitation in the cyanobacterium *Synechococcus* sp. PCC 7002. *Arch Microbiol.* 169:10-19.

Sauer, J., Schreiber, U., Schmid, R., Völker, U. and Forchhammer, K. (2001) Nitrogen starvation-induced chlorosis in *Synechococcus* PCC 7942. Low-level photosynthesis as a mechanism of long-term survival. *Plant Physiol.*, 126, 233-243.

- Schwarz, R., & Forchhammer, K.** (2005) Acclimation of unicellular cyanobacteria to macronutrient deficiency: emergence of a complex network of cellular responses. *Microbiol.* 151:2503-2514.
- Schwarz, D., Orf, I., Kopka, J., & Hagemann, M.** (2013) Recent applications of metabolomics toward cyanobacteria. *Metabolites.* 3:72-100.
- Shastri, A.A. & Morgan, J.A.** (2005) Flux balance analysis of photoautotrophic metabolism. *Biotechnol. Prog.*, 21, 1617 – 1626.
- Shen, G., Antonkine, M.L., van der Est, A., Vassiliev, I.R., Bittl, R., Zech, S.G., Zhao, J., Stehlik, D., Bryant, D.A., & Golbeck, J.H.** (2002) Assembly of photosystem I. II. Rubredoxin is required for the *in vivo* assembly of F_X in *Synechococcus* sp. PCC 7002 as shown by optical and EPR spectroscopy. *J Biol Chem.* 277:20355-20366.
- Shen, G., & Bryant, D.A.** (1995) Characterization of a *Synechococcus* sp. strain PCC 7002 mutant lacking Photosystem I. Protein assembly and energy distribution in the absence of the Photosystem I reaction center core complex. *Photosynth Res.* 44:41-53.
- Shylajanaciyar, M., Dineshababu, G., Rajalakshmi, R., Subramanian, G., Prabakaran, D., & Uma, L.** (2015) Analysis and elucidation of phosphoenolpyruvate carboxylase in cyanobacteria. *Protein J.* 34:73-81.
- Skizim, N.J., Ananyev, G.M., Krishnan, A., & Dismukes, G.C.** (2011) Metabolic pathways for photobiological hydrogen production by nitrogenase- and hydrogenase-containing unicellular cyanobacteria *Cyanothece*. *J Biol Chem.* 787:2777-2786.
- Smith, A.J., London, J., & Stanier, R.Y.** (1967) Biochemical basis of obligate autotrophy in blue-green algae and Thiobacilli. *J Bacteriol.* 94:972–983.
- Srivastava, A.A., Allen, J.P., Vaccaro, B.J., Hirasawa, M., Alkul, S., Johnson, M.K., & Knaff, D.B.** (2015) Identification of amino acids at the catalytic site of a ferredoxin-dependent cyanobacterial nitrate reductase. *Biochem.* 54:5557-5568.
- Stal, L.J. & Moezelaar, R.** (1997) Fermentation in cyanobacteria. *FEMS Microbiol Rev.* 21:179-211.
- Steinhauser, D., Fernie, A.R., & Araújo, W.L.** (2012) Unusual cyanobacterial TCA cycles: not broken just different. *Trend Plant Sci.* 17(9): 503-509.
- Steuer, R., Knoop, H., & Machné** (2012) Modelling cyanobacteria: from metabolism to integrative models of phototrophic growth. *J Exp Bot.* 63:2259-2274.
- Stevens, S.E., Patterson, C.O.P., & Myers, J.** (1973) The production of hydrogen peroxide by blue-green algae: a survey. *J Phycol.* 9:427-430.
- Stevens, S.E. Jr., Balkwill, D.L., Paone, A.M.** (1981) The effects of nitrogen limitation on the ultrastructure of the cyanobacterium *Agmenellum quadruplicatum*. *Arch Microbiol.* 130:204-212.

Stevens, S.E. Jr. and Porter, R.D. (1980) Transformation in *Agmenellum quadruplicatum*. *Proc. Natl Aca. Sci. USA*, 77, 6052-6056.

Struys, E.A., Jansen, E.E.W., Gibson, K.M., & Jakobs, C. (2005) Determination of the GABA analogue succinic semialdehyde in urine and cerebrospinal fluid by dinitrophenylhydrazine derivatization and liquid chromatography-tandem mass spectrometry: application to SSADH deficiency. *J. Inherit. Metab. Dis.* 28: 913-920.

Subramanian, S., Barry, A. N., Pieris, S. & Sayre, R. T. (2013) Comparative energetics and kinetics of autotrophic lipid and starch metabolism in chlorophytic microalgae: implications for biomass and biofuel production. *Biotechnol Biofuels.* 6:150.

Suzuki, E., Ohkawa, H., Moriya, K., Matsubara, T., Nagaike, Y., Iwasaki, I., Fujiwara, S., Tsuzuki, M. and Nakamura, Y. (2010) Carbohydrate metabolism in mutants of the cyanobacterium *Synechococcus elongates* PCC 7942 defective in glycogen synthesis. *Appl Environ Microbiol.* 76:3135-3159.

Szecowka, M., Heise, R., Tohge, T., Nunes-Nesi, A., Vosloh, D., Huege, J., Feil, R., Lunn, J., Nikoloski, Z., Stitt, M., Femie, A.R. and Arrivault, S. (2013) Metabolic fluxes in an illuminated *Arabidopsis* Rosette. *Plant Cell.* 25:649-714.

Taikhao, S., Junyapoon, S., Incharoensakdi, A. and Phunpruch, S. (2013) Factors affecting biohydrogen production by unicellular halotolerant cyanobacterium *Aphanothece halophytica*. *J Appl Phycol.* 25:575-585.

Taikhao, S., Incharoensakdi, A. and Phunpruch, S. (2015) Dark fermentative hydrogen production by the unicellular halotolerant cyanobacterium *Aphanothece halophytica* grown in seawater. *J Appl Phycol.* 27:187-196.

Takabayashi, A., Kishine, M., Asada, K., Endo, T., & Sato, F. (2005) Differential use of two cyclic electron flows around photosystem I for driving CO₂-concentration mechanism in C4 photosynthesis. *Proc Natl Acad Sci USA.* 102:16898-16903.

Tang, J.K., You, L., Blankenship, R.E., & Tang, Y.J. (2012) Recent advances in mapping environmental microbial metabolisms through ¹³C isotopic fingerprints. *J R Soc Interface.* 9:2767-2780.

Tang, K., Tang, Y.J., & Blankenship, R.E. (2011) Carbon metabolic pathways in phototrophic bacteria and their broader evolutionary implications. *Front Microbiol.* 2:165.

Tank, M. & Bryant, D.A. (2015) Nutrient requirements and growth physiology of the photoheterotrophic acidobacterium, *Chloracidobacterium thermophilum*. *Front Microbiol.* 6:1-14

Taparia, T., Mvss, M., Mehrotra, R., Shukla, P., & Mehrotra, S. (2015) Developments and challenges in biodiesel production from microalgae: a review. *Biotechnol Appl Biochem.* Epub. doi: 10.1002/bab.1412.

- Tedesco, M.A. and Duerr, E.O.** (1989) Light, temperature and nitrogen starvation effects on the total lipid and fatty acid content and composition of *Spirulina platensis* UTEX 1928. *J Appl Phycol.* 1:201-209.
- Tong, Y., Yu, J., Maness, P.C., Smith, H.O. & Xu, Q.** (2011) Heterologous expression of *Alteromonas macleodii* and *Thiocapsa roseopersicina* [NiFe] hydrogenases in *Synechococcus elongatus*. *PLoS ONE.* 6:e20126.
- Trevelyan, W.E. & Harrison, J.S.** (1952) Studies on yeast metabolism. I. Fractionation and microdetermination of cell carbohydrates. *Biochem J.* 50:298-303.
- Troshina, O., Serebryakova, L., Sheremetieva, M., & Lindblad, P.** (2002) Production of H₂ by the unicellular cyanobacterium *Gloeocapsa alpicola* CALU 743 during fermentation. *Int J Hydrogen Energy.* 27:1283-1289.
- Varman, A.M., Xiao, Y., Pakrasi, H.B. and Tang, Y.** (2013) Metabolic engineering of *Synechocystis* sp. strain PCC 6803 for isobutanol production. *Appl Environ Microbiol.* 79: 908-914.
- Vu, T.T., Hill, E.A., Kucek, L.A., Konopka, A.E., Beliaev, A. and Reed, J.L.** (2013) Computational evaluation of *Synechococcus* sp. PCC 7002 metabolism for chemical production. *Biotechnol J.* 8:619-630.
- Wang, W., Liu, X. and Lu, X.** (2013) Engineering cyanobacteria to improve photosynthetic production of alka(e)nes. *Biotechnol Biofuels.* 6: 69.
- Wermuth, C.G.** (1979) A convenient synthesis of γ -Ethoxy- γ -butyrolactone and of succinic semialdehyde. *J Org Chem.* 44:2406-2408.
- White D.** (1995) *The physiology and biochemistry of prokaryotes* 3rd edn. Oxford University Press.
- Wiechert, W.** (2001) ¹³C metabolic flux analysis. *Metab Eng.* 3(3):195-206.
- Winkel, B.S.J.** (2004) Metabolic channeling in plants. *Annu Rev Plant Biol.* 55:85-107.
- Wittmann, C.** (2002) Metabolic flux analysis using mass spectrometry. *Adv Biochem Eng Biotechnol.* 74:39-64.
- Woolston, B.M., Edgar, S., & Stephanopoulos, G.** (2013) Metabolic engineering: past and future. *Annu Rev Chem Biomol Eng.* 4:259–288
- Vallino, J.J. & Stephanopoulos, G.** (1994) Carbon flux distributions at the pyruvate branch point in corynebacterium-glutamicum during lysine overproduction. *Biotechnol Progr.* 10:320–326
- Vermaas, W.F.J.** (2001) Photosynthesis and respiration in cyanobacteria. *Encycl Life Sci.* 1-7.

- Vollmar, M., Schlleper, D., Wlwn, M., Buchner, C., & Groth, G.** (2009) Structure of the c14 rotor ring of the proton translocating chloroplast ATP synthase. *J Biol Chem.* 284:18228-18235.
- Vu, T.T., Hill, E.A., Kucek, L.A., Konopka, A.E., Beliaev, A., & Reed, J.L.** (2013) Computational evaluation of *Synechococcus* sp. PCC 7002 metabolism for chemical production. *Biotechnol J.* 8:619-630.
- Xiong, W., Brune, D., & Vermaas, W.F.J.** (2014) The γ -aminobutyric acid shunt contributes to closing the tricarboxylic acid cycle in *Synechocystis* sp. PCC 6803. *Mol Microbiol.* 93:786-796.
- Xu, Y., Alvey, R.M., Byrne, P.O., Graham, J.E., Shen, G. and Bryant, D.A.** (2011) Expression of genes in Cyanobacteria: adaptation of endogenous plasmids as platforms for high-level gene expression in *Synechococcus* sp. PCC 7002. *Methods Mol Biol.* 684: 273-293.
- Xu, Y., Guerra, L.T., Li, Z., Ludwig, M., Dismukes, G.C. & Bryant, D.A.** (2013) Altered carbohydrate metabolism in glycogen synthase mutants of *Synechococcus* sp. Strain PCC 7002: Cell factories for soluble sugars. *Metab Eng.* 16:56-67.
- Xuan, Y.H., Hu, Y.B., Chen, L., Sosso, D., Ducat, D.C., Hou, B. & Frommer, W.B.** (2013) Functional role of oligomerization for bacterial and plant SWEET sugar transporter family. *Proc Natl Acad Sci USA.* 110:E3685–E3694.
- Yamori, W., Shikanai, T. and Makino, A.** (2015) Photosystem I cyclic electron flow via chloroplast NADH dehydrogenase-like complex performs a physiological role for photosynthesis at low light. *Sci Rep.* 5: 13908.
- Yang, C., Hua, Q., & Shimizu, K.** (2002) Quantitative analysis of intracellular metabolic fluxes using GC–MS and two-dimensional NMR spectroscopy. *J Biosci Bioeng.* 93:78–87
- Yoo, S.H., Keppel, C., Spalding, M., & Jane, J.L.** (2007) Effects of growth condition on the structure of glycogen produced in cyanobacterium *Synechocystis* sp. PCC6803. *Int J Biol Macromol.* 40:498-504.
- You, L., Berla, B., He, L., Pakrasi, H.B., Tang, Y.J.** (2014) ¹³C-MFA delineates the photoheterotrophic metabolism of *Synechocystis* sp. PCC 6803 under light- and carbon-sufficient conditions. *Biotechnol J.* 9:684–692. doi:10.1002/biot.201300477
- You, L., He, L., & Tang, Y.J.** (2015) Photoheterotrophic fluxome in *Synechocystis* sp. strain PCC 6803 and its implications for cyanobacterial bioenergetics. *J Bacteriol.* 197:943-950.

- Young, J.D., Shastri, A.A., Stephanopoulos, G. and Morgan, J.A.** (2011) Mapping photoautotrophic metabolism with isotopically nonstationary ^{13}C flux analysis. *Metab. Eng.* 13:656-665.
- Yu, Y., You, L., Liu, D., Hollinshead, W., Tang, Y.J., & Zhang, F.** (2013) Development of *Synechocystis* sp. PCC 6803 as a phototrophic cell factory. *Mar Drugs.* 11:2894-2916.
- Yu, J., Liberton, M., Cliften, P.F., Head, R.D., Jacobs, J.M., Smith, R.D., Koppenaal, D.W., Brand, J.J., & Pakrasi, H.B.** (2015) *Synechococcus elongates* UTEX 2973, a fast growing cyanobacterial chassis for biosynthesis using light and CO_2 . *Sci Rep.* 30:8132. doi: 10.1038/srep08132.
- Yuan, J., Bennett B.D., & Rabinowitz, J.D.** (2008) Kinetic flux profiling for quantitation of cellular metabolic fluxes. *Nat Protoc.* 3:1328-1340.
- Zhang, S. and Bryant A.** (2011) The tricarboxylic acid cycle in cyanobacteria. *Science*, 334, 1551-1553.
- Zhang, S., & Bryant, D.A.** (2014) Learning new tricks from an old cycle: the TCA cycle in cyanobacteria, algae and plants. *Perspect Phycol.* 1:73-86.
- Zhang, S., Liu, Y., & Bryant, D.A.** (2015) Metabolic engineering of *Synechococcus* sp. PCC 7002 to produce poly-3-hydroxybutyrate and poly-3-hydroxybutyrate-co-4-hydroxybutyrate. *Metab Eng.* 32:174-183.
- Zhang, S., & Bryant, D.A.** (2015) Biochemical validation of the glyoxylate cycle in the cyanobacterium *Chlorogloeopsis fritschii* strain PCC 9212. *J Biol Chem.* 290:14019-14030.
- Zhao, H., Wang, P., Huang, E., Ge, Y., & Zhu, G.** (2008) Physiologic roles of soluble pyridine nucleotide transhydrogenase in *Escherichia coli* as determined by homologous recombination. *Ann Microbiol.* 58:275–280.